Università degli Studi di Cagliari

DOTTORATO DI RICERCA

FISICA

Ciclo XXVIII

TITOLO TESI

Computational Investigation on Polycyclic Aromatic Hydrocarbons in the Molecular and Solid Phases

Settore/i scientifico disciplinari di afferenza

FIS 03 / Fisica della Materia

Presentata da: *Roberto Cardia*

Coordinatore Dottorato *Prof. Alessandro De Falco*
Prof. Paolo Ruggerone

Tutor *Prof. Giancarlo Cappellini*
Dott. Giuliano Malloci.

Esame finale anno accademico 2014 – 2015

UNIONE EUROPEA
Fondo sociale europeo

REGIONE AUTONOMA DELLA SARDEGNA

POR SARDEGNA

COMPUTATIONAL INVESTIGATION ON POLYCYCL IC AROMATIC HYDROCARBONS IN THE MOLECULAR AND SOLID PHASES

Effects of functionalization on morphology, electronic excitations, optical and transport properties

Roberto Cardia

Università degli Studi di Cagliari

Facoltà di Scienze

Dipartimento di Fisica

Relatori: *Prof. Giancarlo Cappellini*
Dott. Giuliano Malloci

Coordinatori: *Prof. Alessandro De Falco*
Prof. Paolo Ruggerone

COMPUTATIONAL INVESTIGATION ON POLYCYCLIC AROMATIC HYDROCARBONS IN THE MOLECULAR AND SOLID PHASES

Effects of functionalization on morphology, electronic excitations, optical and transport properties

ROBERTO CARDIA

Università degli Studi di Cagliari
Facoltà di Scienze
Dipartimento di Fisica

Relatori:
Prof. Giancarlo Cappellini
Dott. Giuliano Malloci

Coordinatori:
Prof. Paolo Ruggerone
Prof Alessandro De Falco

Roberto Cardia: *Computational investigation on polycyclic aromatic hydrocarbons in the molecular and solid phases,* Effects of functionalization on morphology, electronic excitations, optical and transport properties, © April 2016

ABSTRACT

In this Thesis we discuss the effects of specific chemical functionalization and partial/complete atomic substitution on the electronic (ground-/excited-state) and charge-transport properties of small organic compounds of interest for molecular electronics.

In particular, we considered several Polycyclic Aromatic Hydrocarbons (PAHs) with different morphologies (small-compact, compact, angular and linear). For these molecules we study the effects of complete substitution of the peripheral H atoms with halogens (F and CL), the functionalization with Triisopropylsilylethynil (TIPS) group, and the partial substitution with chalcogen (S in particular) atoms on several physical properties.

In the first part of this work we report a systematic comparative study on dibenzo[b,def]chrysene (angular) and dibenzo[def,mno]chrysene (compact) polyaromatic hydrocarbons and their bis-triisopropylsilylethynyl (TIPS)-functionalized and perhalogenated (F, Cl) counterparts.

We used all-electrons density functional theory (DFT) and time-dependent DFT (TDDFT) to quantify the effects of morphology and chemical modifications on different physical observables, namely electron affinity, ionization energy, quasi-particle energy gap, optical absorption, exciton binding energy, and molecular reorganization energies for holes and electrons. For this part of the work we used the hybrid exchange-correlation functional B3LYP in conjunction with a gaussian localised basis-set. This adopted combination functional/basis-set has proven to yield good results for polyaromatic hydrocarbons and derivatives.

In the second part of the work we used the same theoretical framework (DFT and TDDFT), to study the electronic, optical, and charge-transport properties of the hexathiapentacene (HTP) molecule. HTP is a derivative of pentacene (PNT) obtained by symmetric substitution of the six central H with S atoms. We discuss in a comparative way the key molecular properties of HTP and PNT. In particular, electron affinities, ionization energies, quasi-particle energy-gaps, optical absorption spectra, exciton binding energies, and reorganization energies for holes and electrons are calculated for the molecules and compared with the corresponding results for PNT, as well as with the available experimental data. The DFT and TDDFT results are also validated by performing many-body perturbation

theory calculations within the GW and Bethe-Salpeter equation formalisms.

In addition, for the crystal structures of PNT and HTP we perfomed DFT-based calculations using a pseudopotentials+plane-waves formalism and adopting the PBE exchange-correlation functional empirically corrected in order to take properly into account dispersive interactions.

The electronic excitations are also obtained within a perturbative B3LYP scheme. A comparative analysis is carried out between the ground-state and excited-state properties of crystalline HTP and PNT linking to the findings obtained for the isolated molecules.

In the last part of this Thesis we investigate the charge-transport properties of different PAHs covering an ample range of structures within catacondensed and pericondensed species. In particular, we considered some linear molecules (anthracene, tetracene, pentacene), some compact molecules (pyrene, and dibenzocrhysene in the angular and compact form) and some ultracompact ones (circumnaphthalene, circumanthracene, circumtetracene). We quantified the effect of complete substitution of the peripheral H with F atoms on the charge-transport properties for both holes and electrons.

To this aim we first derived the key molecular parameters for charge transport (reorganization energy and transfer integral) using all-atoms B3LYP calculations for both unsubstitued and perfluorated species. We then used the above parameters to estimate charge-hopping rates and relative mobilities (with respect to those of pure pentacene which is here considered as a benchmark system for charge-transport) in the high temperatures regime within semi-empirical Marcus theory.

Overall, the results obtained in this Thesis can be summarized as follows:

- Halogenation and TIPS functionalization are an effective way to increase the UV-visible absorption of organic compounds of interest for molecular electronics.
- Following TIPS functionalization and halogen substitution the optical and the quasi-particle energy-gaps appear to be reduced with respect to those of the pure molecules. On the contrary, electron affinities are found to increase, in some cases in a dramatic way (nearly tripled).
- On the other hand, the same chemical modifications on the other hand appear to be detrimental for charge transport in almost all cases considered. A notable exception is represented

by the largest systems investigated, suggesting that molecules with large conjugated cores may show good transport properties even after a complete halogenation.

In conclusion, using state-of-the-art computational techniques, this Thesis presents original results on key molecular properties of different polyaromatic hydrocarbons. We performed a systematic comparative investigation to quantitatively evaluate the effects of different chemical modifications (addition of functional groups or atomic substitution) on the electronic, optical, and charge-transport properties of different materials which are the building blocks of materials widely employed in molecular electronics. Our findings can be possibly used to select tailored chemical modifications to specific compounds for future electronic and optical applications.

PUBLISHED AND SUBMITTED WORKS

PUBLICATIONS

The results of this Thesis have been published in the following three papers:

[1] **R. Cardia**, G. Malloci, A. Mattoni, G. Cappellini, "Effects of TIPS-Functionalization and Perhalogenation on the Electronic, Optical, and Transport Properties of Angular and Compact Dibenzochrysene", *J. Phys. Chem. A* **118**, 5170-5177 (2014)

Submitted Works

[1] **R. Cardia**, G. Malloci, G-M. Rignanese, X. Blase, G. Cappellini, "Electronic, optical, and transport properties of hexathiapentacene in the molecular and crystal structures", **SUBMITTED–**,– (2015)

Works in Preparation

[1] **R. Cardia**, G. Malloci, A. Bosin, G. Serra, G. Cappellini, "Effects of perfluorination on charge-transport properties of molecular materials for organic electronics: the case of PAHs", **in PREPARATION–**,– (2016)

Other publications

[1] **R. Cardia**, C. Melis, L. Colombo, "Neutral-Cluster Implantation in Polymers by Computer Experiments", *J. App. Phys.***113**, 2243070-2243079 (2013)

WORKSHOP, CONGRESSES AND SEMINARS

Posters

1. (**Poster**) E. Molteni, G. Onida, **R. Cardia**, G. Cappellini. "Thymine adsorbed on the Silicon(001) surface: atomic and electronic properties" - Presented at: *7th SCHOOL ON ORGANIC ELECTRONICS: from Semiconductor to Biomolecular*

Interfaces - Como, Italy 14-18/09/15. [Presenting Author E. Molteni]

2. (**Poster**) G. Cappellini, **R. Cardia**, G. Malloci "Computational investigation on the effect of halogen substitution on the electronic, optical, and transport properties of guanine" - Presented at: Ψ_K *2015 Conference - San Sebastian, Spain 06-10/09/15*

3. (**Poster**) G. Cappellini, **R. Cardia**, G. Malloci "Computational investigation on the electronic, optical and transport properties of hexathiapentacene in the molecular and solid phases" - Presented at: *Workshop on Computer Simulations for condensed phase systems: from correlated electrons to novel materials - Rome (CNR Headquarters), Italy 04-06/05/15*. [Presenting Author G. Cappellini]

4. (**Poster**) G. Cappellini, **R. Cardia**, G.-M. Rignanese "Effects of perfluorination on the electronic, optical, and transport properties of polyaromatic hydrocarbons: pentacene and pyrene in the molecular and solid phase" - Presented at: *DPG Conference - Berlin, Germany 14-20/03/15*. [Presenting Author G. Cappellini]

5. (**Poster**) **R. Cardia**, G. Malloci, G. Cappellini "Electronic Optical and Transport Properties of Hexathiapentacene within (TD)DFT schemes" - Presented at: *19th ETSF Workshop on Electronic Excitations - Complex systems in Biology and Nanoscience - Saragoza, Spain 22-26/09/14*. [Presenting Author G. Cappellini]

6. (**Poster**) **R. Cardia**, G. Malloci, A. Mattoni, G. Cappellini "The Role Functionalizations on the Electronic and Optical Properties of Angular and Compact Dibenzochrysene" - Prsented at: *2nd SINFO Workshop on Surfaces, Interfaces and Functionalization Processes in Organic Compounds and Applications - Trieste, Italy 25-27/06/2014*

7. (**Poster**) **R. Cardia**, G. Malloci, G. Cappellini "Electronic excitations and optical properties of angular and compact dibenzochrysene and their derivatives" - Presented at: *19th ETSF Workshop on Electronic Excitations - Applications to functional and energy materials - Luxembourg 1-4/10/2013*. [Presenting Author G. Cappellini]

Conferences

1. (**Conference Oral Contribution (Talk)**) **R. Cardia**, G. Malloci, G. Cappellini "Effects of substitution and functionalization on the electronic, optical, and transport properties of polycyclic aromatic hydrocarbons" - Presented at: Ψ_K *2015 Conference - San Sebastian, Spain 06-10/09/15*

2. (**Conference Oral Contribution (Talk)**) **R. Cardia**, G. Malloci, A. Mattoni, G. Cappellini "Angular and Compact Dibenzochrysene: the Role of Functionalizations on their Electronic and Optical Properties" - Presented at: *European Theoretical Spectroscopy Facility Young Researchers' Meeting - Rome, Italy 12-16/05/14*

3. (**Conference Oral Contribution (Talk)**) "Optical and electronic properties of functionalized polyaromatic hydrocarbons: a computational investigation on perfluorinated circumacenes" - **SUBMITTED TO**: *SPIE Photonics Europe - Bruxelles, Belgium 04-07/04/16*

Seminars

1. (**Seminar Contribution**) G. Cappellini, **R. Cardia**, G. Malloci "Electronic, optical and transport properties of PAHs in the molecular and solid phases: the role of functionalizations" - Presented at: *Istituto Tecnologico de Areonautica di Sao José dos Campos, - Sao Paolo, Brasil 07/10/15*. [Presenting Author G. Cappellini]

2. (**Seminar Contribution**) **R. Cardia**, G. Malloci, G. Cappellini "Role of functionalizations on the electronic, optical and transport properties of PAHs: from molecules to solids" - Presented at: *IFTO-FSU - Jena, Germany 22/07/15*. [Presenting Author G. Cappellini]

COMPUTATIONAL RESEARCH PROJECTS

- "Electronic and optical properties of functionalized dibenzochrysene", **ISCRA C** Class Project; ID: HaloTips - HP10C3IPM4, *29/07/2013 - 29/04/2014*

- "PAHs molecules in the gas and in the solid phase: electronic and optical properties", **ISCRA C** Class Project; ID: PAHMOS - HP10CM9ZL2, *10/04/2014-10/01/2015*

ACKNOWLEDGMENTS

First of all I would like to thank my supervisors Prof. Giancarlo Cappellini and Dr. Giuliano Malloci for their continuous support and motivation. Your guidance and scientific collaboration have been crucial for improving my scientific skills. My PhD experience would not have been as pleasant as it has been without their supervision, patience and help.

My gratitude also goes to Dr. Claudio Melis for having invested a great amount of their time in helping and teaching me many things on computational physics in the first stages of my PhD.

I would like to thank Prof. Gian-Marco Rignanese of the Université Catholique de Louvain, in Louvain-la-neuve (Belgium), for providing me the opportunity to work in a foreign research environment, as well as the opportunity to start a collaboration with his group.

I would also like to thank Dr. Andrea Bosin and Dr. Giovanni Serra for their fundamental technical support.

Non posso poi non ringraziare i miei compagni di avventura del XXVIII ciclo di dottorato: Tommaso, Giuliana, Roberto, Barbara e Laura oltre naturalmente a Claudia, Silvia e tutti gli altri compagni di common room.

Ovviamente il Grazie più grande va ai miei genitori, mia sorella Daniela (con Cristian) e zia Maria e a tutti coloro che hanno avuto la sventura di dovermi sopportare durante questi tre anni di dottorato, Grazie davvero... anche perché so di essere insopportabile quando mi ci metto.

Ringrazio infine tutti gli amici che mi sono stati vicino in questi anni, quelli che avevo quando ho iniziato e che sono rimasti e i nuovi che sono arrivati nel frattempo; in ordine sparso: Dema, Mauri, Sara, Alessandro, Marianna, Melania, Elide, Lucia (da quel di Palermo) e Fabio.

Se alla fine sono riuscito a raggiungere questo traguardo lo devo anche un po' a tutti voi...

La presente tesi è stata prodotta durante la frequenza del corso di dottorato in Fisica dell'Università degli Studi di Cagliari, a.a. 2013/2015 - XXVIII ciclo, con il supporto di una borsa di studio finanziata con le risorse del P.O.R. SARDEGNA F.S.E. 2007-2013 - Obiettivo competitività regionale e occupazione, Asse IV Capitale umano, Linea di Attività l.3.1 "Finanziamento di corsi di dottorato finalizzati alla formazione di capitale umano altamente specializzato, in particolare per i settori dell'ICT, delle nanotecnologie e delle biotecnologie, dell'energia e dello sviluppo sostenibile, dell'agroalimentare e dei materiali tradizionali".

Roberto Cardia gratefully acknowledges Sardinia Regional Government for the financial support of her PhD scholarship (P.O.R. Sardegna F.S.E. Operational Programme of the Autonomous Region of Sardinia, European Social Fund 2007-2013 - Axis IV Human Resources, Objective l.3, Line of Activity l.3.1.)

CONTENTS

ACRONYMS

MO Molecular Orbital

HOMO Highest Occupied Molecular Orbital

LUMO Lowest Unoccupied Molecular Orbital

LED Light Emitting Diode

OFET Organic Field Effect Transistor

OTFT Organic Thin Film Transistor

OLED Organic Light Emitting Diode

OPV Organic Photovoltaic

IE Ionization Energy

EA Electron Affinity

UV ultra-violet

PAH Polycyclic Aromatic Hydrocarbon

TIPS Tri-Isopropylsilylethynyl

DFT Density Functional Theory

QP Quasi-Particle

TDDFT Time-Dependent DFT

MBPT Many Body Perturbation Theory

VdW Van der Waals

BSE Bethe-Salpeter Equation

PNT Pentacene

PFP Perfluoro-Pentacene

HTP Hexa-Thia Pentacene

PYR Pyrene

ANT Anthanthrene

DBC Dibenzochrysene

PF-PYR Perfluoro-Pyrene

PF-ANT Perfluoro-Anthanthrene

PF-DBC Perfluoro-Dibenzochrysene

Part I

SCIENTIFIC CONTEXT AND THEORETICAL FRAMEWORK

1 INTRODUCTION

Contents

1.1 TECHNOLOGICAL BACKGROUND - ORGANIC SEMICONDUCTORS

In the last decades inorganic silicon and gallium arsenide semiconductors, silicon dioxide insulators, and metals such as aluminium and copper have been the backbone of the electronic industry. Since the beginning of the twenty-first century, we are facing a new electronics revolution that has become possible due to the development and understanding of a new class of materials, commonly known as *Organic Semiconductors*. Organic semiconductors are a large family of materials that combine the electronic behavior of semiconducting systems with the chemical and mechanical advantages of organic compounds such as plastics. Thus, the ability to absorb light, conduct electricity, and emit light is combined with a material structure that can easily be modified by chemical synthesis, for example, to design electronic properties such as the desired emission wavelength, to make it soluble, or to allow for mechanically robust, lightweight, and flexible thin films. These characteristics imply that semiconductor applications such as displays, lighting panels, or solar cells may be produced with a variety of solution-processing techniques or vacuum deposition methods. Organic semiconductors are not new. The first studies of the dark and photoconductivity of anthracene crystals (a prototype organic semiconductor) date back to the early twentieth century[2] and, more widely, have been studied since the 1950s.[3] The field of organic semiconductors was influenced greatly by the discovery in the late 1970s that high conductivities could be obtained in π-conjugated polymers, that is, hy-

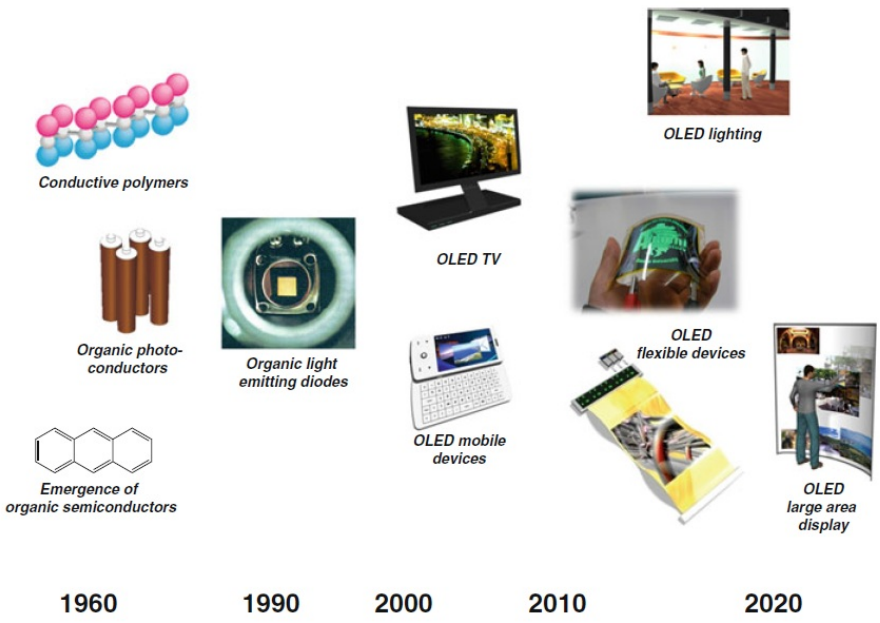

Figure 1: History of research and development of organic semiconductors. Figure taken from [1].

drocarbon chains with alternating single and double bonds, when they are doped. The discovery and development of these conductive polymers was rewarded in 2000 with the Nobel Prize in Chemistry to Heeger, MacDiarmid, and Shirakawa.[4,5]. As an example, the electronic conductivity of these materials lies between that of metals and insulators spanning a broad range between $10^{-6} \div 10^{3}$ $\Omega^{-1}\text{cm}^{-1}$ [6].

It is useful to distinguish between the following three families of organic semiconductors:

1. **Amorphous molecular films:** These are systems made by organic molecules deposited as an amorphous film through evaporation or spin-coating. Thin amorphous films of molecules are employed for device applications such as Light Emitting Diodes (LEDs), and molecularly doped polymer films are used on a large technological scale in xerography.

2. **Molecular crystals:** A crystal consists of a lattice and a basis. In the same way how atoms like silicon can form a crystal by covalent bonding, or sodium and chlorine atoms by ionic bonding, molecules such as anthracene and pentacene can form the basis of a crystal that is held together by Van der Waals (VdW) interactions. The charge mobilities that can be obtained in molecular crystals are high compared to those

in noncrystalline organic materials. This makes them relevant for transistor applications.

3. **Polymer films:** Polymers may be considered a chain of covalently coupled molecular repeated units. Frequently, they are processed from solution, which allows for a range of deposition techniques including simple spin-coating, ink-jet deposition, or industrial reel-to-reel coating. They are more suitable to blending than molecules since polymer blends are thermodynamically more stable and less susceptible to crystallization.

In the present work we study the properties of isolated molecules and of systems belonging to the above second family.

1.2 ORIGIN OF THE ELECTRONIC STRUCTURE IN ORGANIC SEMICONDUCTORS

Organic semiconductors have very different electrical properties when compared to traditional inorganic semiconductors. This section presents a rapid introduction of the electronic structure and charge carrier behavior of an organic semiconductor and an overview on excitons (bound electron-hole pairs), which are coupled optical and electronic processes. Consequently, optoelectronic devices based on organic semiconductors have different operation principles and design requirements compared to those based on traditional inorganic materials. An understanding of organic charge transport and exciton formation is therefore crucial in effective device design and optimization.

All organic semiconducting materials, whether they are small molecules, polymers, or more complex structures, rely on conjugated π-electron systems for conduction. Systems are considered π-conjugated when alternating carbon-containing single and double bonds are present in their molecular structure.

Each carbon atom, considering for example C_2H_4 (see Fig. 2), is sp^2 hybridized, with three sp^2 orbitals created per atom and one leftover unhybridized p_z orbital. The six sp^2 orbitals result in five strong σ-bonds within the system (four C-H bonds and one C-C), with the p_z orbitals around each carbon atom forming a C-C π-bond. Due to the shape of the p_z orbitals, the C-C π-bond has weak interaction due to small electron cloud overlap above and below the molecular plane. The strength of the overlapping σ-bonds leads to strong bonding (σ) and antibonding ($\sigma^\star$) Molecular Orbitals (MOs). The weaker interactions of the parallel p_z orbitals give correspondingly weaker

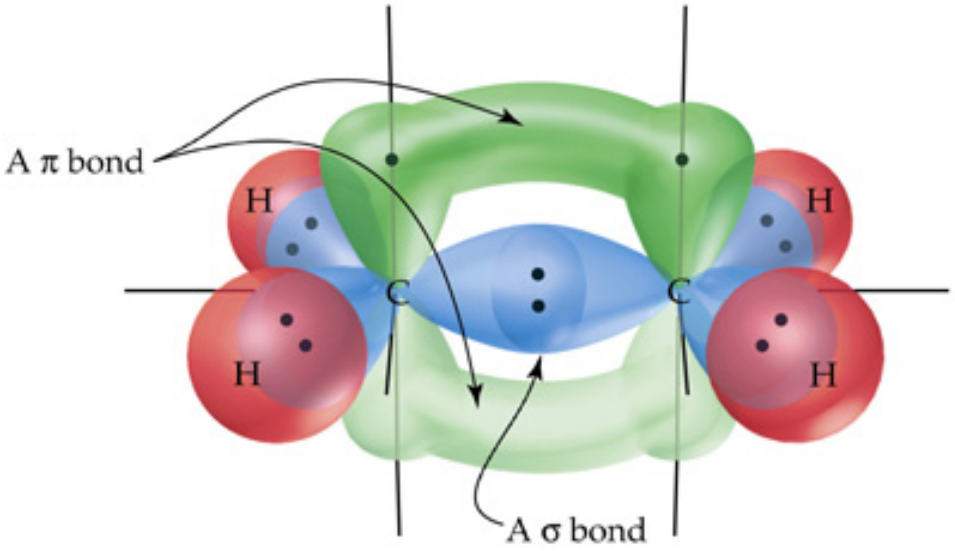

Figure 2: Schematic representation of σ and π bonds in ethylene.

bonding (π) and antibonding ($\pi^\star$) MO energy levels, making the π-$\pi^\star$ transition the smallest possible electronic excitation within the molecule. Because of the importance of the π-$\pi^\star$ transition as the lowest-energy option in a π-conjugated system, the π-bonding MO is called Highest Occupied Molecular Orbital (HOMO) and the $\pi^\star$-antibonding MO is named the Lowest Unoccupied Molecular Orbital (LUMO). The HOMO and LUMO, respectively, are analogous to the valence and conduction bands in inorganic semiconducting materials (see Fig. 3).

Holes and electrons in π-orbitals are the typical charge carriers in organic semiconductors. Charge transport typically depends on the ability of the charge carriers to move from one molecule to another, which depends on the energy gap between HOMO and LUMO levels.

The degree of π-conjugation within an organic solid has a large impact on its electrical properties. Increased conjugation length causes a greater degree of electron delocalization, increasing the mobility of charges through the π-bonding system. Similarly, short conjugation length localizes electrons, reducing their ability to freely move within a system. This is reflected in the polyacenes, conjugated systems of conjoined benzene rings. Increased conjugation (more conjoined benzene rings) corresponds with red-shifted absorption spectra caused by decreasing HOMO-LUMO separation. For example, the absorption maximum of benzene occurs at 255 nm; the increased conjugation in pentacene shifts its absorption maximum to 580 nm.[8] This illustrates the great advantage of organic

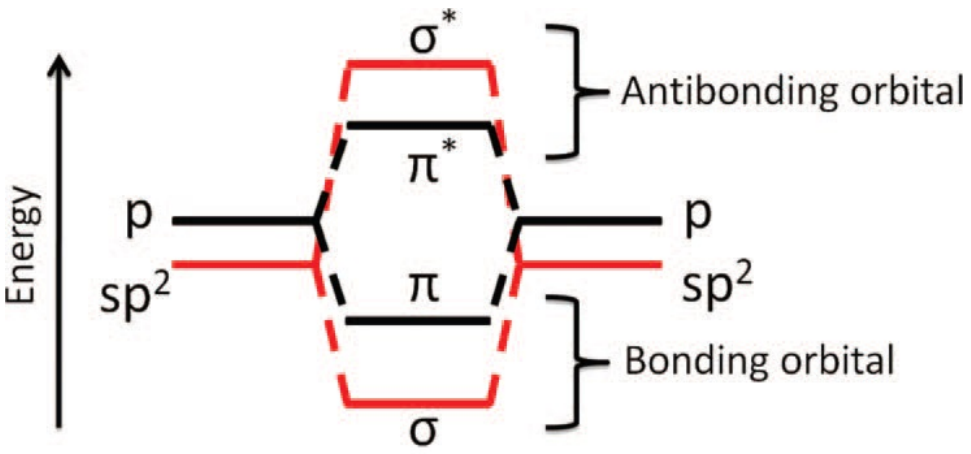

Figure 3: Schematic energy level diagram of a discrete organic molecule. The electronic band gap (HOMO-LUMO) is taken as the π-$\pi^{\star}$ gap. Figure taken from [7].

semiconductors: *simple changes to a base molecule can alter its electronic transport and optical properties*.

1.3 CHARGE TRANSPORT PROPERTIES

Charge transport within organic-based materials is a combination of two processes: intramolecular carrier movement and intermolecular charge transfer. Within a molecule, π-conjugation enables charge carriers to move freely. In organic materials, transport is limited by the weak VdW intermolecular coupling, drastically lowering charge carrier mobility to typical values of $10^{-5} \div 10^{2}$ $cm^2V^{-1}s^{-1}$ within the photovoltaic materials of interest.[9–11] This weak coupling causes a strong localization of charge carriers on individual molecules and this fact prevents continuous band transport. As a matter of fact the intermolecular transport typically occurs through a hopping process as a charge carrier overcomes an energy barrier to move from one molecule to the next. The mobility in this situation is dependent on the energy barrier height, electric field, and temperature. The situation can change substantially based on the degree of interaction between adjacent molecules. In these compounds the interaction is dominated by the Van der Waals interaction force. This can be modelled by a *Lennard-Jones potential*. Small deviations in the intermolecular distance r can have large effects on the degree of interaction within the solid, increasing coupling between molecules, decreasing charge carrier localization, and lowering the energy barrier for hopping transport. In a highly-ordered molecular crystal charge carriers are sufficiently delocalized that band transport is re-

alized, much like in inorganic semiconductors. Charge mobility in highly pure crystals of 5,6,11,12-tetraphenylnaphthacene (rubrene) has reached values of 40 $cm^2V^{-1}s^{-1}$.[12–15]

1.4 EXCITONS

Bound electron-hole pairs, or excitons, are crucial to the operation of optoelectronic organic devices, including Organic Photovoltaics (OPVs) and organic Organic Light Emitting Diodes (OLEDs).[8,16] In OPVs, excitons are the by product of photon absorption, where an electron is excited to the LUMO level of the molecule and coulombically binds with the hole left behind in the HOMO to slightly lower the total system energy. The exciton must then be broken back into free charge carriers (dissociated) to extract power from the device. In OLEDs, the injected charge carriers form excitons in an emissive layer, which then recombine to emit a photon. In either case, an electron and hole are separated by a distance r_c based on the Coulomb attraction force and dielectric constant of the material.

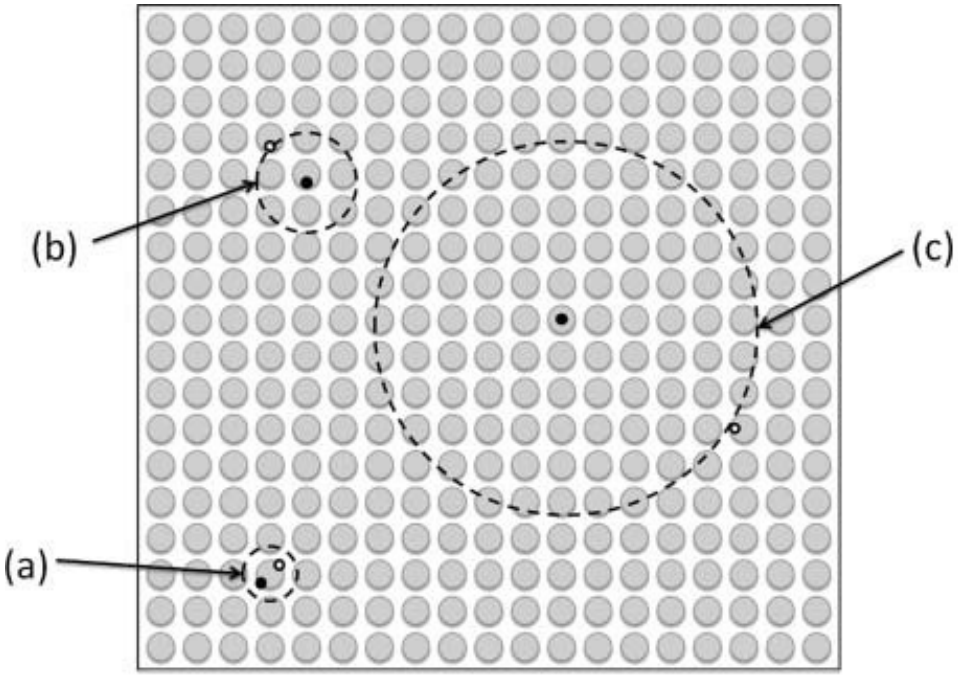

Figure 4: Schematic representation of different classes of excitons: (a) Frenkel (b) charge-transfer exciton and (c) Wannier-Mott, with varying degrees of delocalization indicated. Figure taken from [7]

There are three types of excitons that have been observed: *Frenkel*, charge-transfer excitons (CT), and *Wannier-Mott* (Fig. 4). Frenkel excitons are formed with the electron-hole binding distance smaller

than a single molecule or (in the case of inorganics) the lattice constant of the crystallographic unit cell. CT excitons occur when the bound carriers are delocalized over adjacent molecules. The third class, Wannier-Mott excitons, are found in inorganic semiconductors, where the large dielectric constant screens the coulombian attraction of the electron and hole and allows them to delocalize over a long distance. Binding energies of Frenkel and CT excitons are greater than 0.1 eV; Wannier-Mott binding energies are only a few meV. At room temperatures, Wannier-Mott excitons are dissociated by thermal energy; consequently, inorganic photovoltaics are not considered "excitonic" as any excitons formed upon photon absorption are immediately dissociated into free charge carriers. Bound excitons can move throughout a solid like other fundamental particles. Because excitons are charge neutral, applied electric fields do not control their motion.

Much as is the case with charge carrier transport, the weak intermolecular interactions in organic solids limit exciton mobilities and diffusion lengths; most excitons in organic solids can diffuse on the order of 10 nm prior to recombination,[17–19] though micrometer diffusion lengths have been observed in highly pure rubrene crystals.[20]

The large binding energy of Frenkel and charge transfer excitons does not lend itself to easy dissociation. Thermal dissociation is not practical due to the low decomposition temperatures of organic materials. Excitons can be dissociated by application of an electric field, but the field strength must be in the range of 10^5 to 10^6 V/m to have an appreciable rate of exciton dissociation.[21] The preferred route to induce exciton dissociation is the introduction of a heterojunction between organic materials with differing electron affinities and ionization potentials. When an exciton encounters such an interface, could be energetically favorable for that exciton to dissociate back into free charge carriers.

Considering σ- and π-bonds, the effect of the delocalized π-electrons most obviously appears in the color of the organic systems. The usual organic or plastic materials that are formed only by the σ-bonds do not have colors or are transparent. This is because the σ-bonds are so strong that the electronic excitation energy becomes high and the optical gap energy is much larger than the visible photon energy range. In contrast, when the π-electrons are delocalized over the molecule, the electronic excitation energy considerably decreases, and the materials become colored. Figure 5 presents the optical gap energies of polyacenes (and polyenes), plotted as a function of the number of fused benzene rings and double bonds.

When the molecules become larger and the delocalized π-electrons are more extended, the excitation energy becomes considerably lowered and becomes colored due to the absorption of visible light. In both the polyenes and polyacenes, each carbon has one π-electron along the alternating sequence of single and double bonds in the chemical notation. Actually, however, these π-electrons do not belong to each double bond but rather to a group of atoms along the alternating sequence of single and double bonds. The sequence is often called as conjugated double bonds, which allow a delocalization of π-electrons across all the adjacent aligned p-orbitals.

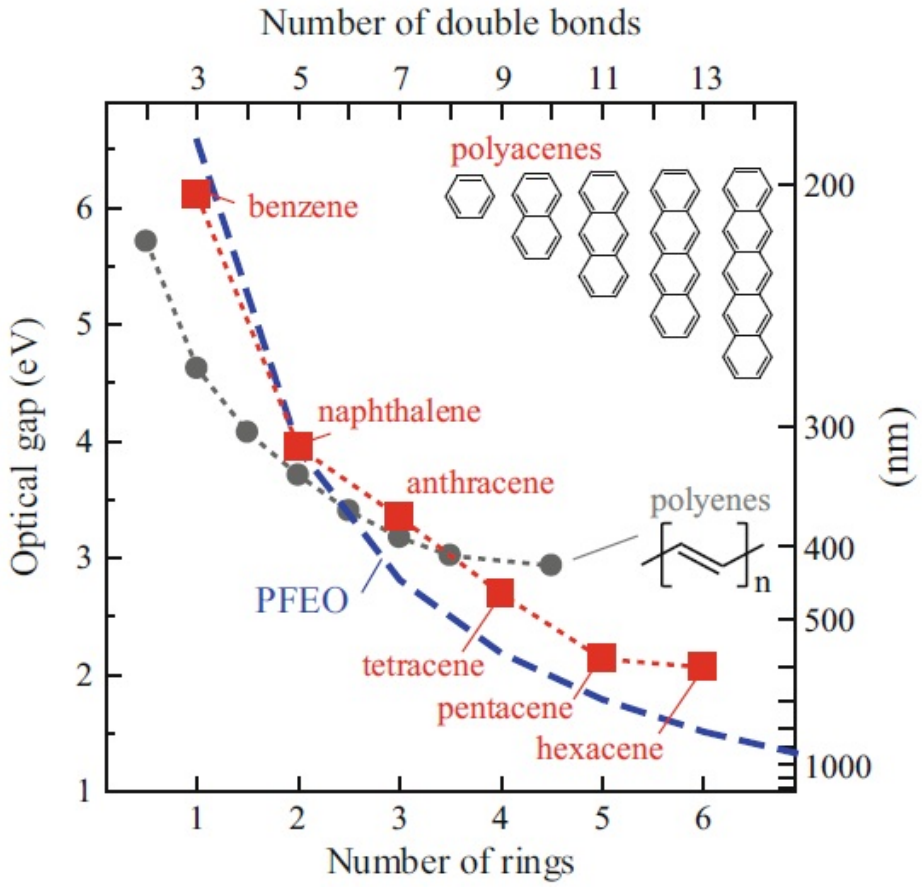

Figure 5: Optical gap energy of polyacenes as a function of number of fused rings or double bonds (red squares); Optical gap energy in polyenes as a function of double bonds (gray circles). Figure taken from [1].

Organic semiconductors are either based on oligomers such as pentacene, anthracene, rubrene, or oligothiophenes, or on polymers such as polypyrrole, polyacetylene, poly(3-hexylthiophene) (P3HT), or poly(p-phenylene vinylene) (PPV). In particular organic semiconductors based on small molecules as polycyclic aromatic hydrocar-

bons (Polycyclic Aromatic Hydrocarbons (PAHs)) are being widely used as active elements in different optoelectronic devices such as Organic Field Effect Transistors (OFETs), OLEDs, and organic photovoltaic (OPV) cells[22]. Linear acenes and heteroacenes, in particular, are p-type semiconductors with good transport properties and are used as hole-transporters in some of the best performing OFETs[23–25]. As compared to polymers, small molecules offer several advantages, such as the possibility to be easily purified by varied techniques and tractable by both evaporation and solution processing methods[23,26]. In addition, their electronic, optical, and transport properties can be tuned via chemical modification or addition of functional groups to the conjugate core[25,27–31].

For example, the modification with strong electronegative substituents is an effective approach for converting p-type organic semiconductors to n-type[25,32]. To produce bipolar transistors, in fact, it would be ideal to have both n-type and p-type organic semiconductors with similar physical and electrical properties[33,34]. In the case of PAHs, however, despite the successes with hole transport, it has turned out to be more difficult to achieve n-type transport (e.g., pentacene OFETs exhibit hole mobilities up to 5 $cm^2/(V \cdot s)$[23] and electron mobilities of 0.04 $cm^2/(V \cdot s)$[33]). Typically, n-type materials based on PAHs are obtained by attaching strong electron-withdrawing groups such as CN[35] to the conjugated core, or by replacing the peripheral hydrogens with halogen atoms (in particular F and Cl)[34,36]. The decreased lowest unoccupied molecular orbital allows electron injection by lowering the charge injection barrier.

Besides the intrinsic semiconductor charge mobility, the device performances strongly depend on crystal structure and thin-film morphology. Supramolecular issues have been therefore extensively addressed in the literature from both the experimental and theoretical points of views, especially for non-functionalized and functionalized linear acenes[37–42]. In particular, the formation of package structures with a high degree of π-overlap is believed to facilitate charge migration[43]. The face-to-face π-stacking motif is thus more efficient for charge transport than the edge-to-face herringbone-packing structures typical of organic semiconductors such as pentacene, rubrene etc.[23,43]. Several studies have shown that the face-to-face π stacking is more common with molecules that possess a two-dimensional extended aromatic system and is rarely observed for linear molecules such as oligoacenes[44]. For PAHs with large conjugated cores, in particular, self-assembly via strong π-π interactions has been demonstated to result in the formation of one-

dimensional nanostructures[45,46], making them promising materials for a multitude of electronic applications[44].

It is known that the tendency to form face-to-face stacked structures can be enhanced by adding peripheral substituents[23,47]. In the field of photovoltaics, in particular, the increased orbital overlap has been shown to be favorable for high efficiency solar cells[48]. For example, the triisopropylsilylethynyl (TIPS) functionalization[23,28] of two nonlinear PAHs, dibenzo[b,def]chrysene and dibenzo[def,mno]chrysene, has been recently found to deliver high power-conversion efficiencies in bulk heterojunction solar cells[26,49,50]. TIPS-functionalization is of particular interest since it changes both the intramolecular electronic structure and intermolecular electronic interactions, thus leading to different ionization energies, electronic energy gaps, and charge injection barriers[30,51]. The unique packing motifs due to TIPS-functionalization[52], in addition, make the precursor solution processable[23,24]. In the case of pentacene, for example, compatibility with relatively low-cost solvent-based processing techniques (e.g., spin coating) as well as printing technologies such as ink-jet printing, has been demonstrated under full-scale production conditions[23,24].

1.5 AIM OF THIS THESIS

The aim of the present Thesis is to study the effects of substitutions and functionalizations, by addition of specific chemical and functional groups, on the electronic, optical and charge transport properties of finite and bulk systems based on specific Polycyclic Aromatic Hydrocarbons (PAHs.) In particular, we have chosen Pentacene (PNT) as a prototype of linear acenes used in organic electronics, *dibenzo[b,def]chrysene* and *dibenzo[def,mno]chrysene* (the former sometimes called simply Dibenzochrysene (DBC) and the latter Anthanthrene (ANT)), as important examples of PAHs used in organic electronics but with different morphology respect to the more usual linear acenes (the first has an angular-shape and the second a compact-shape).

For this purpose we use a set of theoretical and numerical tools based on Density Functional Theory (DFT), Time-Dependent DFT (TDDFT) and Many Body Perturbation Theory (MBPT).

More specifically we wanted to address the following points:

- **Molecular Electronic Properties**:

  Study the effects of perhalogenation (i. e.complete substitution of H with F or Cl) on the Ionization Energy (IE), Electron

Affinity (EA), Quasi-Particle gap (QP_{Gap}) in the case of angular and compact dibenzochrysenes.

Investigation, for the same molecules and the same observables, of the effects of functionalization by addition of Tri-Isopropylsilylethynyl (TIPS) groups.

Study of the differences in terms of IE, EA and QP_{Gap} between pentacene PNT and Hexa-Thia Pentacene (HTP) molecules. HTP is a pentacene derived molecule, obtained by substitution of 6 hydrogens with 6 sulfur (S) atoms.

- **Solid State Electronic Properties**

  Study of the differences in terms of ground-state properties and electronic excitations between pentacene PNT and HTP crystalline molecular solids.

- **Molecular Optical Properties**:

  Calculation of the optical absorption spectra for compact and angular DBC, for PNT and for all substituted and functionalized molecules up to the near UV.

  Prediction of the *optical gap* (E_{opt}) and *exciton binding energy* (E_{Bind}) for all compounds under study.

- **Charge Transport Properties**:

  Computation of molecular reorganization energies for all compounds here considered and comparison of these parameters between pure and derivated molecules.

  Prediction of the transfer integral values in the case of unsubstituted and perfluorinated PNT, DBC,ANT and Pyrene (PYR). Study of the charge hopping rates and mobilities relative to PNT for holes and electrons as a function of the temperature.

Chapter 2 contains the detailed explanation of the theoretical tools used in all parts of this work. Some secondary details are contained in the first part of each Chapter 3, 4, 5.

The investigation on electronic properties and optical spectra of molecular DBCs are addressed in Chapter 3. The same Chapter reports also the results on transport properties for the same molecules (limited to the molecular reorganization energies).

The study of the molecular electronic and optical properties of HTP and PNT instead, are contained in Chapter 4. In the same chapter are also present the results for the corresponding crystalline molecular solids.

Transport properties have been mainly discussed in Chapter 5

2

THEORETICAL METHODS

Contents

Ab-initio simulations (also called first principles simulations) take their name from the fact that they lie on a physical-mathematical theory, from which the properties of the system are derived without the use of empirical parameters. Nowadays, the density functional theory (DFT) is probably the most convenient theory to perform atomistic ab-initio simulations, due to the advantageous scalability of the computational time with the number of electrons of the system[53]. The DFT is able to give a reliable prediction of the ground state properties of a large class of materials. Time-dependent density functional theory (TDDFT) extends the DFT to the study of excited states of the system and the associated observables.[54] This chapter reports an overview of the theoretical methods adopted in the present Thesis.

2.1 INTRODUCTION

In classical physics, the time evolution of bodies positions and velocities are uniquely determined by Newton or more generally by Lagrange or Hamilton equations. In Quantum Mechanics, (QM) particle trajectories have to be forgotten and the time evolution of the system is described by a mathematical tool called wavefunction $\Psi(\mathbf{r},t)$ which characterize the state of the system.

The time evolution of $\Psi(\mathbf{r},t)$ for a single particle can be found solving the *time-dependent* Schrödinger equation:

$$i\hbar\frac{\partial}{\partial t}\Psi(\mathbf{r},t) = -\frac{\hbar^2}{2m}\nabla^2\Psi(\mathbf{r},t) + V(\mathbf{r},t)\Psi(\mathbf{r},t) = \mathbf{H}(\mathbf{r},t)\Psi(\mathbf{r},t) \quad (1)$$

where $\hbar$ is the reduced Planck constant and $V(\mathbf{r},t)$ the potential depending on the position of the particle and the time. The sum of the last two terms represents the time-dependent *Hamiltonian* of the system $\mathbf{H}(\mathbf{r},t)$.

The resolution of the Schrödinger equation allows accessing to the electronic properties of atoms and molecules from first principles. Generally, the phenomena studied in molecular physics and quantum chemistry are stationary so that the potential does not depend on the time parameter but only on the position of the particles. The Eq. 1 then reduces to the *time-independent* equation written for a molecular system:

$$\mathbf{H}\Psi(\bar{R},t) = E_{tot}\Psi(\bar{R},t) \quad (2)$$

where $\Psi(\bar{R},t)$ is the *total wavefunction* of the molecular system that depends on both $\mathbf{r}$ and $\mathbf{R}$ ($\bar{R} = [\mathbf{r},\mathbf{R}]$) which are respectively the electron and the nuclei spatial coordinates, E_{tot} is the *total energy* of the system and $\mathbf{H}$ the *total Hamiltonian* of the molecular system containing M nuclei and N electrons. The total hamiltonian for a multielectronic molecular system can be written as:

$$\begin{aligned}\mathbf{H} &= T_e + T_N + V_{eN} + V_{ee} + V_{NN} \\ &= -\frac{\hbar^2}{2m_e}\sum_{i=1}^{N}\nabla_i^2 + -\hbar^2\sum_{a=1}^{M}\frac{1}{2m_a}\nabla_a^2 \\ &- \frac{1}{4\pi\varepsilon_0}\sum_{i=1}^{N}\sum_{a=1}^{M}\frac{e_i Z_a}{r_{ia}} + \frac{1}{4\pi\varepsilon_0}\sum_{i=1}^{N}\sum_{j>i}^{N}\frac{e_i e_j}{r_{ij}} \\ &+ \frac{1}{4\pi\varepsilon_0}\sum_{A=1}^{N}\sum_{b>a}^{M}\frac{Z_a Z_b}{r_{ab}}\end{aligned} \quad (3)$$

where the *total kinetic energy* is the sum of the electronic (T_e) and nuclear (T_N) kinetic energies, the *total potential energy* is the sum of three components: the attractive interactions between nuclei and electrons (V_{eN}), the repulsive electron-electron interactions (V_{ee}) and the repulsive interactions between the nuclei (V_{NN}). $Z_{a,b}$ are the nucleic charge of atoms A and B, $m_{e,a}$ are the mass of electron and of the atom A, r_{ab} is the distance between nuclei A and B, r_{ia} is the distance between nucleus A and electron i and finally r_{ij} is the distance between electrons i and j.

Please remark that in the previous expressions we omit intentionally to add the spin dependence in the wavefunction since the Hamiltonian operator presented here does not dependent on it.

Analytical solutions of Eq. 2 (with relative expressions of the eigenfunctions and energies) can only be obtained in a few cases; for example:

- Particle in one, two or three dimensional box submitted to a zero potential inside the box and infinite at the boundaries
- Single atom with non interacting electrons
- Hydrogen atom
- Hydrogenoid atomic systems[1]

2.1.1 *Born-Oppenheimer Approximation*

The Schrödinger equation for a multielectronic system is a very difficult problem to solve. The point is to find stationary states of nuclei and electrons in interaction. From the conservation of the momentum and the large difference between the mass between nuclei and electrons (at least, a factor of 1832 between the electron and proton mass), nuclei are expected to be much slower than electrons so that the kinetic energy of the nuclei (T_N) can be neglected. The electrons are then moving in the field created by the fixed nuclei and are supposed to rearrange immediately after any displacement of the atoms. One says that electrons follow adiabatically the movement of the nuclei. This approximation is called the *Born-Oppenheimer approximation* or adiabatic approximation.[55]

The stationary states and eigenvalues of the energy are function of the atomic positions. We can thus define an electronic Hamiltonian

1 Similar class of problems as the hydrogen atom with the same number of electrons but different nuclear charge

which carries a parametric dependence on the nuclear coordinates and depends explicitly on the electron coordinates:

$$\mathbf{H}_{el} = T_e + V_{eN} + V_{ee} \tag{4}$$

the total wavefunction can be factorized as:

$$\Psi(\mathbf{r}, \mathbf{R}) = \sum_i \phi_i(\mathbf{r}, \mathbf{R})\zeta_i(\mathbf{R}) \tag{5}$$

where $\phi_i(\mathbf{r}, \mathbf{R})$ is the electronic wavefunction, $\zeta_i(\mathbf{R})$ is the nuclear wavefunction and the sum goes over all the electronic states..

If we consider the total wavefunction in the form expressed by Eq. 5, the Schrödinger equation can be rewritten as:

$$\mathbf{H}\Psi(\mathbf{r}, \mathbf{R}) = [H_{el}(\mathbf{R}) + T_N + V_{NN}] \sum_i \phi_i(\mathbf{r}, \mathbf{R})\zeta_i(\mathbf{R}) \tag{6}$$

Applying the Born-Oppenheimer approximation, we can neglect the term T_N and the previous equation becomes:

$$\mathbf{H}\Psi(\mathbf{r}, \mathbf{R}) = [\mathbf{H}_{el}(\mathbf{R}) + V_{NN}] \sum_i \phi_i(r, R)\zeta_i(\mathbf{R}) \tag{7}$$

from wich we can obtain a set of equations completely independent by the nuclear wavefunction:

$$\mathbf{H}_{el}\phi(\mathbf{r}, \mathbf{R}) = E_i^{el}(\mathbf{R})\phi_i(\mathbf{r}, \mathbf{R}) \tag{8}$$

where $E_i^{el}(\mathbf{R})$ is the electronic energy for the i-th state. The adiabatic energy E_{ad} (which differs from the total energy by neglecting the nuclear kinetic energy contribution) is obtained as:

$$\sum_i [E_i^{el} + V_{NN}]\phi_i(\mathbf{r}, \mathbf{R})\zeta_i(\mathbf{R}) = E_{\text{ad}} \sum_i \phi_i(\mathbf{r}, \mathbf{R})\zeta_i(\mathbf{R}) \tag{9}$$

If we multiply Eq. 6 by $\phi_j^\star(\mathbf{r}, \mathbf{R})$ and integrate with respect to r we obtain

$$\begin{aligned} \int \phi_j^\star(\mathbf{r}, \mathbf{R})\mathbf{H}\Psi(\mathbf{r}, \mathbf{R})dr &= [E_j^{el}(\mathbf{R}) + V_{NN}]\zeta_j(\mathbf{R}) \\ &\quad + \sum_i \int \phi_j^\star(\mathbf{r}, \mathbf{R})T_N\phi_j(\mathbf{r}, \mathbf{R})\zeta_j(\mathbf{R})dr \\ &= E_{Tot}\zeta_j(\mathbf{R}) \end{aligned} \tag{10}$$

The first term of the second member of equation 10 is the adiabatic energy mentioned above. The second term can be rewritten in another form to let appear the non-adiabatic coupling Θ_{ij}. From these algebraic manipulations, the complete nuclear equation is given by:

$$[T_N + E_j^{el}(\mathbf{R}) + V_{NN}]\zeta_j(\mathbf{R}) + \sum_i \Theta_{ij}\zeta_i(\mathbf{R}) = E_{Tot}\zeta_j(\mathbf{R}) \quad (11)$$

The non-adiabatic coupling accounts for the coupling between electronic and nuclear states and is responsible for transitions between electronic states induced by nuclear motions. These terms are generally of weak importance and are often neglected. However, the non-adiabatic coupling has to be taken into account in order to achieve a good description when electronic states are close to one other or for avoiding crossings [4]. Equation (2.12) is often used to distinguish adiabatic and diabatic representations in the general description of charge transfer in bi-molecular systems. (See Sect. 2.4)

With the Born-Oppenheimer approximation, the Schrödinger equation has been divided in two independent parts, electronic and nuclear; the electronic equation being solved in the field of fixed nuclei; but even using this approximation the problem of finding an analytical solution of the Eq.2 remains unaffordable.

Indeed, in spite of this approximation, the electronic equation can only be solved for few examples:

- The problem of M nuclei and one electron (such as the ion H_2^+)
- Within the independent model which is the problem of N non interacting electrons and M nuclei

The last case introduces important notions in quantum-chemistry and is detailed in the section 2.1.2.

2.1.2 *Independent Electron Model*

To try to approximate a multielectronic wavefunction, Hartree[56,57] (1928), introduced the idea of a self-consistent field with particular reference to valence electrons and groups of core electrons. The wave function of an electron ψ_i is determined from the field of the nucleus and the other electrons in a selfconsistent fashion. One starts with an approximate field and iterates until input and output fields for all electrons are the same. In this approach the wave function of the N-electron system can be approximated by the product of N single-particle functions:

$$\Psi(\mathbf{r}_1, \sigma_1; \mathbf{r}_2, \sigma_2; \ldots; \mathbf{r}_N, \sigma_N) = \psi_1(\mathbf{r}_1, \sigma_1)\psi_2(\mathbf{r}_2, \sigma_2)\ldots\psi_N(\mathbf{r}_N, \sigma_N) \quad (12)$$

where r_i is the ith electron coordinate and σ_i is the spin term [2].

Each of the wavefunctions $\psi_i(\mathbf{r}_i, \sigma_i)$ is solution of the single electron Schrödinger equation:

$$\hat{h}_i \psi_i(\mathbf{r}_i, \sigma_i) = \left(-\frac{\hbar^2}{2m} \nabla^2 + \Phi_i + V_{ext} \right) \psi_i = \varepsilon_i \psi_i \tag{13}$$

where ε_i is the energy eigenvalue of the single electron state ψ_i, $\hat{h}$ is the one-electron hamiltonian[3] V_{ext} is the nuclei potential and Φ_i is the "mean field" potential due to the interaction with other electrons which can be obtained by the Poisson equation:

$$\nabla^2 \Phi_i = 4\pi e^2 n(\mathbf{r}) = 4\pi e^2 \sum_{j=1}^{N} |\psi_j|^2 \tag{14}$$

In agreement with the Pauli exclusion principle, a multifermionic wavefunction must be antisymmetric, i. e.

$$\Psi(\mathbf{r}_1, \sigma_1; \ldots; \mathbf{r}_i, \sigma_i; \mathbf{r}_j, \sigma_j; \ldots; \mathbf{r}_N, \sigma_N) = -\Psi(\mathbf{r}_1, \sigma_1; \ldots; \mathbf{r}_j, \sigma_j; \mathbf{r}_i, \sigma_i; \ldots; \mathbf{r}_N, \sigma_N) \tag{15}$$

but the product wavefunction 12 does not respect this antisymmetry. Fock[58] and Slater[59] (1930) demonstrated that replacing Eq. 12 by a determinant of such functions led to equations that were only a little more complicated, while satisfying the Pauli principle. This determinantal function is known as *Slater Determinant*[59] and can be written as:

$$\Psi(\mathbf{r}_1, \sigma_1; \ldots; \mathbf{r}_N, \sigma_N) = \frac{1}{\sqrt{N!}} \begin{vmatrix} \psi_1(\mathbf{r}_1, \sigma_1) & \psi_1(\mathbf{r}_2, \sigma_2) & \ldots & \psi_1(\mathbf{r}_N, \sigma_N) \\ \psi_2(\mathbf{r}_1, \sigma_1) & \psi_2(\mathbf{r}_2, \sigma_2) & \ldots & \psi_2(\mathbf{r}_N, \sigma_N) \\ \vdots & \ddots & \ddots & \vdots \\ \vdots & \ddots & \ddots & \vdots \\ \vdots & \ddots & \ddots & \vdots \\ \psi_N(\mathbf{r}_1, \sigma_1) & \psi_N(\mathbf{r}_2, \sigma_2) & \ldots & \psi_N(\mathbf{r}_N, \sigma_N) \end{vmatrix} \tag{16}$$

This form satisfy condition required for a multi-fermionic system expressed by Pauli's principle which states that any two electrons

2 Actually the single electron wavefunction $\psi_1(\mathbf{r}_1, \sigma_1)$ can be factorized as $\psi_i(\mathbf{r}_i, \sigma_i) = \psi_i(\mathbf{r}_i)\sigma_1(\omega_i)$ in which $\psi_i(\mathbf{r}_i)$ is the spatial wavefunction and $\sigma_1(\omega_i)$ is spin wavefuncion

3 Composed by the sum of the total kinetic energy, the electron-nuclei attraction and the nuclei-nuclei repulsion operators $\hat{h}_i = T_{e,j} + V_{eN,j}$

can not occupy the same spin-orbital. This follows immediately from the fact that the determinant in equation 16 vanishes if any two spinorbitals are identical.

The pure independent model represents a rough approximation (for instance, the total energy of helium shows that the system is much more stabilized by more than 30 eV compared to the experiment). A better model to describe the electronic states is required and is achieved with two main ways Hartree-Fock formalism and Density Functional Theory.

2.2 DENSITY FUNCTIONAL THEORY (DFT)

The density functional theory (DFT)[53] is founded on the hypothesis that a multi-electron system and all the observables associated with it can be described univocally by its electronic density $n(r)$. This means that, for a system with N electrons, instead of calculating the multielectronic wavefunction $\Psi(\mathbf{r}_1, \mathbf{r}_2, \ldots, \mathbf{r}_N)$ (that is a function of 3N variables) one can calculate the density n(r) that has just three variables. From a practical point of view, the advantage of the DFT is linked to the fact that the computational cost of the variational procedure grows relatively slowly with the number N of electrons in the system. It can be demonstrated[53] that the computational time t follows the relationship

$$t \sim N^{\alpha} \tag{17}$$

with $\alpha \simeq 2 \div 3$. The first steps towards the Density Functional Theory were made by the Thomas-Fermi model[60,61] and just after by the Thomas-Fermi-Dirac model which succeeded in giving quantitative results of atomic properties. However, these earlier models were not able to describe molecules that were predicted to be unstable. The modern DFT begins with publication of the demonstrations of the two famous Hohenberg and Kohn theorems[62]:

Theorem 1 (of Hoenberg and Khon)**.** *For any system of interacting particles in an external potential $V_{ext}(\boldsymbol{r})$, the potential $V_{ext}(\boldsymbol{r})$ is determined uniquely, except for a constant, by the ground state particle density $n_0(\boldsymbol{r})$*

Theorem 2 (of Hoenberg and Khon)**.** *An universal functional for energy $E[n]$ in terms of the density $n(\boldsymbol{r})$ can be defined, valid for any external potential $V_{ext}(\boldsymbol{r})$. For any particular $V_{ext}(\boldsymbol{r})$, the exact ground state energy of the system is the global minimum value of this functional, and the density $n(\boldsymbol{r})$ that minimizes the functional is the exact ground state density $n_0(\boldsymbol{r})$.*

The variational principle on the energy was the basis of the formulation of the exact density functional formalism given by Hohenberg and Kohn (1964)[62]. First they showed that there is a one-to-one relationship between the external potential $V_{ext}(\mathbf{r})$ and the (nondegenerate) ground state wave function Ψ, and that there is a one-to-one relationship between Ψ and the ground state density $n(\mathbf{r})$ of an N-electron system:

$$n(\mathbf{r}) = \int d\mathbf{r}_2 \dots d\mathbf{r}_N \Psi^*(\mathbf{r}, \mathbf{r}_2 \dots d\mathbf{r}_N)\Psi(\mathbf{r}, \mathbf{r}_2 \dots d\mathbf{r}_N) \tag{18}$$

where the spin coordinates are not shown explicitly. The knowledge of the density then determines the external potential within a constant, so that all terms in the Hamiltonian are known. These ideas can be applied to the total energy using the variational principle. For this purpose, Hohenberg and Kohn defined the functional $F[n(\mathbf{r})]$, which is "universal" in the sense that it is valid for any external potential $V_{ext}(\mathbf{r})$, this functional can be expressed as:

$$F[n(\mathbf{r})] = \langle \Psi_N | T + V_{ee} | \Psi_N \rangle \tag{19}$$

and showed that the energy functional $E[n(\mathbf{r}), V_{ext}(\mathbf{r})]$ satisfies a variational principle:

$$E_{GS} = \min_{n(\mathbf{r})} E[n(\mathbf{r}), V_{ext}(\mathbf{r})] \tag{20}$$

where

$$E[n(\mathbf{r}), V_{ext}(\mathbf{r})] = \int d\mathbf{r} V_{ext}(\mathbf{r}) n(\mathbf{r}) + F[n(\mathbf{r})] \tag{21}$$

The minimization is performed in [62] over all nondegenerate densities that can be derived from the ground state of some external potential.

2.2.1 *The Kohn-Sham equations*

The task of finding good approximations to the energy functional $E[n, V_{ext}]$ is greatly simplified if we use the decomposition introduced by Kohn and Sham (1965)[63]

$$F[n] = T_s[n] + \frac{1}{2} \int n(\mathbf{r}) \Phi(\mathbf{r}) d\mathbf{r} + E_{xc}[n(\mathbf{r})] \tag{22}$$

T_s is the kinetic energy that a system with density n would have in the absence of electron-electron interactions, Φ is the classical Coulomb potential for electrons, and E_{xc} defines the exchange-

correlation (XC) energy.[4] T_s is not the true kinetic energy T, but it is of comparable magnitude and is treated here without approximation. All terms in Eq. 22 other than the exchange-correlation energy E_{xc} can be evaluated exactly, so that approximations for this term are crucial in density functional applications. The variational principle applied to Eq. 22 yields:[64]

$$\frac{\delta E[n, V_{ext}]}{\delta n(\mathbf{r})} = \frac{\delta T_s}{\delta n(\mathbf{r})} + V_{ext}(\mathbf{r}) + \Phi(\mathbf{r}) + \frac{\delta E_{xc}[n]}{\delta n(\mathbf{r})} = \epsilon \tag{23}$$

where ϵ is the Lagrange multiplier associated with the requirement of constant particle number.

If we compare this with the corresponding equation for a system with the same density in an external potential $V(\mathbf{r})$ but without electron-electron interactions, we obtain:

$$\frac{\delta E[n]}{\delta n(\mathbf{r})} = \frac{\delta T_s}{\delta n(\mathbf{r})} + V(\mathbf{r}) = \epsilon \tag{24}$$

We see that the mathematical problems are identical, provided that:

$$V(\mathbf{r}) = V_{ext}(\mathbf{r}) + \Phi(\mathbf{r}) + \frac{\delta E_{xc}[n]}{\delta n(\mathbf{r})} \tag{25}$$

The solution of Eq. 24 can be found by solving the Schrödinger equation for a noninteracting particles system:

$$\left[-\frac{1}{2}\nabla^2 + V(\mathbf{r})\right]\phi_i(\mathbf{r}) = \varepsilon_i\phi_i(\mathbf{r}) \tag{26}$$

yielding:

$$E = \sum_{i=1}^{N}\varepsilon_i + E_{xc}[n(\mathbf{r})] - \int V_{xc}(\mathbf{r})n(\mathbf{r}')d\mathbf{r}' + \frac{1}{2}\int\frac{n(\mathbf{r})n(\mathbf{r}')}{|\mathbf{r}-\mathbf{r}'|}d\mathbf{r}d\mathbf{r}' \tag{27}$$

and

$$n(\mathbf{r}) = \sum_{i=1}^{N}|f_i\phi_i(\mathbf{r})|^2 \tag{28}$$

The functions ϕ_i are the Kohn-Sham orbitals, and the occupation numbers f_i are noninteger at zero temperature when the orbitals are degenerate at the Fermi level and Fermi-Dirac occupancies at nonzero temperatures. The condition 25 can be satisfied in a self-consistent procedure.

4 In the world of wave functions, the "correlation energy" is defined as the difference between the exact and Hartree-Fock (variationally optimized single Slater determinant) energies.

The solution of this system of equations leads to the energy and density of the lowest state and all quantities derivable from them. The formalism can be generalized to the lowest state with a given symmetry[65] or other constraints[66]. Instead of seeking these quantities by determining the wave function of the system of interacting electrons, the DFT method reduces the problem to the solution of a singleparticle equation of Hartree form.

The difficulty in finding the self-consistent solution of the KS equations is contained in the exchange-correlation term $E_{xc}[n(\mathbf{r})]$ which is actually unknown. In principle, if one were able to determine $E_{xc}[n(\mathbf{r})]$ exactly, the Kohn-Sham equations would include all the many-body effects. However, the complexity of the multielectrons interaction prevents an exact solution and approximations needs to be adopted to solve the problem.

2.2.2 *Exchange-Correlation energy approximations*

For many materials (especially metals), the screening effect on a reference electron exerted by the other electrons is sufficient to screen it completely on a distance of about the Fermi wavelength $\lambda_F(r) = [3\pi^2 n(r)]^{1/3}$.

This means that a reference electron does not feel the charge distribution for distances longer than λ_F (the so called nearsightedness of the electron). Hence, its exchange-correlation (XC) energy depends only on the charge distribution $n(r)$ in its proximity.

These considerations are the foundations of the *Quasi-Local Approximation*(QLA) for the XC energy $E_{xc}[n(\mathbf{r})]$]:

$$E_{xc}[n(\mathbf{r})] = \int e_{xc}(\mathbf{r}, [n(\tilde{\mathbf{r}})])n(\mathbf{r})d\mathbf{r} \tag{29}$$

where e_{xc} is the one-electron XC energy. The approximation is called *quasi-local* because e_{xc} in the coordinates $\mathbf{r}$ depends only by the charge distribution in $\tilde{\mathbf{r}}$, where $\tilde{\mathbf{r}}$ differs from $\mathbf{r}$ for a distance of the order of λ_F. The QLA can be implemented in a code for atomistic simulations in different ways. The *Local Density Approximation* (LDA) assumes that the one electron XC energy e_{xc} in $\mathbf{r}$ with density $n(\mathbf{r})$ is the same of a uniform electron gas with density $n(\mathbf{r})$:

$$E_{xc}^{LDA}[n(\mathbf{r})] = \int e_{xc}(\mathbf{r}, [n(\mathbf{r})])n(\mathbf{r})d\mathbf{r} \tag{30}$$

In the case of uniform gas of electrons the XC energy can be considered as the sum the exchange energy and the correlation energy ($e_{xc} = e_x + e_c$) which are given by[67,68]:

$$e_x(n) = -\frac{0.458}{r_s} \tag{31a}$$

$$e_c(n) = \frac{0.44}{r_s + 7.8} \tag{31b}$$

where r_s is the radius of the average sphere of volume occupied by each electron. When the density is not uniform the Eqs. 31a and 31b can still be adopted with a variable $r_s(\mathbf{r})$. This is a good approximation if the density is almost constant[62], as well as at high densities, where the kinetic energy dominates the exchange and correlation terms[63].

In molecular systems, the electron density is typically rather far from being spatially uniform and there are good reasons to intuitively believe that the LDA will have limitations. One way to improve the description of the exchange-correlation functional is to make it not only depending on the local density $n(\mathbf{r})$, but also on the direction of the density gradient $\nabla n(\mathbf{r})$, in some extent to region of space where the density is not uniform. This approximation is known as *Generalized Gradient Approximation* (GGA):[69]

$$E_{xc}^{GGA}[n(\mathbf{r}, \nabla n(\mathbf{r}))] = \int e_{xc}(\mathbf{r}, [n(\mathbf{r})], \nabla n(\mathbf{r})) n(\mathbf{r}) d\mathbf{r} \tag{32}$$

Most of the exchange-correlation functionals are then constructed with a correction term added to the LDA functional. Among all the exchange or correlation potentials, a distinction has to be made between those containing experimental parameters and those which do not contain any of them. The GGA functionals has been implemented in a lot of ways, with different complexity, accuracy and computational cost. Among the most widespread implementations, we mention the Vosko-Wilk-Nusair (1980)[70] functional, the Lee-Yang-Parr (1988)[71], and the Perdew-Burke-Ernzerhof (1996) functional.[72] which is used in a part of this work.

A possible improvement of the GGA functional consist to allow the exchange-correlation functionals to depend on high order derivative of the electronic density. These functionals are called *Meta-GGA* ones.

Meta-GGA XC functionals are constructed including, in addition to the charge density and his gradient, also the orbital kinetic energy density, defined as:

$$\tau(\mathbf{r}) = \frac{1}{2} \sum_{1}^{\text{occ.}} |\nabla \psi_i(\mathbf{r})|^2 \tag{33}$$

or the laplacian of the density $l(\mathbf{r}) = \nabla^2[n(\mathbf{r})]$. This approximation can be expressed by=

$$E_{xc}^{MGGA}[n(\mathbf{r}), \nabla n(\mathbf{r}), \nabla^2[n(\mathbf{r})], \tau(\mathbf{r})] = \\ = \int e_{xc}\left(\mathbf{r}, [n(\mathbf{r})], \nabla n(\mathbf{r}), \nabla^2 n(\mathbf{r}), \tau(\mathbf{r})\right) n(\mathbf{r}) d\mathbf{r} \tag{34}$$

An example of implementation of this kind of functional is the Tao-Perdew-Staroverov-Scuseria (TPSS, 2003)[73].

2.2.3 *Hybrid Functionals*

The basic idea behind the hybrid functional construction is given by the *Adiabatic Connection Method*. The system that we should describe is a system of N electrons in interaction. Let us imagine that we can smoothly move from a non-interacting system to a fully interacting one. Using the Hellmann-Feynman theorem[74], the exchange-correlation energy can then be computed as:

$$E_{xc} = \int_0^1 \langle \psi(\alpha) | \, V_{xc}(\alpha) \, | \psi(\alpha) \rangle \, d\alpha \tag{35}$$

where α describes the extent of electronic interactions ranging from 0 to 1 in which 0 and 1 means respectively no-interactiong and fully interacting system. For $\alpha = 0$ the system is without correlation, in this case, the wavefunction of the system is a Slater determinant and the exchange-correlation potential reduces to the Hartree-Fock exchange potential.

In other terms *Hybrid Functionals* (sometimes called Hyper-GGA functionals) incorporate a portion of exact exchange from the Hartree-Fock theory with the approximate exchange and correlation estimated using LDA, GGA, etc. The exact exchange functional is expressed in terms of Kohn-Sham orbitals rather than the density and, for this reason, it is also referred as *Implicit Density Functional*.

Since the exchange-correlation potential as well as the wavefunction for $\alpha \neq 0$ are not known, the value of the integral can only be approximated. Different attempts were made with a weighted sum of the L(S)DA and GGA exchange and correlation functionals. This leads to the development of several important hybrid functionals for example B3LYP (Becke 3-parameter Lee-Yang-Parr)[75] which is one of the most used hybrid functionals and has been extensively used also in the present thesis. This functional, which incorporates

the 20 % of the exact Hartree-Fock exchange, can be described by the following expression:

$$E_{XC}^{\mathrm{B3LYP}} = E_X^{\mathrm{LDA}} + \alpha(E_X^{\mathrm{HF}} - E_X^{\mathrm{LDA}}) + \beta(E_X^{\mathrm{GGA}} - E_X^{\mathrm{LDA}}) + E_C^{\mathrm{LDA}} + \gamma(E_C^{\mathrm{GGA}} - E_C^{\mathrm{LDA}}) \tag{36}$$

with: $\alpha = 0.2$, $\beta = 0.72$ and $\gamma = 0.81$. These mixing parameters are obtained by fitting experimental atomic energies, electron affinities and ionization potentials..

The hybridization allows to improve the estimation of several chemical and physical properties, including the molecular energy levels and the bond lengths of different molecular systems.

2.3 EXCITED STATES

2.3.1 Δ-*Self Consistent Field Method*

While Density Functional Theory (DFT) has been successfully applied to obtain the ground state electronic properties of a large class of materials, it is well recognized that the use of Kohn-Sham eigenvalues to determine the quasi-particle properties of many-electrons systems yields, by and large, results in disagreement with experiments.[76]

For example, the well-known band-gap problem for bulk semiconductors arises from a severe underestimate (even exceeding 50%) of the electronic excitation energies with respect to available experimental results (optical absorption, direct and inverse photoemission).[77,78]

In optical absorption experiments, in particular, an electron excited into a conduction state interacts with the resulting hole in the previously occupied state and two-particles (excitonic) effects must be properly considered.[77]

For finite systems it is possible to obtain accurate excitation energies using the so-called delta-self-consistent-field (ΔSCF) approach.[76,77] This method, successfully applied to obtain the quasi-particle energies for several clusters and isolated molecules,[79,80] consists in evaluating total energy differences between the self-consistent calculations performed for the system with N and $N \pm 1$ electrons, respectively.

At the optimized geometry of the neutral system it's possible to evaluated the vertical electron affinity ($\mathrm{EA_V}$) and the vertical first ionization energy ($\mathrm{IE_V}$) as a difference between the total energies

of neutral (E_N) and charged molecules: cation ($E^{(N)}_{N+1}$) and anion ($E^{(N)}_{N-1}$)).

$$EA_V = E_N - E^{(N)}_{N-1} \tag{37a}$$

$$IE_V = E^{(N)}_{N+1} - E_N \tag{37b}$$

Within the same framework, is also possible to calculate the adiabatic electron affinity (EA_A) and adiabatic first ionization energy (IE_V) in the same way but using the cation and anion total energies ((E_{N+1}) and (E_{N-1}) respectively) calculated at their proper equilibrium geometry:

$$EA_V = E_N - E_{N-1} \tag{38a}$$

$$IE_V = E_{N+1} - E_N \tag{38b}$$

This enabled the calculation of the quasiparticle-corrected HOMO-LUMO gap (QP_{Gap}) of the neutral systems; this quantity is usually referred to as the fundamental energy gap and is rigorously defined within the Δ-SCF scheme[81] as:

$$QP_{Gap} = IE_V - EA_V = E^{(N)}_{N+1} + E^{(N)}_{N-1} - 2E_N \tag{39}$$

In the framework of Δ-SCF it is also possible to express the QP_{Gap} with the following approximate expression:

$$QP_{Gap} = \varepsilon^{n+1}_{n+1} - \varepsilon^{n}_{n} \tag{40}$$

where ε^{j}_{i} are the i^{th} Kohn-Sham eigenvalue of the j-electron system. The results obtained using the above Eqs. 39 and 40 tend to coincide as the system gets larger and the orbitals more delocalized.

2.3.2 *Time-Dependent Density Functional Theory (TDDFT)*

The *Time-Dependent Density Functional Theory* (TDDFT) is an extension of DFT that is suitable to investigate the properties and dynamics of multi-electron systems in the presence of time-dependent potentials (i.e. excited states). Through TDDFT it is possible to calculate excitation energies, frequency-dependent response properties, and photoabsorption spectra. Similarly to DFT, TDDFT is based on the fundamental hypothesis that the time-dependent wave function can be replaced by the time-dependent electronic density to derive the effective potential of a fictitious non-interacting system.

TDDFT is based on an extension of the HK Theorems previously seen in the Sect. 2.2 known as *Runge-Gross Theorem*[54] (RG) which states that:

Theorem 3 (of Runge and Gross)**.** *Given initial state at time t_0, the single particle potential $V(\mathbf{r},t)$ leading to a given density $n(\mathbf{r},t)$ is uniquely determined so that the map $V(\mathbf{r},t) \mapsto n(\mathbf{r},t)$ is invertible. As a consequence of the bijective map $V(\mathbf{r},t) \leftrightarrow n(\mathbf{r},t)$, every observable $O(t)$ is unique functional of the time-dependent electronic density $n(\mathbf{r},t)$.*

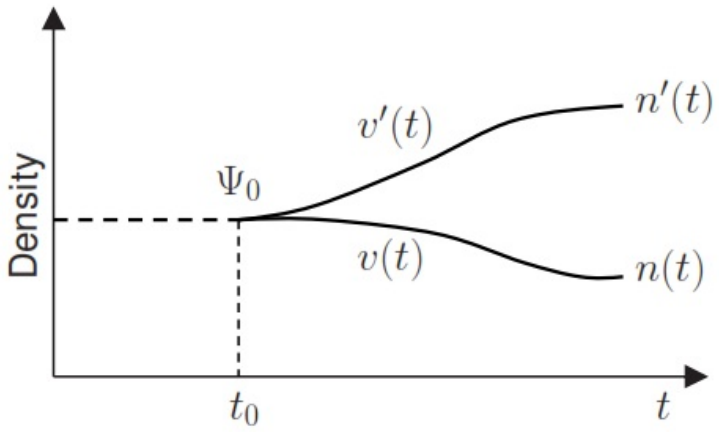

Figure 6: Illustration of the Runge-Gross theorem. Figure taken from [82]

From the RG theorem, and in a similar way to the KS construction for the ground state density, we may build a time-dependent KS scheme. For that purpose, we have to introduce an auxiliary system of N noninteracting electrons, subject to an external potential v_{KS}. This potential is unique, by virtue of RG theorem applied to the noninteracting system, and is chosen such that the density of the KS electrons is the same as the density of the original interacting system. These Kohn-Sham electrons obey the time-dependent Schrödinger equation:

$$i\hbar\frac{\partial}{\partial t}\phi_i(\mathbf{r},t) = \left[-\frac{\hbar^2}{2m}\nabla^2 + v_{KS}([n];\mathbf{r},t)\right]\phi(\mathbf{r},t) = \mathbf{H}_{KS}([n];\mathbf{r},t)\phi_i(\mathbf{r},t) \tag{41}$$

from which we can obtain the electronic density of the interacting system from the Kohn-Sham orbitals as:

$$n(\mathbf{r},t) = \sum_{i=1}^{N} |\phi_i(\mathbf{r},t)|^2 \tag{42}$$

The time-dependent Kohn-Sham potential (v_{KS}) in Eq. 41 is usually written as the sum of three terms:

$$v_{KS}([n];\mathbf{r},t) = v_{ext}(\mathbf{r},t) + v_{Hartree}([n];\mathbf{r},t) + v_{XC}([n];\mathbf{r},t) \tag{43}$$

where the first one is the external potential (usually due to the nuclei), the second one (Hartree term) accounts for the classical electrostatic interaction between electrons:

$$v_{Hartree}([n];\mathbf{r},t) = \int \frac{n(\mathbf{r},t)}{|\mathbf{r}-\mathbf{r'}|} d^3r' \tag{44}$$

and the final term (XC potential) includes all the many-body effects. In the same way previously seen for the ground-state DFT, also in this case, $v_{XC}([n];\mathbf{r},t)$ has an extremely complex (and essentially unknown) functional dependence on the density. This dependence is clearly nonlocal, both in space and in time, i.e., the potential at time t and position $\mathbf{r}$ can depend on the density at all other positions and all previous times (due to causality).

2.3.2.1 *Linear Response Theory*

The starting point in the linear response theory establish that a small external perturbation (spin-independent) $\delta v_{ext}(\mathbf{r},\omega)$ will induce a density response $\delta n(\mathbf{r},\omega)$.

For a finite system the photoabsorption cross section is proportional to the imaginary part of the dynamic polarizability:[83]

$$\sigma(\omega) = \frac{4\pi\omega}{3c}\Im\left\{\sum_\gamma \alpha_\gamma(\omega)\right\} \tag{45}$$

where c is the speed of light, $\gamma = x,y,z$ and $\alpha_\gamma(\omega)$ is given by

$$\alpha_\gamma(\omega) = -\int d^3r \int r_\gamma \sum_{\sigma\sigma'} \chi_{\sigma\sigma'}(\mathbf{r},\mathbf{r'};\omega) d^3r r'_\gamma \tag{46}$$

with the sum over the spin states σ,σ'. The function χ is called *Linear Density Response Function* of the system and measures the change of the density when the system is perturbated by a small change of the external potential.

$$\delta n_\sigma(\mathbf{r},\omega) = \sum_\sigma{}' \int \chi_{\sigma\sigma'}(\mathbf{r},\mathbf{r'};\omega)\delta v_{ext}(\mathbf{r},\omega) d^3\mathbf{r'} \tag{47}$$

Let $\{\varphi_{j\sigma}(\mathbf{r})\}$ be the ground-state Kohn-Sham wave functions of the system. Apply a perturbation of the form $\delta v_{ext}(\mathbf{r},t)) =$

$-\kappa_0 r_v \delta(t)$. The amplitude κ_0 must be small in order to keep the response of the system linear. This perturbation excites all frequencies of the system with equal weight. At $t = 0^+$ the Kohn-Sham orbitals are:

$$\varphi_{j\sigma}(\mathbf{r}, t = 0^+) = \mathrm{e}^{i\kappa_0 \mathbf{r}} \varphi_{j\sigma}(\mathbf{r}) \tag{48}$$

These orbitals are then further propagated for a finite time. The dynamical polarizability can then be obtained from:

$$\alpha_\gamma(\omega) = -\frac{1}{\kappa_0} \int r_\gamma \delta n(\mathbf{r}, \omega) d^3 r \tag{49}$$

In the previous expression, $\delta n(\mathbf{r}, \omega)$ stands for the time Fourier transform of $n(\mathbf{r}, t) - \tilde{n}(\mathbf{r})$ where $\tilde{n}(\mathbf{r})$ is the ground-state density of the system. This prescription has been used with considerable success to calculate the photoabsorption spectrum of several finite systems, from small molecules [see, e.g., References 84 and 85] to biological systems[86]. As it is based on the propagation of the Kohn-Sham equations, this approach can be easily extended to study non-linear responses, or to treat cases where the external field is not a small perturbation. However, if our sole objective is the calculation of the linear excitation spectrum, it is possible to use linear response theory to evaluate χ directly.

2.3.3 *GW Method*

We have seen that, in the DFT-KS scheme, the response of a system of interacting electrons, of Hamiltonian

$$H = \sum_{i=1}^{N} \left[-\frac{\hbar^2}{2m} \nabla_i^2 + V_{ext}(\mathbf{r}) \right] + \sum_{i<j}^{N} \frac{e_i e_j}{|\mathbf{r}_i - \mathbf{r}_j|} \tag{50}$$

to an external potential V_{ext} is that of independent particles responding to an effective potential.

A similar, though much older, idea is that the long-range, and relatively strong, Coulomb forces could screen the individual electrons, with a surrounding charge cloud of the other electrons. This leads us to the concept of quasi-particle,[87] i.e. an electron plus its screening cloud. Thus, the response of strongly interacting particles can be described in terms of weakly interacting quasi-particles which interact via a screened rather than the bare Coulomb potential(see Fig. 7). This scheme has also two advantages:

1. Permits to better represent the electrons in a many-body framework.

2. Allows to use a perturbative expansion, with respect to the quasi-particle interaction

The last point has given to this approach the name *Many Body Perturbation Theory* (MBPT).

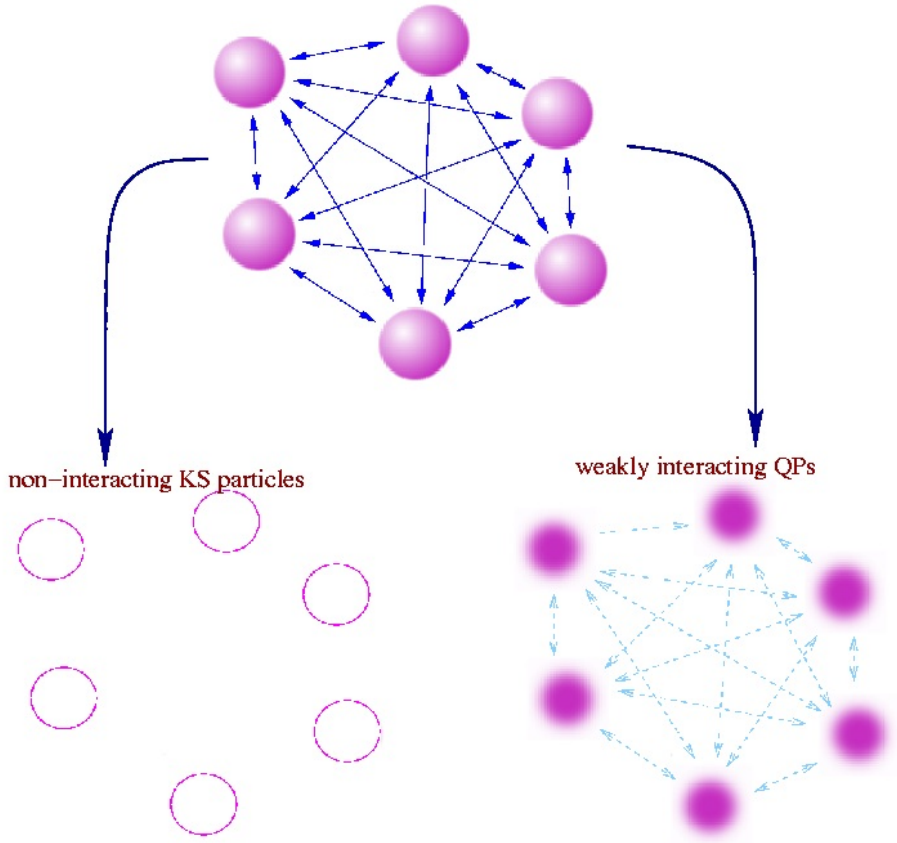

Figure 7: An interacting particles system can be mapped onto a non-interacting particles system (DFT-KS theory) or onto a weakly interacting particles (quasi-particles) system (Green function - MBPT). Figure taken from [88]

Quasi-particles states are not eigenstates of the N-electrons Hamiltonian 50, therefore their lifetimes are not infinite. Moreover, the screening can lead to an "effective mass" different from that of the bare particle. All the differences between quasi-particles and bare particles can be contained in a non-local, non-hermitian, energy-dependent operator called *Self Energy* (Σ), which contains all the many-body exchange and correlation effects. In this MBPT scheme, the quasi-particle energies and wavefunctions are determined by solving the Schrödinger-like equation:

$$\left[-\frac{\hbar^2}{2m}\nabla^2 + v_{ionic}(\mathbf{r}) + v_{hartree}(\mathbf{r})\right]\phi_i(\mathbf{r},\omega) + \\ + \int \Sigma(\mathbf{r},\mathbf{r'};\omega)\phi_i(\mathbf{r'},\omega)d\mathbf{r'} = E_i\phi_i(\mathbf{r},\omega) \tag{51}$$

this equation is called the quasi-particle equation ($\omega = E_i$). In a solid, the index i represent the usual couple of parameters $(\mathbf{k}, n)$ respectively the wave vector and the band index.

2.3.3.1 *Single Particle Green's Function*

The expectation value (on the ground state $|N\rangle$) of any single-particle operator is determined by the knowledge of the time ordered single-particle Green function[87]

$$G(1,2) = -\frac{i}{\hbar}\langle N|T[\psi(1)\psi^\dagger(2)]|N\rangle = \begin{cases} -\frac{i}{\hbar}\langle N|[\psi(1)\psi^\dagger(2)]|N\rangle & t_1 > t_2 \\ \frac{i}{\hbar}\langle N|[\psi^\dagger(2)\psi(1)]|N\rangle & t_1 < t_2 \end{cases} \tag{52}$$

The terms ψ and $\psi^\dagger$ representing the creation and annihilation fermion field operators, and where the five coordinates $(\mathbf{r}_i, \sigma_i, t_i)$ of the ith electron are represented by the symbol i (so the function $G(a,b)$ actually is $G(\mathbf{r}_a, \sigma_a, t_a; \mathbf{r}_b, \sigma_b, t_b)$).

By inserting a complete set of (N-1) and (N+1) particles state in 52 and taking the Fourier transform in time, it can be seen that G has poles at the electron addition and removal energies. Among the observables described by single-particle operator, there are the density, the quasi-particle energies and lifetimes, or even the total energy of the system..

The Green function $G(1,2)$ is also called *Propagator* since it describes the probability amplitude for the propagation of an electron from position r_2 at time t_2 to the position r_1 at time t_1. If $t_1 < t_2$, the same $G(1,2)$ describes the propagation of a hole.

2.3.3.2 *Hedin's Formalism*

In this section we just schematically sketch the principal ideas associated with the underlying Green's function formalism[89] and the functional derivative approach[90] to many-body perturbation theory, namely:

- The (charged) excitation energies associated with adding or removing an electron from the system can be properly defined as the poles in the energy representation of the one-particle time-ordered $G(1,2)$ Green's function which measures the amplitude of probability to find an electron (a hole) in position and time $(2 = r_2, t_2)$ after its introduction in the system at $(1 = r_1, t_1)$.
- The equation of motion, or time-dependent Schrödinger equation for operators, that may be used to determine $G(1,2)$, involves a two-body Green's function $G_2(1,2,3,4)$, initiating a hierarchical chain of increasing order Green's function with increasing complexity.
- The needed two-body G_2 operator can be expressed as a function of the derivative of the one-body $G(1,2)$ Green's function with respect to an external perturbation, allowing to introduce quantities familiar within linear response theory, namely the susceptibility of the system (or irreducible polarizability) $P(1,2)$, that relates the change of the charge density in (1) with respect to an external perturbation acting in (2), the energy-dependent dielectric function $\epsilon(1,2)$ and the related screened Coulomb potential $W(1,2)$.

The quantities defined here above are however not given in closed form, but are related by a set of coupled equations, traditionally labelled Hedin's equations[91,92] in condensed matter physics:

$$G(12) = G_0(12) + \int G_0(13)\Sigma(34)G(42)d(34) \tag{53a}$$

$$\Sigma(12) = i \iint G(13)\Gamma(32;4)W(41)d(34) \tag{53b}$$

$$W(12) = v(12) + \int v(13)P(34)W(42)d(34) \tag{53c}$$

$$P(12) = -i \int G(13)G(41)\Gamma(34;2)d(34) \tag{53d}$$

$$\Gamma(12;3) = \delta(12)\delta(13) + \int \frac{\delta\Sigma(12)}{\delta G(45)} G(46)G(75)\Gamma(67;3)d(4567) \tag{53e}$$

where $v(12) = v(\mathbf{r}_1, \mathbf{r}_2)\delta(t_1.t_2)$ is the bare Coulomb potential, 53a is the *Dyson Equation* for the Green function (G), 53b the Self Energy (Σ), 53d the *Irreducible Polarizability* (or susceptibility; P), 53c the Screened Coulomb Interaction (W), 53e the Vertex Function (or three

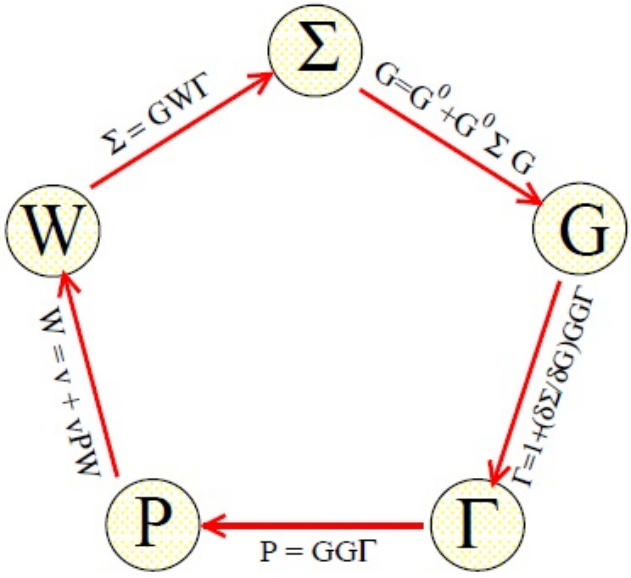

Figure 8: Self consistent Hedin's full cycle. Figure taken from [88]

body vertex correction; Γ) and G_0 is the Independent Green function. The self consistent full cycle, based on Eq.53 is reported in Fig. 8.

Such set of equations can in principle be solved iteratively, starting from a zeroth-order system where the self-energy is zero, namely the *Hartree mean-field solution*, yielding to first-order: $\Gamma(12;3) = \delta(12)\delta(13)$. This approximation for the vertex correction yields the well known GW approximation for the self-energy. If we rewrite these equations in the energy representation (see Ref 93) we can see that the summations over occupied and empty states lead to an $O(N^4)$ scaling for GW calculations with respect to system size, a scaling larger than the standard $O(N^3)$ scaling for DFT calculations with (semi)local functionals[93].

In principle the cycle showed in 8 should continue until self-consistency is reached. But in practice, a full self-consistent resolution of the Hedin's equations has never been pursued (essentially for the complexity of the vertex term calculation). Instead, real implementations of the method usually stop once obtained the $\Sigma = G_0W_0$ (i.e. after a single cycle), or search for the self-consistency of a reduced set of equations (mainly short-cutting the vertex function). These GW approximations (GWA) are called *non-self-consistent* and *self-consistent*, respectively.

The GWA consists, essentially, in short-cutting the "Hedin's pentagon" (as show in Fig. 9), avoiding the calculation of the vertex function Γ set to a delta function:

$$\Gamma(1,2,3) \simeq \delta(1,2)\delta(1,3) \tag{54}$$

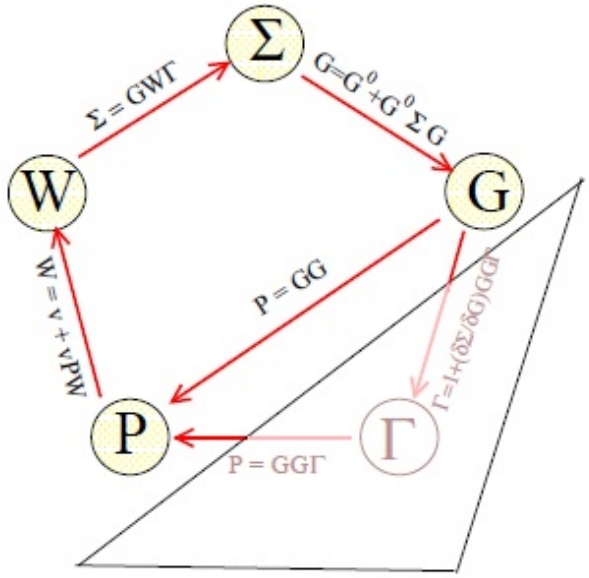

Figure 9: Self consistent Hedin's cycle for GW approximation. Figure taken from [88]

In many cases, the mean-field starting point is never the Hartree solution, but more traditionally the DFT KS eigenstates which represent in general the best available mean-field starting point. This leads to the standard single-shot perturbative G_0W_0 treatment where the exchange-correlation contribution to the DFT KS eigenvalues is replaced by the GW self-energy operator expectation value onto the frozen KS DFT eigenstates, namely

$$E_n^{QP} = \varepsilon_n^{DFT} + \left\langle \phi_n^{DFT} \middle| \Sigma^{GW}(E_n^{QP}) - v^{XC,DFT} \middle| \phi_n^{DFT} \right\rangle \tag{55}$$

2.3.4 *Bethe-Salpeter Equation (BSE)*

GW calculations aim at obtaining accurate quasi-particle energies, such as the electronic affinity, ionization potential, and more generally the entire band structure of a given system, to be compared, e.g. to direct and inverse photoemission experiments, the Bethe-Salpeter formalism tackles the problem of the neutral optical excitations, namely excitations where the electron does not leave the system and interacts through the (screened) Coulomb potential with the hole left in the occupied bands. As such, the *Bethe-Salpeter equation*

(BSE), originally derived in the 50s[94] and adapted in the mid-1960s by Sham and Rice in the context of condensed matter physics[95–97], is a two body electron-hole eigenvalue problem, very much as the proton-electron hydrogenoid textbook exercise, but in an environment that provides screening through Coulomb and Pauli repulsion between electrons. As another familiar reference for solid state physicists, it can be considered as a generalization of the Elliott[98] (or Mott-Wannier) approach to delocalized excitons in semiconductors.

Three independent ab-initio implementations were developed simultaneously in 1998[99–101] Because BSE calculations require as an input the GW quasi-particle energy levels, GW-BSE calculations on molecular systems (e. g.fullerenes or porphyrins) have also emerged rather recently after initial studies on small molecules[102,103] or bulk organic semiconductors.[104–106]

The treatment of excitons and resulting optical spectra, i. e.the full excitonic problem, requires practically to set up and diagonalize an electron-hole Hamiltonian $\hat{H}$. Within Hedin's GW scheme and a restriction to static screening this two-particle Hamiltonian reads for singlet excitations in matrix form as:[92,107]

$$\begin{aligned}\hat{H}(vc\mathbf{k}, v'c'\mathbf{k'}) = &[\epsilon_c^{QP}(\mathbf{k}) - \epsilon_v^{QP}(\mathbf{k})]\delta_{vv'}\delta_{cc'}\delta_{\mathbf{kk'}} \\ &- \int d^3\mathbf{r}\int d^3\mathbf{r'}\psi^\star_{c\mathbf{k}}(\mathbf{r})\psi_{c'\mathbf{k'}}(\mathbf{r})W(\mathbf{r},\mathbf{r'})\psi_{v\mathbf{k}}(\mathbf{r'})\psi^\star_{v'\mathbf{k'}}(\mathbf{r'}) \\ &+ 2\int d^3\mathbf{r}\int d^3\mathbf{r'}\psi^\star_{c\mathbf{k}}(\mathbf{r})\psi_{v\mathbf{k}}(\mathbf{r})\bar{v}(\mathbf{r},\mathbf{r'})\psi_{c'\mathbf{k'}}(\mathbf{r'})\psi^\star_{v'\mathbf{k'}}(\mathbf{r'})\end{aligned} \tag{56}$$

where matrix elements between KS wave functions of CB states and VB states occur. Contributions to Eq. 56 which destroy particle number conservation have been omitted. The first term describes the noninteracting quasielectron quasihole pairs. The second term accounts for the screened electron-hole Coulomb attraction with the statically screened Coulomb potential $W(\mathbf{r},\mathbf{r'})$. The third contribution, governed by the nonsingular part of the bare Coulomb interaction $\bar{v}(\mathbf{r},\mathbf{r'})$ represents the electron-hole exchange or crystal local-field effects.[92,108] After diagonalization of the exciton matrix, or, more precisely, solving the homogeneous BSE or stationary two-particle Schrödinger equation with the eigenvalues E_Λ and the eigenfunctions $A_\Lambda(vc\mathbf{k})$ of the pair states Λ one can obtain the frequency-dependent macroscopic dielectric function including excitonic effects as:

$$\varepsilon_{\alpha\alpha}(\omega) = \delta_{\alpha\alpha} + \frac{16\pi e^2\hbar^2}{V}\sum_{\Lambda}\left|\sum_{cv\mathbf{k}}\frac{\langle c\mathbf{k}|v_\alpha|v\mathbf{k}\rangle}{\epsilon_c(\mathbf{k})-\epsilon_v(\mathbf{k})}A_\Lambda(vc\mathbf{k})\right|^2 \cdot\left[\frac{1}{E_\Lambda-\hbar(\omega+i\gamma)}+\frac{1}{E_\Lambda+\hbar(\omega+i\gamma)}\right] \tag{57}$$

where v_α is the corresponding cartesian component of the single-particle velocity operator, γ is the pair damping constant and V is the he crystal volume. The details of the standard scheme using the direct diagonalization of Eq. 57 have been discussed in Ref. 92,107–109.

2.4 CHARGE TRANSPORT PROPERTIES

Organic molecular solids have an important position nowadays in basic and applied research. In particular with respect to transport processes; in fact π-conjugated molecular, oligomeric, and polymeric materials are of great interest as alternatives to traditional inorganic materials for many low-cost organic-based electronic applications, including thin film transistors (OTFTs), light-emitting diodes (OLEDs), and photovoltaic cells, owing to device processing ease, mechanical flexibility and a large synthetic palette from which properties can be designed into the molecular or polymeric structure. However many fundamental questions concerning how charge is transported through these functional organic molecular solids remain unresolved.

In particular, why certain molecular materials favor the transport of holes versus electrons (i.e., positive and negative polarons, respectively) and how molecular and crystal structure parameters influence relative carrier mobility magnitudes are far from being completely understood.[110–112]

In typical organic transport media, very small bandwidths (<1eV) dictate that charge motion occurs by hopping. The electron-hopping process is generally portrayed as a self-exchange electron-transfer reaction between neighboring molecules within the framework of Marcus theory.[110,113–117] The rate constant for electron transfer (i.e., polaron hopping) is then defined in an Arrhenius-like form:

$$K_{ET} = \frac{4\pi}{h}\frac{t_{12}^2}{\sqrt{4\pi\lambda k_B T}}\exp\left(-\frac{\lambda}{4k_B T}\right) \tag{58}$$

In the Eq. 58 λ is the reorganization energy for the intermolecular electron transfer, t_{12} is the electronic coupling element (transfer in-

tegral), between neighboring molecules, h is the Planck's constant, k_B is the Boltzmann constant and T is the absolute temperature.

The reorganization energy λ can be separated into the sum of two primary components: i) the medium reorganization energy (i.e., outer-sphere reorganization energy, λ_0) that arises from modifications to the medium polarization due to the presence of an excess charge; and ii) the intramolecular reorganization energy (i.e., inner-sphere reorganization energy, λ_i) that provides a measure of the intramolecular electron-vibration interaction for the sequential reduction and oxidation processes of polaron hopping. Along with the original dielectric continuum model put forth by Marcus, numerous explorations into expressions to describe λ_0 are currently ongoing.[114–116,118–122]

The parameter λ_i can be determined quantum-chemically from the individual relaxation process energies for the neighboring electron-donor and electron-acceptor species; as an example, λ_i for the reduction of an electron-acceptor (neutral species, λ_1) via oxidation of a doublet electron-donor (radical-anion, λ_2), (see Fig. 10) can be obtained by following expression:

$$\lambda = \lambda_1 + \lambda_2 = (E_0^{-1} - E_0^0) + (E_{-1}^0 - E_{-1}^{-1}) \tag{59}$$

E_0^0 and E_{-1}^{-1} are the total energies of the neutral and anion in their equilibrium structures, respectively, E_{-1}^0 is the total energy of the anion in the neutral geometry, and E_0^{-1} is the total energy of the neutral in the anion geometry. The first term λ_1 accounts for the relaxation of the charged state, the second one λ_2 corresponds to the radical anion formation.

Following the work of Siebbeles et al.[123,124] and Coropceanu et al.[125,126], the electronic Hamiltonian of a simple two-site (i.e., dimer pair) tight-binding model[16] can be written as

$$\hat{H} = \begin{pmatrix} e_1 & t_{12} \\ t_{21} & e_2 \end{pmatrix} \tag{60}$$

The electronic coupling (transfer integral) is defined by the matrix element $t_{12} = t_{21} = \langle \Psi_1 | \hat{H} | \Psi_2 \rangle$, where Ψ_1 and Ψ_2 are diabatic state wave functions for neighboring molecules. Within the one-electron approximation, the diabatic states are associated with localized monomer orbitals φ_i, here considered to be orthogonal. Assuming that the dimer highest-occupied molecular orbital (HOMO) [lowest-unoccupied molecular orbital (LUMO)] and HOMO-1 [LUMO+1] result solely from the interaction of the monomer HOMOs [LU-

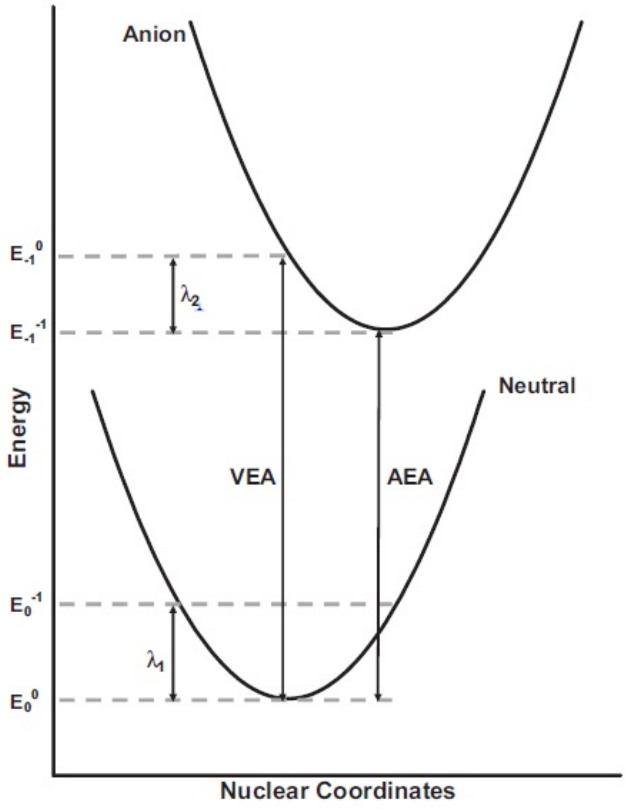

Figure 10: Energy diagram of ionization processes

MOs], the transfer integral for hole (Eq. 61a) [electron, Eq. 61b] transfer can be expressed as:

$$t_{12}^{h} = \left\langle \varphi_1^H | \hat{H} | \varphi_2^H \right\rangle \tag{61a}$$

$$t_{12}^{e} = \left\langle \varphi_1^L | \hat{H} | \varphi_2^L \right\rangle \tag{61b}$$

The diagonal elements of the matrix (60) are the site energies, which originate from differences in either molecular geometry or intermolecular polarization of localized electronic states, and are expressed as:

$$e_1 = \left\langle \varphi_1^{H[L]} | \hat{H} | \varphi_1^{H[L]} \right\rangle \tag{62a}$$

$$e_2 = \left\langle \varphi_2^{H[L]} | \hat{H} | \varphi_2^{H[L]} \right\rangle \tag{62b}$$

Solving the determinant of this matrix provides the relationship between the transfer integral, site energy, and expected degree of energetic splitting of the dimer molecular orbitals (ΔE_{12}) via:[127]

$$\Delta E_{12} = \sqrt{(e_1 - e_2)^2 + (2t_{12})^2} \tag{63}$$

Usually, in the one-electron approximation, the monomer orbitals used to define the diabatic states of the dimer are nonorthogonal. Therefore, ΔE_{12} in a nonorthogonal basis should be written as:

$$\Delta E_{12} = \frac{\sqrt{(\tilde{\varepsilon}_2 - \tilde{\varepsilon}_1)^2 + 4[\tilde{t}_{12}^2 - \tilde{t}_{12}S_{12}(\tilde{\varepsilon}_2 + \tilde{\varepsilon}_1) + \tilde{\varepsilon}_2\tilde{\varepsilon}_1 S_{12}^2]}}{1 - S_{12}^2} \tag{64}$$

where $\tilde{\varepsilon}_1$, $\tilde{\varepsilon}_2$ and $\tilde{t}_{12}$ are the site energies and electronic coupling in the nonorthogonal basis and S_{12} is the spatial overlap between the molecular orbitals on the monomers.[126] Equation 64 is rewritten as Equation 63 in a symmetrically orthonormalized basis when:[127]

$$\varepsilon_{1,2} = \frac{1}{2}\frac{(\tilde{\varepsilon}_1 + \tilde{\varepsilon}_1) - 2\tilde{t}_{12}S_{12} \pm (\tilde{\varepsilon}_1 - \tilde{\varepsilon}_2)\sqrt{1 - S_{12}^2}}{1 - S_{12}^2} \tag{65}$$

and

$$t_{1,2} = \frac{\tilde{t}_{12} - \frac{1}{2}(\tilde{\varepsilon}_1 + \tilde{\varepsilon}_1)S_{12}}{1 - S_{12}^2} \tag{66}$$

As with the reorganization energy, quantum-chemical calculations can provide access to estimates for the electronic coupling element. The most common means of estimating t_{12} is the *Energy-Splitting in Dimer* (ESID) model[3].

Due to computational ease and feasibility, the transfer integral for hole [electron] transfer is generally taken as half the energetic difference of the HOMO and HOMO-1 [LUMO and LUMO+1] energy levels of a molecular dimer:

$$t_{12}^h = \frac{\varepsilon_{\mathrm{HOMO}} - \varepsilon_{\mathrm{HOMO-1}}}{2} \tag{67a}$$

$$t_{12}^e = \frac{\varepsilon_{\mathrm{LUMO+1}} - \varepsilon_{\mathrm{LUMO}}}{2} \tag{67b}$$

The ESID model strictly implies that differences in the site energies given in the equations 62 are necessarily zero or negligible ($e_1 \simeq e_2$). Recent works[125,126] , however, has indicated that this assumption is often invalid in organic crystalline semiconductors and, thus, t_12

should be evaluated as a function of the entire dimer Hamiltonian (EDH).[123,125,126] As Eq. 63 reveals, neglect of site energy inequality can lead to overestimations of the transfer integral. For example, along the diagonal direction of herringbone crystals (e.g., pentacene, when only one inequivalent molecule is present in the crystal structure), the molecular sites are equivalent as long as all the neighboring molecules are taken into account. However, when a dimer is extracted from the crystalline environment, the two herringbone-packed molecules are no longer equivalent and an artificially created site energy difference has to be properly taken into account to evaluate the electronic coupling.[126]

2.5 NUMERICAL METHODS, TOOLS AND SIMULATION SOFTWARES

2.5.1 *Basis Sets*

Most calculational methods of quantum chemistry represent the N-electron wavefunction as a linear combination of Slater determinants, constructed of one electron functions + molecular spin orbitals. They are written in terms of atomic spin orbitals or similar functions.

A molecular orbital is approximated as a linear combination of atomic orbitals LCAO (quantum superposition of atomic orbitals). For a given basis set of atomic orbitals $\{\phi_j\}$, the ith molecular orbital ψ_i can be obtained as:

$$\psi_i = \sum_{j=1}^{k} c_{i,j}\phi_j \tag{68}$$

with $c_{i,j}$ the coefficient of expansion, and K the total number of atomic orbital functions, called *Basis Functions*. The choice of appropriate basis set has a great importance in quantum chemical calculations, because the quality of all the results obtained will ultimately depend on the accuracy of this basis set. A correct basis set should reproduce the physics of the problem, ensure rapid convergence as the number of basis function increases, allow fast calculation of all integrals of interest (to save computational time) and vanish at large distance from the nuclei.

The two commonly used types of atomic orbital functions used to obtain the combination showed in Eq 68, are the Slater-Type Orbitals[128] (STO) and Gaussian-Type Orbitals[129] (GTO).

The STO basis functions (proposed by Slater in 1930) are based on hydrogenic like wavefunctions and have the two following possible form (in polar and cartesian coordinates respectively):

$$\phi^{\mathrm{STO}}_{\zeta,l,m}(r,\theta,\varphi) = Nr^{l}Y_{lm}(\theta,\varphi)e^{-\zeta r} \tag{69a}$$

$$\phi^{\mathrm{STO}}_{\zeta,l_x,l_y,l_z}(x,y,z) = N\bar{x}^{l_x}\bar{y}^{l_y}\bar{z}^{l_z}e^{-\zeta|r|} \tag{69b}$$

Instead the GTO basis functions (introduced by Boys in 1950) have the forms:

$$\phi^{\mathrm{GTO}}_{\zeta,l,m}(r,\theta,\varphi) = Nr^{l}Y_{lm}(\theta,\varphi)e^{-\zeta r^2} \tag{70a}$$

$$\phi^{\mathrm{GTO}}_{\zeta,l_x,l_y,l_z}(x,y,z) = N\bar{x}^{l_x}\bar{y}^{l_y}\bar{z}^{l_z}e^{-\zeta r^2} \tag{70b}$$

In the Eq.s 69 and 70 $\bar{x},\bar{y},\bar{z} = (x_c - x_N, z_c - z_N, z_c - z_N)$ are the difference between the nuclei coordinates (subscript N) and the coordinates of the center of the function (subscript c), N is a normalization constant, $Y_{lm}(\theta,\varphi)$ is the angular part (a spherical harmonic function), $r^{l}e^{-\zeta r}$ is the radial part, l and m are the atomic quantum numbers and r and ζ are the radial distance and the orbital exponent respectively. The orbital exponent, ζ, governs the size of the orbital (large ζ gives tight function, small ζ gives diffuse function) and it is chosen for each (n, l) separately, where n is the principal quantum number. The terms l_x, l_y, l_z (referred to as angular momentum $L = l_x + l_y + l_z$) determines the type of orbital ($L = 0,1,2,3,4,5,6$ designated as s, p, d, f, g, h, i).

Slater type orbitals have the correct functional behaviour near the nucleus with a cusp in the origin, the correct $1/r$ decay at long distances and, in general, are more convenient when high accuracy is needed for atomic and diatomic systems (ab-initio methods), or where all three- and four-centre integrals are neglected (e. g.semi-empirical methods) as well as in cases where Coulomb energy is calculated by fitting the density into a set of auxiliary functions instead of computing the exact exchange energy (in DFT). However, use of STO functions is time-consuming for computing the two-electron molecular integrals and difficult to be differentiated analytically.

For these reasons, in order to speed up molecular integral evaluation the Gaussian-type orbitals in turn can be used.

From a computational point of view GTO functions, are more simple to treat (this implies, for example, a fast calculation of molecular

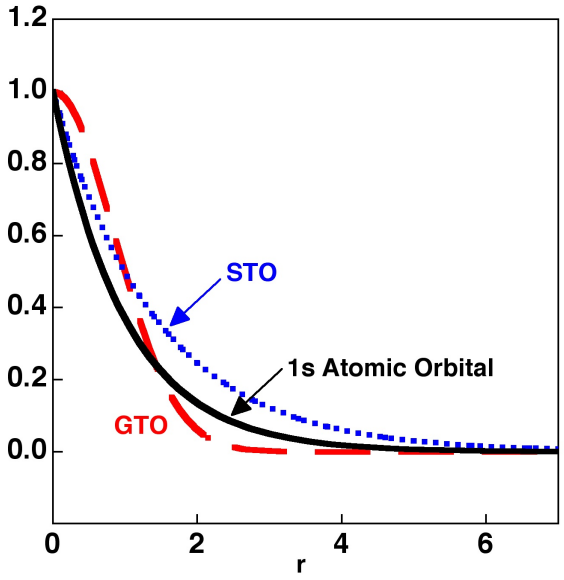

Figure 11: Comparison between Gaussian (red) Slater (blue) type functions and an 1*s* type real atomic orbital

integrals) and can be differentiated in an easy way any number of times. Gaussians are very useful and computationally efficient because the product of any two gaussians is just another gaussian, and the sum of two gaussians is easily evaluated (see Fig. 12).

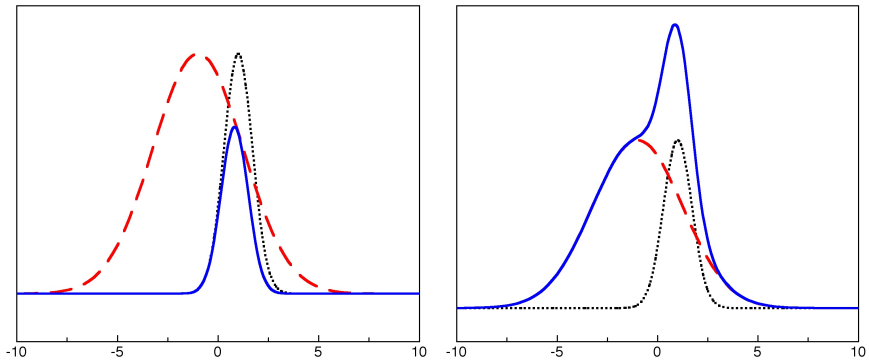

Figure 12: Product (a) and sum (b) of different GTO.

This property is very important in quantum chemistry because we have to evaluate integrals of the form given below. The first is called a "4-center integral" and is easily reduced to a "2-center integral" when using gaussians.

$$\underbrace{\int \overbrace{g_1 g_2}^{g_a} \frac{1}{r_{12}} \overbrace{g_3 g_4}^{g_b} d\tau}_{\text{4-center integral}} = \underbrace{\int g_a \frac{1}{r_{12}} g_b d\tau}_{\text{2-center integral}} \tag{71}$$

in wich the terms g_k are GTO funtions.

On the other hand, despite of the numerical advantages, the GTO, have however some serious shortcomings. The main of these are: the poor description of the electron density near the nuclei due to the fact that, unlike the STO, the GTO do not have a cusp at the origin, and have, instead, a too quick decay for $r \to \infty$ thus underestimating long range interactions. For this reasons replacing a STO by a single Gaussian function leads to unacceptable errors.

However, this problem can be overcome introducing the *Contracted Gaussian-type Orbital* (CGTO) which is represented as a linear combination of primitive GTO functions that imitate the behavior of specific STO orbitals ($\phi_\mu^{\text{STO}}(\mathbf{r}, \zeta)$).

$$\phi_\mu^{\text{CGTO}}\left(\mathbf{r}, N, \{d_{p,\mu}, \zeta_{p,\mu}\}\right) = \sum_{p=1}^{N} d_{p,\mu} \phi_\mu^{\text{GTO}}(\mathbf{r}, \zeta_{p,\mu}) \tag{72}$$

where $d_{p,\mu}$ are the coefficients of the primitive gaussian functions $\phi_\mu^{\text{GTO}}(\mathbf{r}, \zeta_{p,\mu})$ and N is the number of functions in the combination.

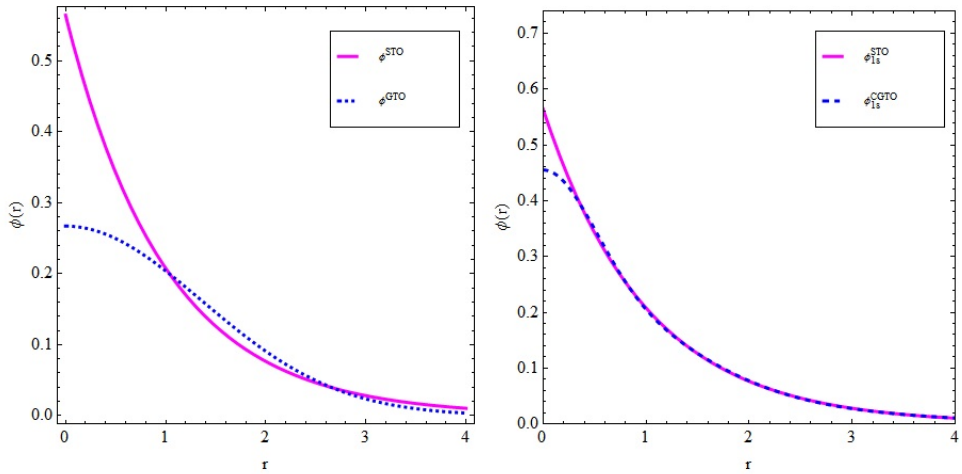

(a) (b)

Figure 13: (a) Comparison between a Slater $\phi_{1s}^{\text{STO}}(1.0; \mathbf{r})$ and Gaussian $\phi_{1s}^{\text{GTO}}(0.270; \mathbf{r})$ functions.
(b) Comparison of the same Slater function ($\phi_{1s}^{\text{STO}}(1.0; \mathbf{r})$) and the Contracted GTO $\phi_{1s}^{\text{CGTO}}(\mathbf{r}) = 0.445\phi_{1s}^{\text{GTO}}(0.110; \mathbf{r}) + 0.535\phi_{1s}^{\text{GTO}}(0.406; \mathbf{r}) + 0.154\phi_{1s}^{\text{GTO}}(2.228; \mathbf{r})$. Figure taken from [130]

As can be seen from Figure 13, a single GTO differs significantly from STO while CGTO of three GTO shows a reasonable approximation of STO, except at very small and very large electron-nucleus separation.

Apart from the choice of STO or GTO type of functions, the most important factor is the number of basis functions used in the basis set. Based on this, the commonly used basis sets can be classified into the following types:

MINIMAL BASIS SET: Represents the smallest number of basis functions needed to the correct numerical description of the atomic orbitals. A minimal basis set (MBS) contain the minimum number of basis functions that are needed for each inner-shell and valence-shell orbital. In particular if we use STO functions a MBS uses 1 STO to describe each atomic orbital in the ground state of an atom. For shells with more than one angular component this means one function for each angular component. If we use GTO functions we can obtain a minimal set using the so called STO-nG in which each atomic orbital is modelled by a linear combination of n-gaussians, where the coefficients and exponents of the GTOs are fitted to the corresponding atomic orbital[5] (n usually have values from 1 to 6 and the computational cost increases not linearly with n).

MULTIPLE ζ BASIS SET: Basis set constructed by replacing each GTO (or STO) of a minimal basis set by 2 (Double-ζ; DZ), 3 (Triple-ζ; TZ), 4 (Quadruple-ζ; QZ) or more (5-ζ, 6-ζ ecc.) GTOs (or STOs) each having different orbital exponent ζ. The use of multiple ζ basis sets allows the needed radial flexibility in the description of the electronic cloud. The tighter functions (closer to the nuclei, larger exponent) can be used to describe the σ-bond with a large coefficient, while the more diffuse function (further from the nuclei small exponent) can be used primarily for describing the π-bond. The increasing of the number of basis functions that describe the atomic orbitals thus allows for a much better description of the fact that the electron distribution is different in different directions.

SPLIT VALENCE: The core (inner-shell) electrons of an atom are less affected by the chemical environment than the valence-shell electrons. A split valence basis set (SV) is a numerical

5 More precisely the coefficients of each combination of GTO are fitted to the corresponding Slater type orbital of the minimal STO basis set that provides the best description of the orbital

simplification of multiple ζ basis sets in which the core shells are treated with a minimal basis set while the valence shells are treated with a larger basis set. In other words, each orbital of a core-shell is represented by a single function, while two or more functions are used to represent each valence shell atomic orbital.

POLARIZATION FUNCTIONS: Since atomic orbitals are distorted in shape and have their centers of charge shifted upon molecule formation, the improvement of basis set for this polarization can be done by adding higher angular momentum functions to the basis set to allow for angular flexibility. In this functions l quantum numbers are greater than the maximum l of the valence shell of the ground-state atom (e. g.p functions for the hydrogen, d functions for carbon ecc.).

DIFFUSE FUNCTIONS: Are additional functions with very small ζ exponents added to a split valence basis set. Diffuse functions have small orbital exponent that makes the electron distribution very broad and are needed whenever loosely bound electrons are present (for example anions or excited states) or when the property of interest is dependent on the wave function tail (for example polarizability). Diffuse functions are necessary for correct description of anions and weak bonds (e.g. hydrogen bonds) and are frequently used for calculations of properties (e. g.dipole moments, polarizabilities, etc.) and to treat very electronegative atoms (e. g.fluorine).

In this Thesis we have used, for the molecular calculations, the Pople type[131] localized basis set 6-31+G*. The Pople basis sets are usually identified using the notation *n-ijkw*G where:

- n: defines the number of primitive Gaussians functions used to describe the core atomic orbitals.
- i,j,k and w represent the number of primitives for contractions in the valence shell. The ij notation defines sets of valence double-ζ quality, ijk the triple-ζ valence sets, $ijkw$ the quadruple-ζ quality and so on. In other words the number of digits after the symbol "-" identify the number of basis that compose the valence orbitals and the explicit value of i,j,k and w tells us the number of gaussian functions that forms the linear combination for each base.

Within this notation are also used the symbols "+" and "++" to indicate the presence of diffuse functions for heavier atoms (except

hydrogen and helium) (+) and for all atoms (++), (including H and He).

Another possible symbols in the Pople notation are "⋆" and "⋆⋆" which denotes the presence of polarization functions. Even in this case the one symbol indicates the presence of these functions with the exception of lightest atoms, the double symbol, instead, confirms the presence of diffuse functions also for He and H.

2.5.2 *Plane Wave Functions*

Rather than using basis functions aimed at modelling the atomic orbitals (STOs or GTOs previously seen in Sect. 2.5.1), and forming linear combination of these to describe orbitals for the whole system, one may use functions aimed directly at the full system. For modelling extended (infinite) systems, for example a unit cell with periodic boundary conditions, this suggests the use of functions with an "infinite" range. The outer valence electrons in metals behave almost like free electrons, which leads to the idea of using solutions for the free electron as basis functions. The solutions to the Schrödinger equation for a free electron in one dimension can be written either in terms of complex exponentials or sine and cosine functions and for these functions, the energy depends quadratically on the k factor.

For infinite systems, the molecular orbitals coalesce into bands, since the energy spacing between distinct levels vanishes. The electrons in a band can be described by orbitals expanded in a basis set of plane waves, which can be written as:

$$\phi_i(\mathbf{r}) = \mathrm{e}^{i\mathbf{k}\cdot\mathbf{r}} \tag{73}$$

For a systems like an ideal crystal, the solution of the corresponding Kohn-Sham equations implies both an infinite number of wave functions and an infinite basis set. These limitations can be avoided by the use of periodic boundary conditions together with Bloch's theorem.[132] The former means that for a given bulk volume, the lenght of its sides will be taken as an spatial period, defining a discrete set of possible $\mathbf{k}$ wave vectors for electrons in the crystal. The latter, Bloch's theorem, states that obeying lattice periodicity the single particle wave function can be written as a plane wave modulated by a function with the same translational symmetry as the crystal:

$$\phi_i(\mathbf{r}) = \mathrm{e}^{i\mathbf{k}\cdot\mathbf{r}}\, u_i(\mathbf{r}) \tag{74}$$

The periodic function can be expanded in the set of plane waves whose wave vectors correspond with the reciprocal lattice vectors, assuring cell periodicity:

$$u_i(\mathbf{r}) = \sum_{\mathbf{G}} c_{i,\mathbf{G}}\, e^{i\mathbf{G}\cdot\mathbf{r}} \tag{75}$$

If we replace Eq. 75 in Eq. 74 obtain:

$$\phi_{i,\mathbf{k}}(\mathbf{r}) = \sum_{\mathbf{G}} c_{i,\mathbf{k}+\mathbf{G}}\, e^{i(\mathbf{k}+\mathbf{G})\cdot\mathbf{r}} \tag{76}$$

Hence, a superposition of plane waves is a rather general expression for any single particle state in a periodic system. The value of $\mathbf{k}$ in the latter equation plays the role of a new quantum number which characterizes each state, and the initial task of getting an infinite number of electronic wave functions is replaced by the determination of a finite number of occupied states at an infinite number of k wave vectors.

The wave vector $\mathbf{k}$ plays the same role as the exponent ζ in a GTO (see Eq. 70), and is related to the energy. As seen in Eq. 73, $\mathbf{k}$ can also be thought of as a frequency factor, with high $\mathbf{k}$ values indicating a rapid oscillation. The permissible $\mathbf{k}$ values are given by the unit cell translational vector $\mathbf{t}$, i. e. $\mathbf{k}\cdot\mathbf{t} = 2\pi m$, with m being a positive integer. This leads to a typical energy spacing between k vectors of 0.01 eV, and the size of the basis set is thus uniquely characterized by the highest energy k vector included.

In order to determine the electronic potential, occupied states should be known at the full set of $\mathbf{k}$ points, which is again an infinite task. However, due to the small changes in this states for close k points and also to the symmetry properties of reciprocal space, it is possible to obtain a very good approximation using a reduced set of k points.[132] This works not only for the electronic potential but in general to integrals of periodic functions in reciprocal space.

Thus, only a finite set of points in the irreducible Brillouin zone are actually needed for the solution of Kohn-Sham equations.[133] Among different methods for defining an appropriate set of k points found in literature, the one proposed by Monkhorst and Pack[134] has gain great popularity, it could be said it is the mainstream method for Brillouin zone sampling and can be found in almost any electronic structure software. It produces uniform sets of points which are easily generated for any kind of lattice.[133] The quality of such a set can be progressively improved by increasing its density of points. Correspondingly, total electronic energy will approach to the infinite k set limit. Therefore, convergence of energy upon the Brillouin zone sampling can be assessed systematically.

We have seen that it is possible to represent the electronic wave function as the sum of plane waves in Eq. 75. In order to obtain a good approximation to the electronic potential a finite set of k points can be used. However, each of these functions is an expansion of plane waves that involves an infinite number of elements. Usually, the magnitude of superposition coefficients decrease with kinetic energy of the corresponding plane wave. The relative importance of low kinetic energy plane waves allows for the truncation of the expansion, hence a finite representation of electronic wave functions is possible. Plane wave kinetic energy is given by:

$$T_{\text{pw}} = \frac{1}{2}|(\mathbf{k}+\mathbf{G})|^2 \tag{77}$$

The error brought on by basis truncation can be systematically reduced by increasing the number of allowed plane waves. The dimension of plane waves basis set is determined the value of the maximum kinetic energy, usually known as *Cutoff Energy* (E_{cut}):

$$\frac{1}{2}|(\mathbf{k}+\mathbf{G}_{\text{max}})|^2 = E_{\text{cut}} \tag{78}$$

Plane wave basis sets tend to be significantly larger than typical

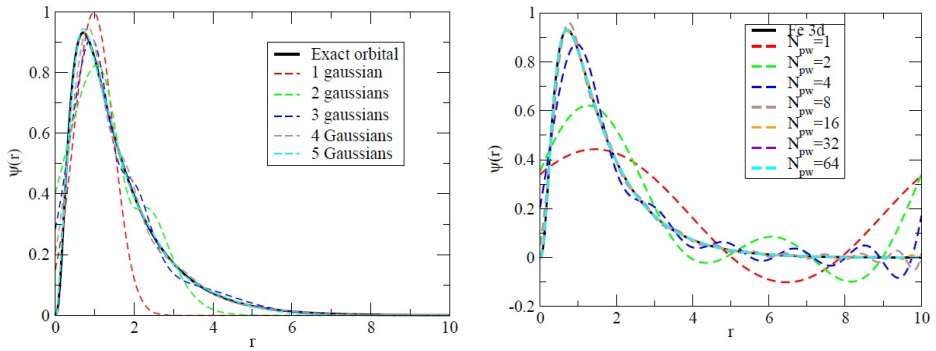

(a) (b)

Figure 14: Comparison between number of GTO functions (a) and plane wave functions (b) to obtain a good approximation of an atomic orbital (Fe 3d orbital in both cases)

Gaussian basis sets; for example a cutoff energy of $\sim$ 200 eV corresponds to a set of $\sim$ 20000 functions[135]. An example of the highest number of functions (as compared with localized basis fnctions) needed to obtain a good approximation with plane waves is showed in Fig. 14.

Plane wave basis functions are ideal for describing delocalized slowly varying electron densities, such as the valence bands in a

metal. The core electrons, however, are strongly localized around the nuclei, and the valence orbitals have a number of rapid oscillations in the core region to maintain orthogonality. Describing the core region adequately thus requires a large number of rapidly oscillating functions, i. e.a plane wave basis with very large $k_{\max}$.[135] The singularity of the nucleus-electron potential is furthermore almost impossible to describe in a plane wave basis, and this type of basis set is therefore used in connection with pseudopotentials (Section 2.5.3) for smearing the nuclear charge and modelling the effect of the core electrons. Note that a pseudopotential is also required for smearing the potential near the nucleus in hydrogen, even though hydrogen does not have core electrons.[135]

2.5.3 *Ionic Pseudopotentials*

Systems involving elements from the lower part of the periodic table have a large number of core electrons.These are, as already mentioned, unimportant in a chemical sense, but it is necessary to use a large number of basis functions to expand the corresponding orbitals, otherwise the valence orbitals will not be properly described (due to a poor description of the electron-electron repulsion). In the lower half of the periodic table relativistic effects further complicate matters.

These two problems may be solved simultaneous by modelling the core electrons by a suitable function, and treating only the valence electrons explicitly. The function modelling the core electrons is usually called Pseudopotential (PP) (or Effective Core Potential (ECP))[6].

Molecular systems have traditionally been described by gaussian functions, while plane waves have been favoured for extended (periodic) systems, and this difference has resulted in some differences for the corresponding pseudopotentials. When using Gaussian functions for describing the valence orbitals, it is natural to also use Gaussian functions to describe the ECP. Since Gaussian functions are continuous, there is no fixed distance to characterize the extent of the core potential and the quality of the ECP is determined by the number of electrons chosen to be represented by the ECP. It's known that the outer $(n+1)$s-, $(n+1)$p- (and (n)d-orbitals constitute the valence space. This "full-core" potentials give reasonable geometries, but the energy calculations are not always satisfactory. Better results can be obtained by also including the orbitals in the

6 PP is usually adopted in the physics area, ECP in the chemistry area.

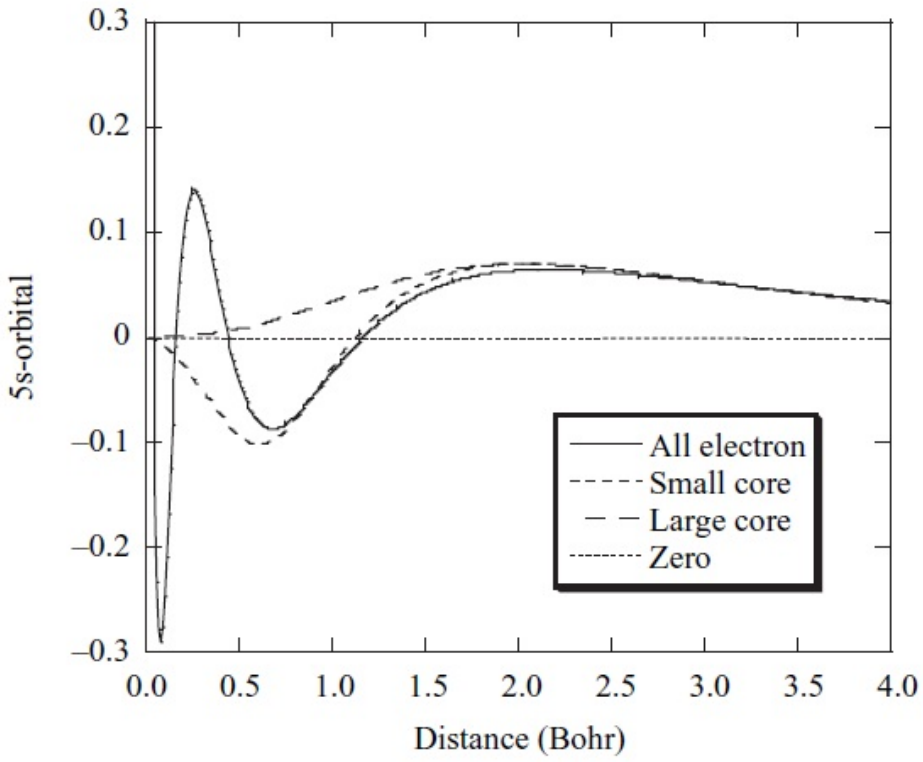

Figure 15: The 5*s*-orbital for *Ag* with either an all-electron, large-core or small-core effective core potential (plot taken from [135])

next lower shell in the valence space, albeit at an increase in the computational cost. The first approach, that includes in the PP all the shells with the exception of the valence space is called *Large Core ECP*, the second approach, which descrives as all-electron the valence space end the first lower electronic shell is called *Small Core ECP*. An example of the differences resulting for these two different choices (and the relative comparison with an all-electron approach) is shown in Fig. 15.

Part II

RESULTS

3

MOLECULAR PROPERTIES OF SUBSTITUTED PAHS: DIBENZOCHRYSENES

Contents

3.1 INTRODUCTION

Calculations of the electronic, optical, and transport properties of the building blocks of organic seminconductors can contribute to the knowledge of their properties and provide guidelines for future dedicated research[28,30,41,42,136]. The aim of this section of the Thesis is to computationally evaluate the effect of TIPS functionalization and substitutions with halogen atoms (F, Cl), on the electronic, optical, and transport properties of prototypical nonlinear PAHs. In particular, we considered two derivatives of chrysene ($C_{18}H_{12}$), namely dibenzochrysene (DBC) molecules, obtained by the addition of two benzene rings in different positions: dibenzo[b,def]chrysene ($C_{24}H_{14}$) which has angular morphology (angular DBC), and dibenzo[def,mno]chrysene ($C_{22}H_{12}$) which is compact in shape (compact DBC). All the molecules investigated, in both unsubstituted and substituted/functionalized forms, are schematically depicted in Fig.16 and 17.

We used Density Functional Theory (DFT)[53] and Time dependent DFT (TDDFT)[83] to quantify the effects of morphology and functionalization/substitution on the electronic, optical, and transport properties. In particular, we compared electron affinities, ionization energies, fundamental gap, optical absorption, and molecular reorganization energies for holes and electrons. For both TIPS functionalization and halogen substitutions, we found larger electron affinities (nearly tripled for perchlorinated molecules), and a lowering of the fundamental gap (up to 22%). For TIPS function-

alization we also observe a small lowering of the ionization energies while for the halogen substitutions these values increase up to ∼17%. The effect of perhalogenation and TIPS functionalization is always to increase molecular reorganization energies for both holes and electrons. Concerning the optical properties, we observe a red-shift of the optical onset in all cases; for TIPS-functionalization, in particular, we additionally found a remarkable enhancement of the absorption in the visible region.

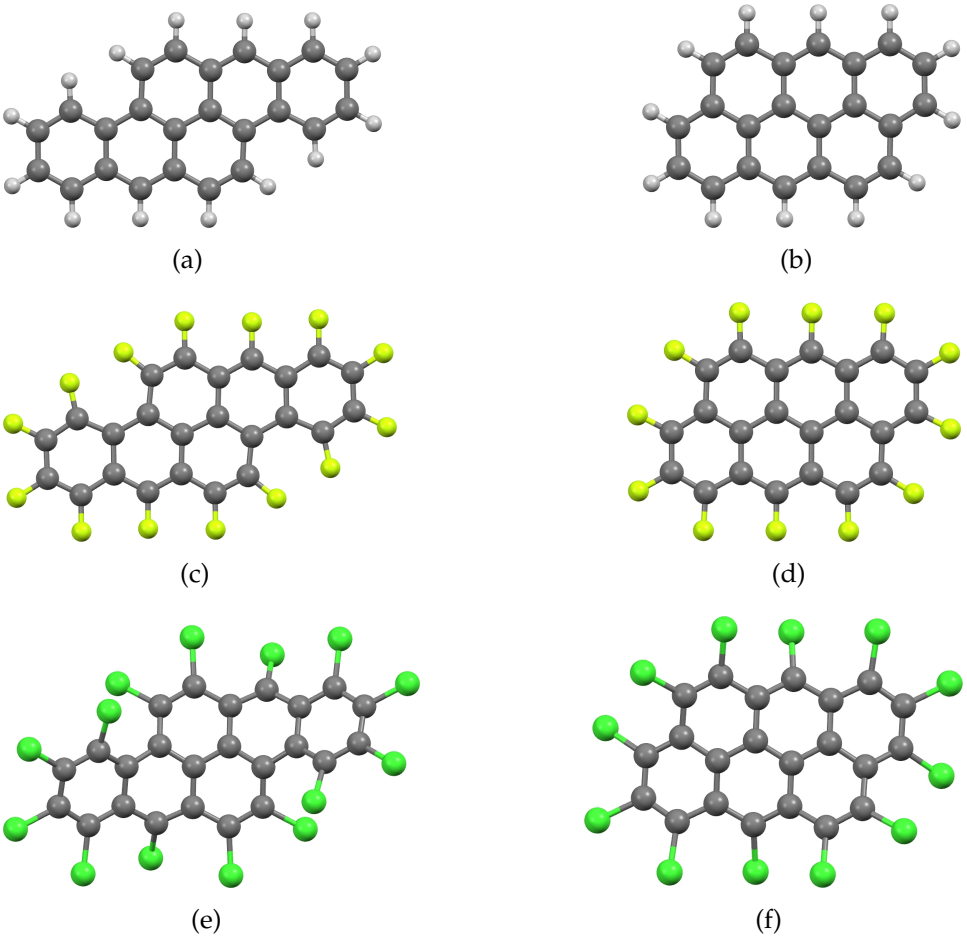

Figure 16: Sticks and balls representation of dibenzo[b,def]chrysene ($C_{24}H_{14}$) or angular DBC, (a), dibenzo[def,mno]chrysene ($C_{22}H_{12}$) or compact DBC, (b), and their perfluorinated [$C_{24}F_{14}$ (c); $C_{22}F_{12}$ (d)] and perchlorinated [$C_{24}Cl_{14}$ (e); $C_{22}Cl_{12}$ (f)] counterparts.

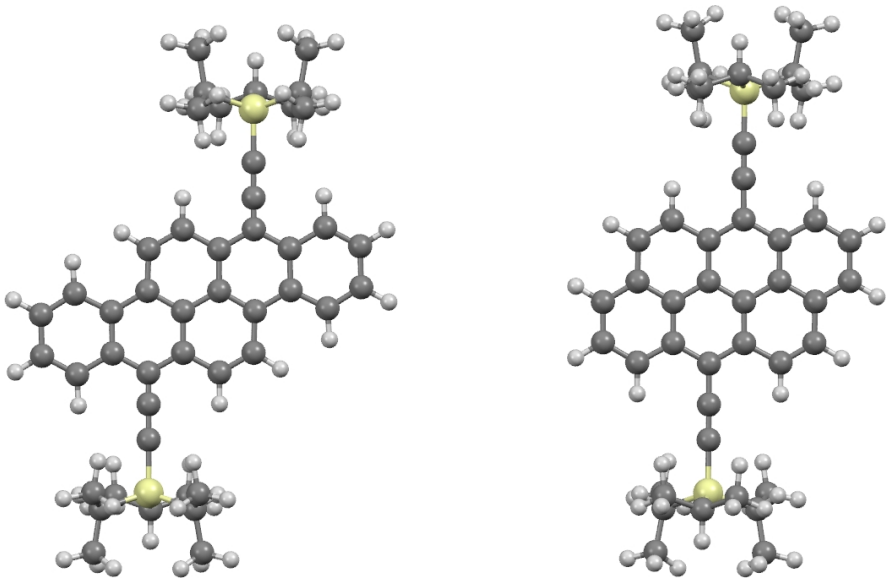

(a) (b)

Figure 17: Sticks and balls representation of TIPS-functionalized angular DBC (a) and TIPS-functionalized compact DBC (b).

3.1.1 *Assessment of the Computational Scheme*

The use of the B3LYP functional is rather standard and some limitations are well documented, such as the system-size-dependent errors found for the lowest short-polarized electronic transitions of oligoacenes[137]. As to the molecular properties of interest in this work, however, we have recently checked for different families of PAHs both the sensitivity of our calculations to different functionals, and their reliability in comparison with available experimental data[138,139]. With the only exception of the ionization energy and the fundamental gap, which were better described using the local-density approximation or range-separated functionals[140], we found that the hybrid B3LYP functional yields the overall best performance. To further asses this choice we performed additional benchmark calculations using the long-range corrected functionals CAM-B3LYP[141]and ωB97X-D[142]. Both methods have been devised to handle the wrong asymptotic behaviour of B3LYP which decays faster than $1/R$ for large distances R from the nuclei; the ωB97X-D scheme, moreover, includes empirical atom-atom dispersion corrections. Table 1 reports the comparison between B3LYP, CAM-B3LYP, and ωB97X-D for tetracene, pyrene, and chrysene, three prototypical PAHs with linear, compact, and angular morphology, respectively. We considered the three lowest electronic transi-

tions (usually described by Clars's notation *p*, *α*, *β*), vertical ionization energy IE_V, vertical electron affinity EA_V, fundamental gap E_{gap}, and exciton binding energy E_{bind}. Overall, the B3LYP functional yields the best agreement with the available experimental data. The only exceptions are again represented by ionization energy and fundamental gap, whose mean relative errors, however, are close to those found with the long-range corrected functionals (5 vs. 3% and 4 vs. 2%, respectively).

Besides the absolute values of the molecular properties of interest, this work aims also at quantifying how much these same quantities change upon chemical modification. We have therefore checked the comparison between B3LYP, CAM-B3LYP,and *ω*B97X-D in predicting the changes of selected properties of angular and compact DBC upon chemical modification. We found that the relative variations predicted by the different functionals follow similar trends. The main conclusions of this work, therefore,are not expected to vary considerably with respect to methodology issues.

As a further check we evaluated the effect of adding an empirical dispersion correction term[146] to the B3LYP functional (B3LYP-D) in the case of TIPS-functionalized species. For these molecules, in fact, long-range interactions between the TIPS group and the molecular core are expected to play a role. For both angular and compact DBC we indeed found a slight variation between the ground-state geometries optimized at B3LYP and B3LYP-D levels (root-mean-square-displacement less than 1Å). In particular, the two geometries differ for a rotation of $\sim 20^\circ$ of the TIPS group with respect to the plane of the molecule. The corresponding electronic properties (energies of the frontier molecular orbitals, IE_V, EA_V, and E_{gap}), however, are not greatly affected by these variations and found to be coincident within numerical errors.

Finally, while the performances of the B3LYP functional for the calculation of the molecular reorganization energy λ in conjugated materials can be improved by precisely calibrated DFT functionals[136,147], its use in the present work is justified since it is expected to describe reasonably the differences occurring upon TIPS-functionalization or halogen substitution.

Ground-state geometry optimizations were performed without symmetry constraints in all cases considered. The optimized structures obtained were then confirmed as being the true minima by performing the vibrational frequency analysis. The minimum-energy configurations of TIPS-functionalized and perfluorinated species were found to preserve the planar geometry of their parent molecules. On the contrary, for both angular and compact DBC, per-

Method	p	α	β	IE_V	EA_V	E_{gap}	E_{bind}
			Pyrene ($C_{16}H_{10}$)				
B3LYP	3.66	3.73	4.57	7.14	0.31	6.83	3.17
CAM-B3LYP	3.96	3.94	5.03	7.26	0.26	7.00	3.04
ωB97X-D	3.98	3.96	5.06	7.26	0.22	7.04	3.06
EXP	3.71	3.33	4.56	7.43	0.41	7.02	3.31
			Tetracene ($C_{18}H_{12}$)				
B3LYP	2.45	3.47	4.62	6.55	1.00	5.55	3.10
CAM-B3LYP	2.80	3.66	4.88	6.68	0.95	5.73	2.93
ωB97XD	2.85	3.69	4.92	6.68	0.89	5.79	2.94
EXP	2.62	3.12	4.55	6.97	1.07	5.90	3.18
			Chrysene ($C_{18}H_{12}$)				
B3LYP	3.80	3.73	4.60	7.25	0.19	7.06	3.26
CAM-B3LYP	4.17	4.04	5.03	7.45	0.07	7.38	3.21
ωB97X-D	4.20	4.06	5.09	7.45	0.01	7.44	3.24
EXP	3.87	3.44	4.64	7.60	0.40	7.20	3.33
			Mean realative error (%)				
B3LYP	3	11	1	5	28	4	3
CAM-B3LYP	7	18	9	3	43	2	7
ωB97X-D	8	18	10	3	54	2	6

Table 1: Comparison between B3LYP, CAM-B3LYP, and ωB97X-D (data in eV) for the lowest electronic transitions p, α, β, ionization energy IE_V, electron affinity EA_V, fundamental gap E_{gap}, and exciton binding energy E_{bind}. Experimental IE_V and EA_V, as well as B3LYP data, are taken from Ref. [143] Experimental electronic transitions are taken from Ref. [144] for tetracene, and from Ref. [145] for pyrene and chrysene.

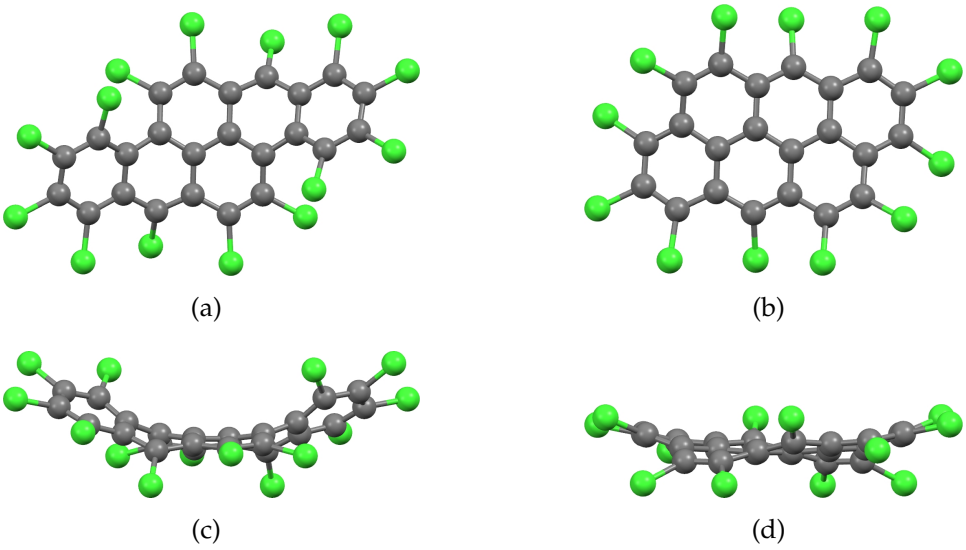

Figure 18: Top (a,b) and side (c,d) views of the optimized structures of pechlorinated angular DBC ($C_{24}Cl_{14}$, left) and perchlorinated compact DBC ($C_{22}Cl_{12}$, right))

chlorination breaks this planar symmetry (see top and side views in Fig.18). This effect appears to be more pronounced for angular DBC than for compact DBC, as shown by the computed root-mean-square-displacements (considering only the backbone Carbon atoms) of 0.7 and 0.3Å, respectively. The Cl atoms belonging to the same benzene ring remain on the same side (above or below the plane), while adjacent Cl atoms of different rings stay on opposite sides. Overall, for both angular and compact DBC, the peripheral Cl atoms are related by an inversion center. Note that similar findings have been previously found for chlorinated tetracene molecules[41]. In particular, 5,6,11,12-tetrachlorotetracene was predicted to adopt a "Z" shape form, in agreement with X-ray data.

3.2 ELECTRONIC PROPERTIES

In the present paragraph we consider the modifications of the electronic properties of DBC's. All the computed observables for both dibenzo[b,def]chrysene (angular DBC) and dibenzo[def,mno]chrysene (compact DBC) molecules, have been reported in Table 2, in their unsbubstituted, perfluorinated, perchlorinated, and TIPS-functionalized forms. A visual inspection of the changes occurring upon chemical substitution/functionalization is given in Figures 19 and 20.

	IE_A	EA_A	IE_V	EA_V	E_{gap}	E_{opt}	E_{bind}	λ_h	λ_e
Angular	6.39	1.11	6.45	1.03	5.42	2.67	2.75	0.12	0.16
Cl	7.01	3.02	7.12	2.90	4.22	1.94	2.27	0.22	0.23
F	7.35	2.51	7.47	2.39	5.08	2.36	2.72	0.25	0.26
TIPS	6.12	1.76	6.20	1.64	4.56	2.28	2.27	0.16	0.22
Compact	6.46	1.06	6.52	0.97	5.55	2.80	2.75	0.11	0.15
Cl	7.24	2.85	7.36	2.71	4.65	2.26	2.39	0.23	0.27
F	7.49	2.32	7.63	2.18	5.45	2.69	2.75	0.26	0.27
TIPS	6.17	1.70	6.25	1.59	4.66	2.40	2.26	0.16	0.21

Table 2: Physical observables in comparison between unsubstituted, perchlorinated, perfluorinated, and TIPS-functionalized angular and compact DBC molecules. Adiabatic and vertical ionization energies (IE_A, IE_V), adiabatic and vertical electron affinities (EA_A, EA_V), fundamental gaps (E_{gap}), first optically active transition (E_{opt}), exciton binding energy (E_{bind}), and molecular reorganization energies for holes and electrons (λ_h, λ_e) have been computed at the B3LYP/6-31+G* level. All values are given in eV.

We first consider the comparison between angular and compact unsubstituted molecules. The ionization energy IE of compact DBC is slightly larger (∼1%) as compared to that of angular DBC. The situation is reversed for the electron affinity EA which is larger (∼5%) for angular DBC. As a consequence, the corresponding fundamental gaps E_{gap} are nearly coincident, 5.42(5.55) eV for the angular(compact) case, respectively. The slighlty larger value for the latter case (0.13 eV, an increase of ∼2%) can be attributed to the more localized nature of compact DBC. Since the optical absorption onset E_{opt} follows the same trend of E_{gap} (see discussion in the next Section), being slightly higher for compact DBC, the resulting exciton binding energies E_{bind} turn out to be nearly coincident (2.75 eV).

We now move to the effect of chemical modifications. As shown in Table 2, for both angular and compact DBC TIPS functionalization reduces slightly the IE (∼4%), increases considerably the EA (∼60%), lowers the E_{gap} (∼16%), and reduces the E_{bind} (∼18%); the latter effect being due to a 15% reduction of E_{opt} (see Figure 21 and discussion in the next Section). On the other hand, the effect of complete halogenation for both compact and angular DBC is to increase both IE and EA and, consequently, lower the fundamental gap E_{gap}. Upon fluorination, a sizeable rise of the IE (∼1.0-1.1

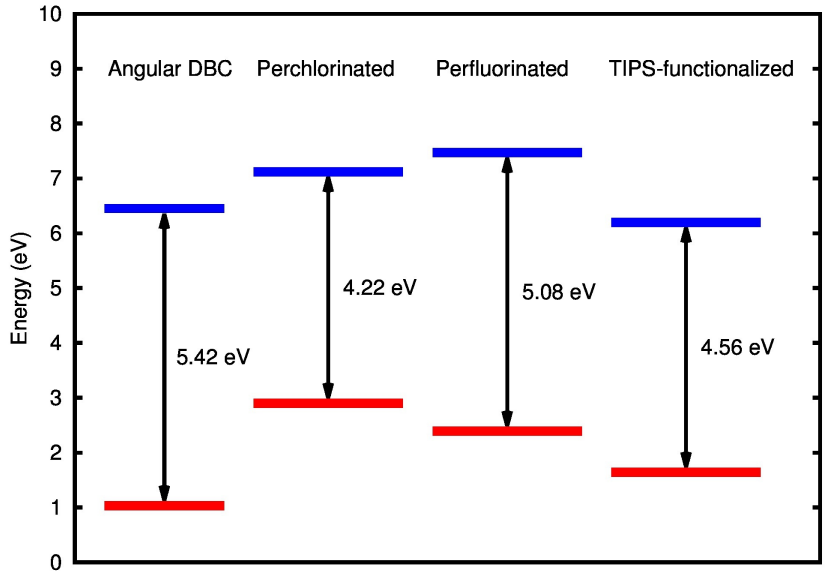

(a)

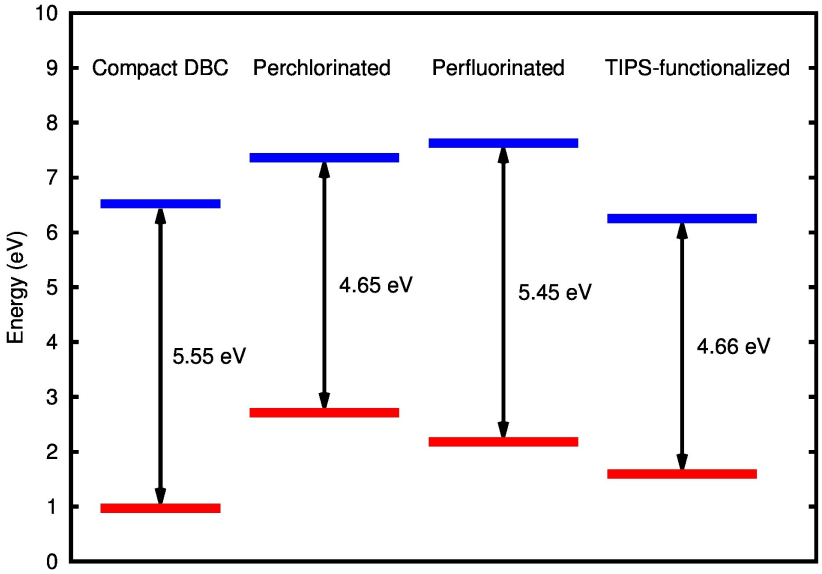

(b)

Figure 19: Vertical ionization energies (blue lines), vertical electron affinities (red lines) and fundamental gap (black arrows) for angular DBC (a), compact DBC (b) and their perhalogenated and TIPS-functionalized counterparts.

eV, %15) and a still larger increase of the EA (∼1.3-1.4 eV) is observed in both cases, which results in a reduction of E_{gap} by about 0.3(0.1) eV for angular(compact) DBC, respectively. Similarly to the case of the unsubstituted molecules, since E_{opt} is reduced by almost

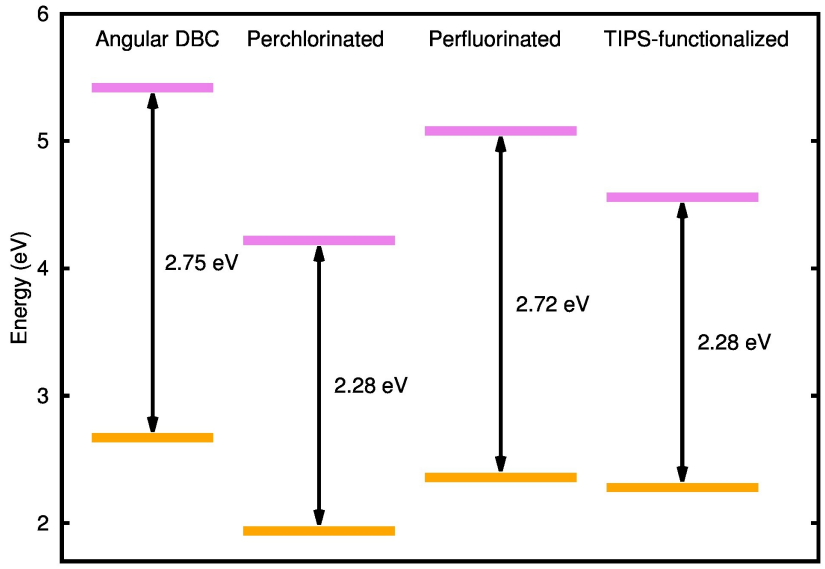

(a)

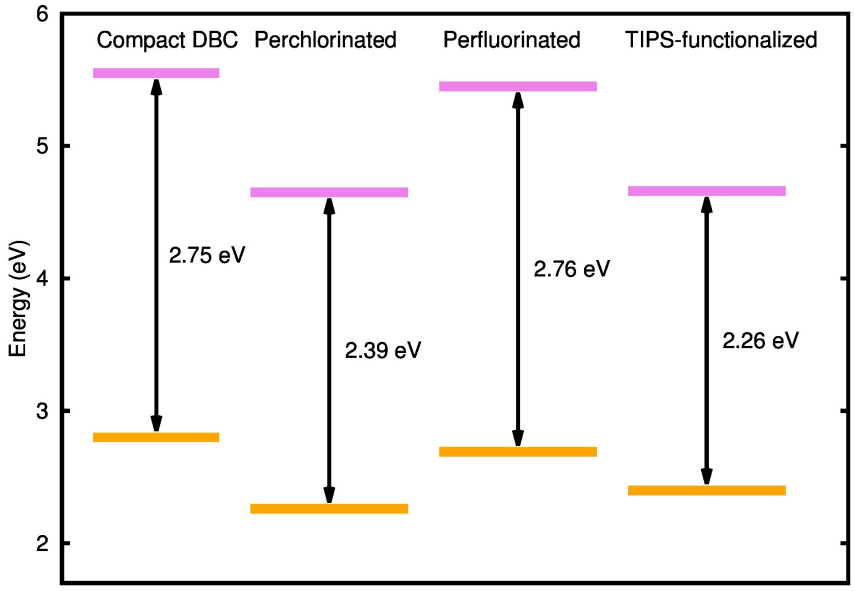

(b)

Figure 20: Fundamental gap (violet line), optical onset (orange line) and exciton binding energies (black arrows) for angular DBC (a), compact DBC (b) and their perhalogenated and TIPS-functionalized counterparts.

the same amount as E_{gap}, the corresponding E_{bind} turn out to be almost unaffected by perfluorination. Following perchlorination, the IE increases by ∼0.6-0.8 eV (∼10%) for angular and compact DBC, respectively. An even larger increase of the EA is observed also in

this case (∼1.7-1.9 eV), which results in a severe reduction of E_{gap} by about 0.9(1.2) eV for the compact(angular) perchlorinated molecule. Since E_{opt} is more redshifted for perchlorination than for perfluorination (see next Section), at variance with the latter case we observe a reduction of E_{bind} by 0.4-0.5 eV in comparison with the parent molecules. By comparing the effects of halogen substitutions, we found that the EA increases more than IE either for F- and for Cl-, in both angular and compact DBC. This effect is found to be more pronounced for Cl- than for F-substitution which in turn yields smaller fundamental gaps for the former case. Our findings are consistent with previous results for Cl- and F-substituted pentacenes[27] and can be attributed to the larger electron withdrawing tendency of Cl with respect to F[27,148].

Summing up, ionization energies are found to be enhanced following halogen substitution, and reduced for TIPS functionalization. On the other hand, we found larger electron affinities for all substitutions/functionalizations, in the order Cl-, F-, TIPS-modification. Notably, the EA of perchlorinated molecules are nearly tripled with respect to their parent molecules for both angular and compact morphologies. In both compact and angular DBC, the above trends reflect in a general reduction of the fundamental gap upon chemical modification.

3.2.1 *Charge Transport Properties*

In this section we present the study of transport properties of functionalized DBC's only relatively to a single transport parameter: λ. For the full treatment, see Chapter 5. Concerning transport properties, the molecular reorganization energies for holes and electrons (λ_h, λ_e) reported in Table 2 are visually sketched in Fig. 21. We found that λ_h and λ_e are very similar for the two unsubsituted DBC. The compact molecule appears to be slightly better for both hole and electron transport; this fact agrees with previous studies showing the good transport properties of compact PAHs[139,147]. The effect of perhalogenation and TIPS functionalization is always to increase both λ_h and λ_e, which results in a worsening of the transport properties for all cases considered. In particular, for both angular and compact DBC, λ_h appears to be more affected than λ_e in all cases. In addition, larger increases are observed upon halogen substitution with respect to TIPS functionalization. As an example, in the case of compact DBC, while F substitution gives rise to an increase of about 140% (80%) for λ_h (λ_e), respectively, for the TIPS case we observe an increase of about 45% (40%) for the same quantities.

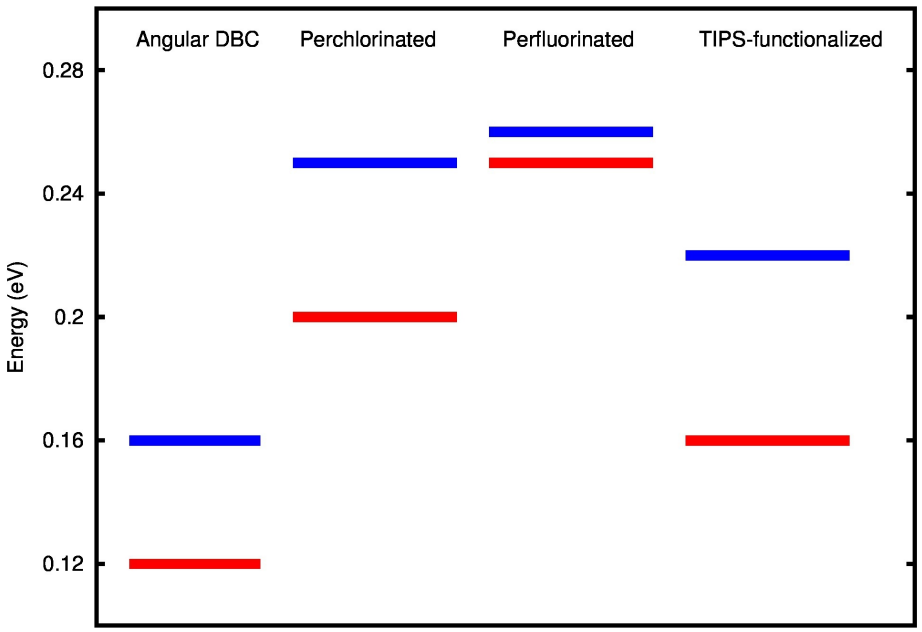

(a)

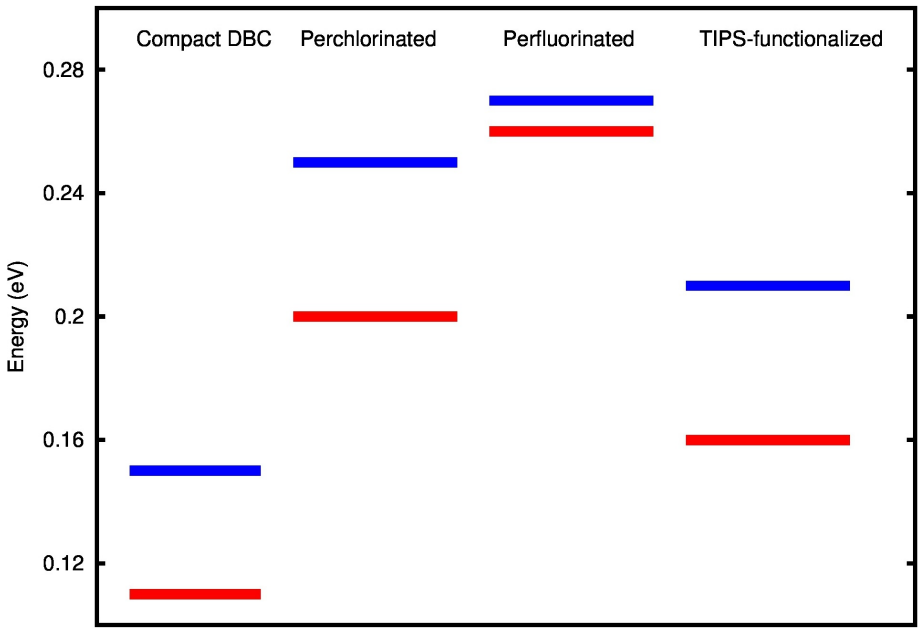

(b)

Figure 21: Molecular reorganization energies for electrons (blue line) and holes (red line) for Angular DBC (a), Compact DBC (b) and their perhalogenated and TIPS-functionalized counterparts.

3.3 OPTICAL PROPERTIES

Figure 22 displays the comparison between the absorption spectra of unsubstituted and functionalized DBC molecules in the

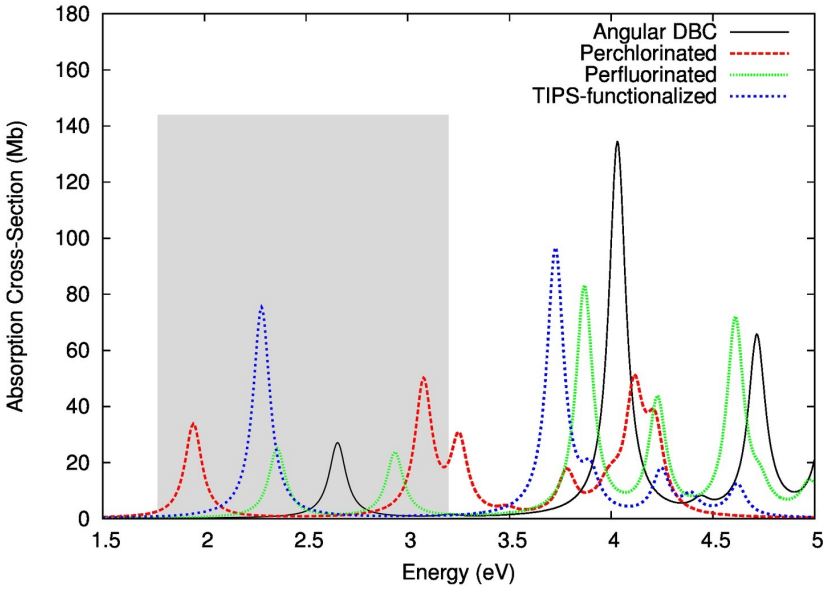

(a)

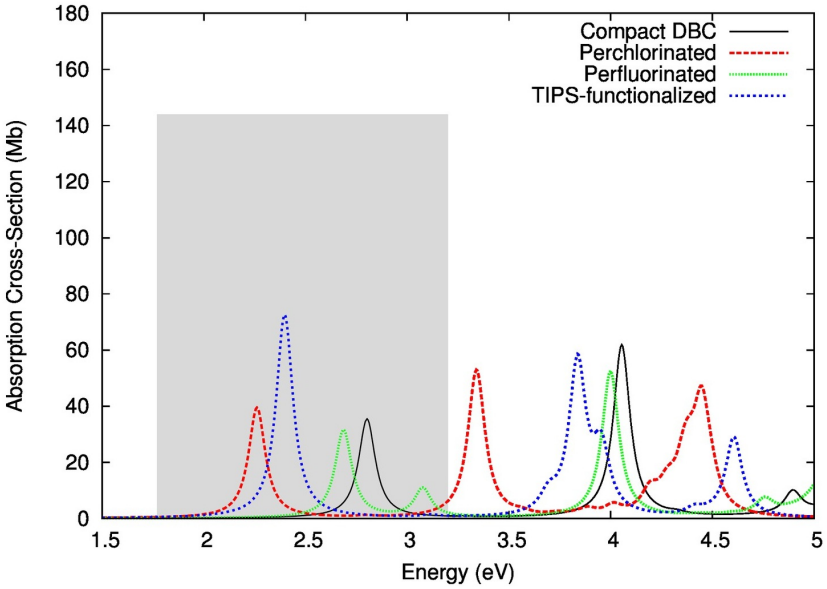

(b)

Figure 22: Absorption spectra of angular DBC (left) and compact DBC (right) for the unsubstituted (black line), perchlorinated (red line), perfluorinated (green line), and TIPS-functionalized (blue line) molecules; the light gray area represents the visible region. The absorption cross-sections are expressed in Megabarns (1 Mb = 10^{-18} cm^2).

visible/near-UV region up to about 5 eV, as given by B3LYP/6-31+G* TDDFT calculations. The absorption spectrum of angular DBC is characterized by the presence of three peaks, the first one

in the visible region (2.7 eV), a stronger peak at about 4.0 eV, and another transitions at 4.7 eV. The absorption spectrum of compact DBC shows only two absorption peaks in the same region, at about 2.8 and 4.1 eV, in order of increasing intensity. The effect of perfluorination for angular DBC is the replacement of the original 2.7 eV peak with two new bands with similar intensity at 2.4 and 2.9 eV. Also the main peak at 4.0 eV is splitted in two weaker peaks at 3.9 and 4.2 eV respectively, while the third one is red-shifted by about 0.1 eV. Perfluorination of compact DBC produces a slight redshift of the whole spectrum, with the additional occurrence of a weak band at about 3.1 eV. Consistently with previous TDDFT calculations for TIPS-functionalized oligoacenes[149], the effect of TIPS functionalization is to redshift the whole spectrum and to greatly enhance the absorption in the visible region. In particular, the new absorption onset appears at 2.3 eV and 2.4 eV for angular and compact DBC, respectively, with a redshift of about 0.4 eV with respect to the unsubstituted molecule in both cases. Finally, the effect of perchlorination produces again a redshift of the absorption spectrum, which is the largest one as compared to the other modifications. In particular, the absorption onset is found to be redshifted by $\sim$0.7 and 0.5 eV for the angular and compact cases, respectively. In addition, while an almost rigid shift of the spectrum occurs for the compact case, a more complex pattern with two additional substructures at 3.1 and 3.3 eV is observed for the angular perchlorinated molecule. Overall, for both angular and compact DBC, halogen substitution and TIPS-functionalization give rise to a redshift of the absorption onset which reflects the fundamental gap reduction predicted by ΔSCF calculations.

3.4 CONCLUSIONS

We presented a systematic comparative study of dibenzo[b,def]chrysene (angular) and dibenzo [def,mno]chrysene (compact) in their unsubstituted, halogen-substituted (F, Cl), and TIPS-functionalized forms. By combining DFT and TDDFT calculations performed at the B3LYP/6-31+G* level, we computed ionization energies, electron affinities, fundamental gap, exciton binding energies, and molecular reorganization energies for both holes and electrons. We found larger electron affinities for all functionalizations, in the order Cl, F, TIPS. Ionization energies are found to be enhanced following halogen substitution, and reduced for TIPS functionalization. In both compact and angular molecules, the above trends reflect in a general reduction of the

fundamental gap upon chemical modification. Transport properties, in relation to λ, appear to worsen in all cases, as shown by the increase of the molecular reorganization energies due to chemical modification. As for the optical absorption spectra, substitution/-functionalization reshifts the onset energy in all cases. In addition, the modified molecules display more structured spectra in terms of higher intensities (TIPS) and number of transitions falling in the visible/near-UV range (F, Cl). The exciton binding energy are reduced in the Cl and TIPS functionalized molecules and nearly unchanged for the F substitution. Our systematic quantitative evaluation of the effect of morphology and functionalization on the electronic, optical, and transport properties of dibenzochrysenes can help in the choice of the best candidate molecule in the design of new optoelectronic devices based on such compounds.

4

FROM MOLECULAR TO BULK PROPERTIES. THE CASE OF HEXATHIAPENTACENE

Contents

4.1 INTRODUCTION

As previously seen in the general introduction polycyclic aromatic hydrocarbons (PAHs) are being largely used as active components in different kind of devices such as organic field effect transistors (OFETs), organic light emitting diodes (OLEDs), and organic photovoltaic (OPV) cells[22]. Linear acenes, in particular, are *p*-type semiconductors with good transport properties and are commonly employed as hole-transporters in OFETs[23–25]. These devices consist of either single or multiple semiconducting parts which are usually assembled in layered (e.g., OFETs and OLEDs) or blended (e.g., OPV-bulk heterojunction) arrangements[150]. Small molecules offer several advantages in comparison to polymers: they can be easily purified by different techniques and processable by both evaporation and solution processing methods[26]. In addition, the electronic, optical and transport properties of small molecules can be fine-tuned via chemical modification or the addition of specific functional groups to the conjugate core[25,28–31]. For example, the modification with strong electronegative substituents is an effective approach for converting *p*-type organic semiconductors to *n*-type[25,32].

To produce bipolar transistors, it would be ideal to have both *n*-type and *p*-type organic semiconductors with similar physical and electrical properties[33,34]. In the case of PAHs, however, despite the successes with hole transport, it has turned out to be more difficult to achieve *n*-type transport (e.g., pentacene OFETs exhibit hole mobilities up to 5 $cm^2/(V \cdot s)$[23] and electron mobilities

of 0.04 $cm^2/(V \cdot s)$[33]). Typically, *n*-type materials based on PAHs are obtained by attaching to the conjugate core strong electron-withdrawing groups such as CN[35], or by replacing the peripheral H with halogen atoms (in particular F and Cl)[34,36]. The decreased lowest unoccupied molecular orbital allows electron injection by lowering the charge injection barrier.

Besides the intrinsic semiconductor charge mobility, the device performances are strongly dependent on crystal structure and thin-film morphology. These issues have been therefore extensively addressed in the literature, especially for non-functionalized and functionalized linear acenes and heterocyclic derivatives.[37–40,151] In particular, the face-to-face π-stacking motif is believed to be more efficient for charge transport than the edge-to-face herringbone-packing structures typical of organic semiconductors such as pentacene, rubrene etc.[23,152]. It is known that the tendency to form face-to-face stacked structures can be enhanced by adding peripheral substituents[23,47]. Inspired from studies on tetrathiafulvalene (TTF) derivatives whose transport properties are enhanced by the presence of S-S interactions[153,154], some groups have started introducing S atoms in the periphery of oligoacenes in order to provide an alternative charge transport pathway other than the "natural" π-π one[47,155].

Calculations of the electronic, optical, and transport properties of the building blocks of organic semiconductors can contribute to understand their properties and can provide guidelines for future dedicated researches[28,30]. The aim of this chapter of this Thesis is to theoretically evaluate the effect of a speific S-functionalization on the electronic, optical and transport properties of linear PAHs in the molecular and in the crystalline phase. We consider hexathiapentacene (HTP, $C_{22}H_8S_6$), a derivative of pentacene (PNT, $C_{22}H_{14}$) obtained by the symmetric substitution of 6 central H with S atoms (a representation of the two molecules is given in Fig. 23). We use Density Functional Theory (DFT)[53] and Time dependent DFT (TDDFT)[83] to determine the effects of this particular substitution on the electronic, optical, and transport properties of the molecules. In particular, we compare electron affinities, ionization energies, quasi-particle gap, optical absorption and molecular reorganization energies for holes and electrons. Finally, we also investigate the electronic properties HTP and PNT molecular crystals within the DFT framework either in the ground state and in the excited one.

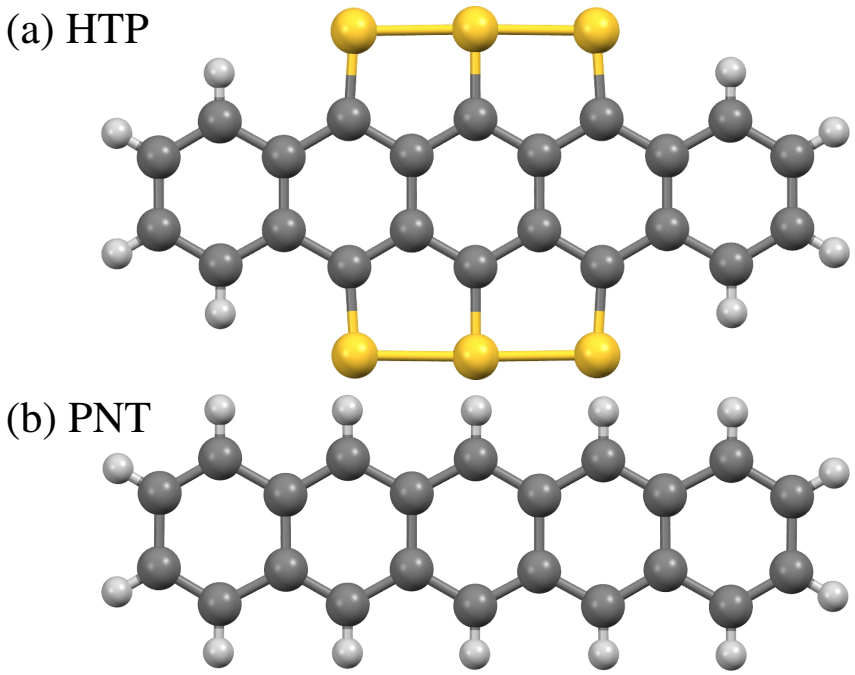

Figure 23: Ball-and-stick representation of (a) hexathiapentacene (HTP) [$C_{22}H_8S_6$] and (b) pentacene (PNT) [$C_{22}H_{14}$] molecules.The C, S, and H atoms are represented in grey, yellow, and white, respectively.

4.1.1 *Assessment of the Computational Scheme*

For the molecules, DFT calculations have been performed using the NWChem package[156]. Following previous works[138,139,144,157] geometry optimization has been carried out using the hybrid exchange-correlation functional B3LYP[75], in combination with the 6-31+G* basis-set, a valence double-ζ set augmented with d polarization functions and s and p diffuse functions. The equilibrium C-S distance was found to be 1.72 Å (1.75 Å for the central S atoms), this corresponds to an increase of 58% (61%) with respect to the corresponding C-H bond length in the PNT molecule. The other C-C and C-H lengths in the S-substituted molecules remained unchanged.

The adiabatic electron affinities and ionization energies have been calculated via total energy differences. The vertical ionization energies (IE_V) and electron affinities (EA_V) have been evaluated at the relaxed geometry of the neutral molecules. This procedure enabled the calculations of the quasi-particle gap which is rigorously defined in the ΔSCF scheme as[80,81]:

$$E_{\text{gap}} = \text{IE}_V - \text{EA}_V = (E_{N+1} - E_N) - (E_N - E_{N-1}), \qquad (79)$$

E_N being the total energy of the N-electron system.

Using TDDFT, the excitation energies and the electronic absorption spectra in the visible/near-UV regions have also been obtained. The calculations were performed with the NWChem package adopting the same level of theory B3LYP/6-31+G*. We used the frequency-space implementation based on the linear response of the density matrix, in which the poles of the linear response function correspond to vertical excitation energies and the pole strengths to the corresponding oscillator strengths. Knowing the first optically active transition E_{opt}, the exciton binding energy have been estimated through the difference $E_{\text{bind}} = E_{\text{gap}} - E_{\text{opt}}$.

The DFT and TDDFT calculations are corroborated by many-body perturbation theory (MBPT) calculations within the *GW* and Bethe-Salpeter equation (BSE) formalisms,[92] using the same geometries and basis set as that used at the DFT/TDDFT level. Our *GW*/BSE calculations are performed with the Fiesta package[158–160] and take as an input the same B3LYP/6-31+G* Kohn-Sham eigenstates as generated by the NWChem package, allowing comparison with the TD-B3LYP calculations on equal footing. Following a recent benchmark study of the optical absorption energies of a large standard set of organic molecules[160], we perform partially self-consistent *GW* calculations, namely reinjecting self-consistently the corrected quasiparticle energies in the construction of the Green's function *G* and the screened Coulomb potential *W*. This was shown to lead to an excellent agreement with the so-called "best theoretical estimates" provided by high-level quantum chemistry techniques[160]. Our BSE calculations are performed beyond the Tamm-Dancoff approximation, namely mixing excitations and de-excitations. More details about the methodology can be found in Ref.[160].

Conductivity in organic molecular semiconductors is known to occur via a hopping mechanism in which charge carriers jump between adjacent molecules, usually under the effect of an external applied field. This process, treated within the semiclassical Marcus theory, is described by associating to electron transfer an overall rate constant proportional to $\exp\left[-\lambda/(4k_{\text{B}}T)\right]$ (where k_{B} is the Boltzmann constant and T the temperature[110,136]). The quantity λ, the molecular reorganization energy or intramolecular coupling, affects critically the charge-transfer process: low values of the reorganization energy imply high transfer rates. λ can be computed via the "four-point method" as the sum of two contributions[110,136] (for more details see Eq. 59 in Sect. 2.4).

In the present paper we present results also on the electronic and optical properties of PNT and HTP in the solid phase, i.e. in the corresponding molecular crystal structures. For the corresponding

PNT and HTP solid phases, all DFT calculations have been performed with the ABINIT code[161–163]. We relaxed both the atomic positions and the cell parameters by minimizing the forces acting on the atoms (reaching less than 1 meV/Å) and the stresses (reaching less than 1 kPa). The relaxed cell parameters (reported in Table 3) are in excellent agreement (with an average error smaller than 1% the experimental values taken from Refs. 151 and 47 for PNT and HTP, respectively). Their unit cells are characterized by the triclinic space group $P\bar{1}$ and contain two molecules. They are displayed in Fig. 24.

PNT and HTP show very similar H-H bonds (see distances d_1 and d_2 in Fig. 24) connecting the molecules along the long molecular axes. In contrast, the bonding between molecules in the other two directions is very different in PNT and HTP. In the former, H atoms are connected to C atoms (distances d_3 and d_4); while, in the latter, S-S bonds are formed leading to a very different arrangement of the molecules in the two crystals. Both PNT and HTP exhibit a herringbone pattern with herringbone angles θ of 50°. Three more angles are used to describe the orientation of the molecules inside the crystal: δ, the angle between the long molecular axes, χ_1 and χ_2 the angles between each long molecular axis and the reciprocal lattice vector $\mathbf{c}^*$ (which is perpendicular to lattice vectors **a** and **b**). In PNT, the long molecular axes of the molecules are nearly parallel to each other (δ is almost zero). This is very different in HTP for which δ=25°. The values of χ_1 and χ_2 are also very different in both cases.

The particular π-stacking structure of HTP can be ascribed to the sulfur atoms which prevent the edge-to-face interactions of the molecular units of PNT. In fact face to face stacking, which is believed to be more efficient in transport that the herringbone one, has been proven to be favored with added peripheral subsittuent atoms.[47] Moreover a short S-S atoms distance results which can be ascribed to the electrostatic intermolecular attraction between the partial positive charge of the outer S atoms with the partial negative charge of the central S atom of neighboring molecules.[47]

We employed Troullier-Martins pseudopotentials[164] and a plane-wave expansion of the wavefunctions using an energy cutoff E_{cut} of 50 Ry. The Brillouin zone (BZ) was sampled using a 4×4×4 grid. The exchange-correlation (XC) energy was approximated using the the PBE[72] generalized gradient approximation functional with the addition of the Grimme semiempirical D3 long-range dispersion correction[165] combined with Becke-Jonson damping[166].

For the electronic band structures, the electronic properties relying on the DFT eigenvalues lead to a well known underestimation

Table 3: Theoretical and experimental lattice parameters for the solid phases of hexathiapentacene [47] and pentacene [151].

	a (Å)	b (Å)	c (Å)	$\alpha(^\circ)$	$\beta(^\circ)$	$\gamma(^\circ)$
HTP						
PBE	3.875	14.263	16.465	72.865	89.087	84.157
Expt.	3.894	14.334	16.551	72.458	88.886	84.169
PNT						
PBE	6.231	7.656	14.427	76.862	88.087	84.451
Expt.	6.266	7.775	14.530	76.475	87.682	84.684

of the band gap in particular with semilocal functionals such as PBE. MBPT calculations should in principle be performed. But this task is very demanding and beyond the scope of our study. Hybrid functionals have been proposed as a cheaper alternative approach to cure the band-gap problem. In recent studies[167,168], it was pointed that the inverse of the macroscopic dielectric constant provides a "reasonable" value for the fraction of exact exchange to be included in the hybrid functional. In organic crystals such as HTP and PNT, the typical dielectric constant is of the order of 4 to 5, leading empirically to 20 or 25% of exact exchange. This points to the well-known B3LYP functional that contains 20% of exact exchange. In the spirit of the single-shot G_0W_0 formalism, we have therefore performed a perturbative B3LYP correction to the PBE electronic energies $\varepsilon_{n\mathbf{k}}^{\mathrm{PBE}}$ as:

$$\varepsilon_{n\mathbf{k}}^{\mathrm{B3LYP}} = \varepsilon_{n\mathbf{k}}^{\mathrm{PBE}} + \langle \psi_{n\mathbf{k}}^{\mathrm{PBE}} | V_{\mathrm{xc}}^{\mathrm{B3LYP}} - V_{\mathrm{xc}}^{\mathrm{PBE}} | \psi_{n\mathbf{k}}^{\mathrm{PBE}} \rangle, \tag{80}$$

assuming that the PBE $\psi_{n\mathbf{k}}^{\mathrm{PBE}}$ are very close to the B3LYP ones.

Notice that the use of B3LYP exchange-correlation (XC) functional both for the solid and molecular phases of PNT and HTP permits us to treat XC effects for consistency on the same footing for the two phases.

4.2 MOLECULAR ELECTRONIC PROPERTIES

Table 4 reports all the computed observables for HTP and PNT molecules together with the corresponding experimental data when available.

The difference between theory and experiments is always under 8% showing the accuracy of the computational procedure adopted.

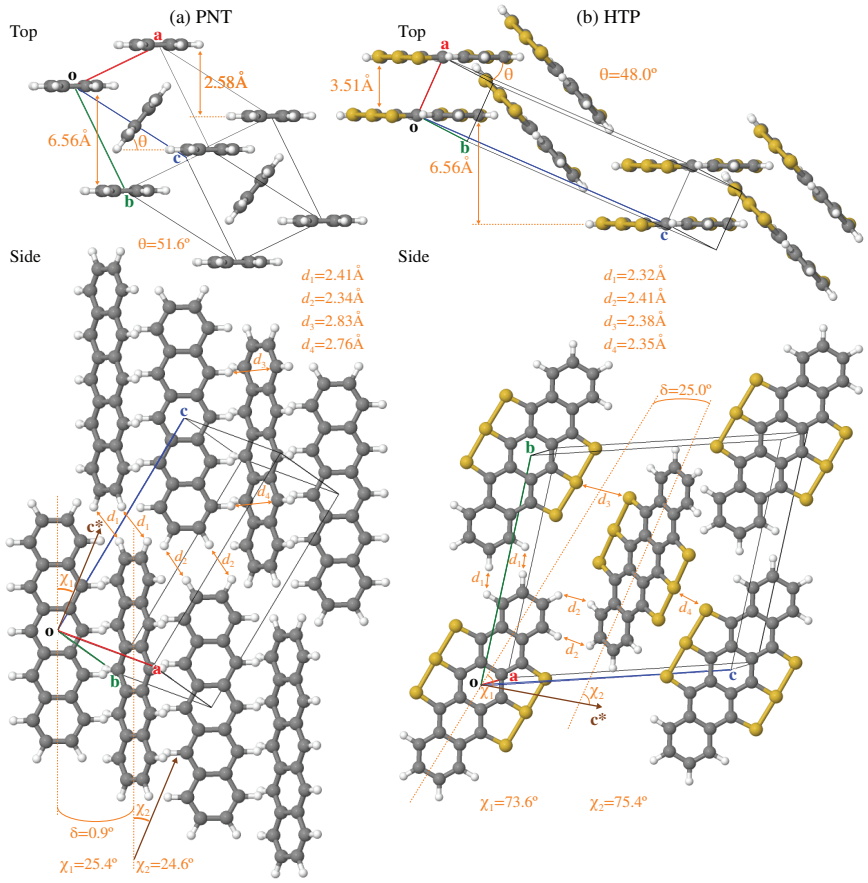

Figure 24: Ball-and-stick representation of the unit cells of crystalline (a) HTP and (b) PNT. In the upper panels, the top view is reported parallel to the vector orthogonal to the two directions normal to the molecules. In the lower panels, the side view is generated such that one of the two molecules is in the plane. Various distances and angles (see text) are reported directly in the figure. Only selected repeated images are reproduced in order to ease the visual perception. The C, S, and H atoms are represented in grey, yellow, and white, respectively.

For the absolute IP (or AE) values, the aug-cc-pVTZ basis had to be used for the *GW* calculations. Indeed, they converge more slowly with basis size as compared to ΔSCF DFT calculations. Explicit comparisons between the 6-31+G* and aug-cc-pVTZ *GW* values confirm however that the (HOMO-LUMO) gap is converged within 10 meV at the 6-31+G* level, indicating that occupied/unoccupied states are affected very similarly by basis set changes.

With respect to the parent molecule the HTP shows an increase of the ionization energies (IE) by 10% (∼0.6 eV for both the adiabatic and vertical quantities) and a sensible rise of the electron affinities (EA) up to 60% (about 0.86 eV for both vertical and adiabatic quanti-

Table 4: Calculated observables for HTP and PNT molecules: adiabatic and vertical electron affinities (EA_A, EA_V) and ionization energies (IE_A, IE_V), quasi-particle corrected HOMO-LUMO gaps (E_{gap}), molecular reorganization energies for holes and electrons (λ_h, λ_e). The experimental data from HTP and PNT are from Refs. [47] and [139]. All values are given in eV.

	IE_A	IE_V	EA_A	EA_V	E_{gap}	E_{opt}	E_{bind}	λ_h	λ_e
HTP									
B3LYP	6.70	6.76	2.34	2.27	4.49	1.79	2.70	0.13	0.14
GW	–	6.78	–	2.35	4.44	1.56	2.88	–	–
Expt.		–		–	–	1.61	–	–	–
PNT									
B3LYP	6.12	6.16	1.48	1.41	4.75	1.91	2.84	0.09	0.13
GW	–	6.42	–	1.48	4.95	1.84	3.11	–	–
Expt.		6.59		1.39	5.20	1.91	2.89	0.10	–

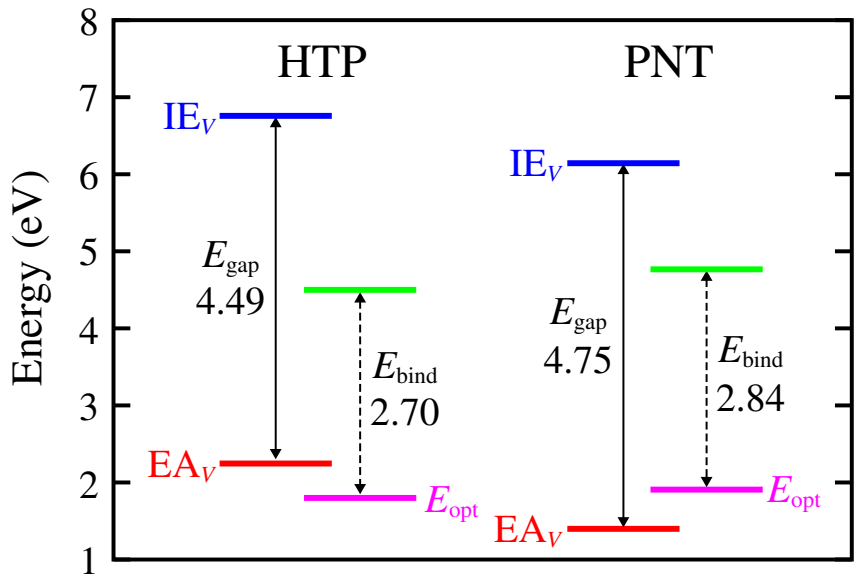

Figure 25: Schematic representation of the electronic and optical properties of the HTP and PNT molecules. The vertical ionization energies (IE_V) and electron affinities (EA_V) are indicated by blue and red lines, respectively, with the quasiparticle gap (E_{gap}) represented by the solid arrows. The optical onsets (E_{opt}) are reported using solid magenta lines and the exciton binding energies (E_{bind}) are indicated by the dashed arrows.

ties). The quasi-particle gap (E_{gap}) is consequently reduced by 5.5% (0.26 eV). The optical absorption onset (E_{opt}) is found to be red-shifted by about 6% (0.12 eV). The difference between this quantity and the E_{gap} provides an estimate of the exciton binding energy (E_{bind}) which appears to be reduced by 5% (0.14 eV).

Since molecular reorganization energies are found to increase for both holes and electrons after the substitution by S atoms, a worsening of those transport properties depending of these particular parameters could be expected.

The effect appears to be more pronounced for p-transport (λ_h rises by 41%, 0.04 eV) than for n-transport (λ_e increases by only 8%, 0.01 eV).

4.3 MOLECULAR OPTICAL PROPERTIES

Figure 26 displays the absorption spectra in the visible region (in the energy range from 1.5 to 3.75 eV) of HTP and PNT as computed using the frequency-space implementation of TDDFT in NWCHEM.

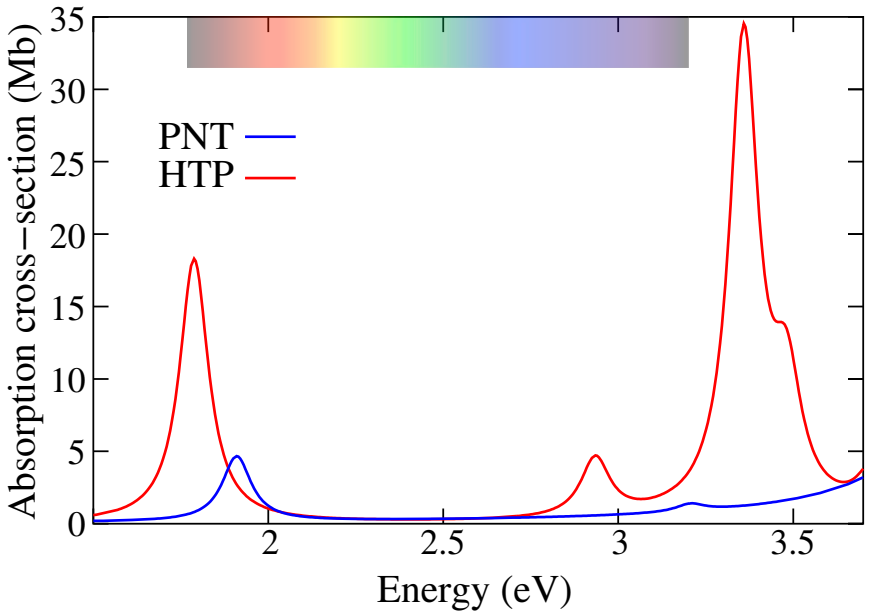

Figure 26: (Color online) Comparison between the computed TDDFT absorption cross section (in Mb) of molecular PNT (blue solid line) and HTP (red solid line) as a function of energy (in eV).

For the energy-range considered, PNT shows only a very small absorption peak (4.7 Mb) at 1.91 eV and results almost inactive in the remaining part of the visible range. At variance with PNT, HTP shows a redshift of the optical onset (with a reduction of -0.12 eV) with an enhancing of this absorption structures, the amplitude of

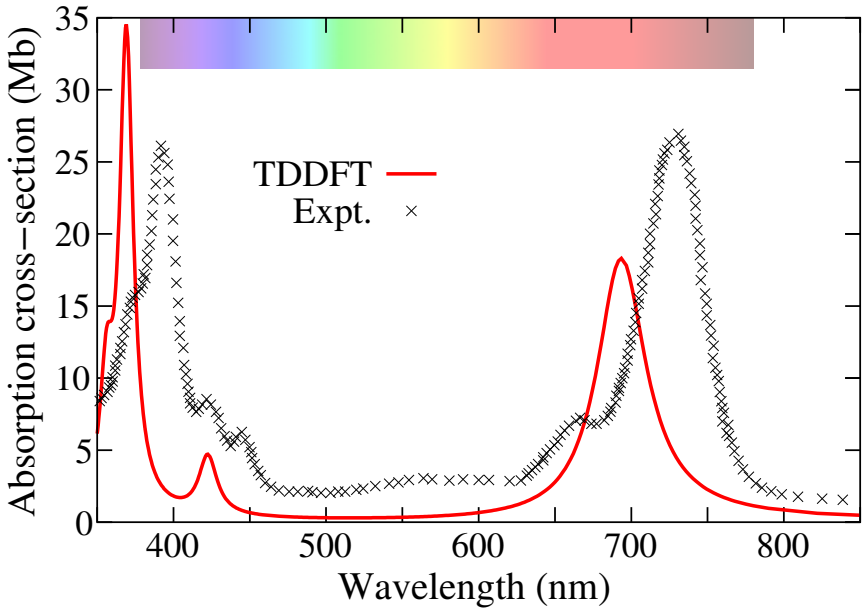

Figure 27: (Color online) Comparison between the computed TDDFT (red solid line) and experimental (black crosses) absorption cross section (in Mb) of molecular HTP as a function of the wavelength (in nm). The experimental data are taken from Ref. [47].

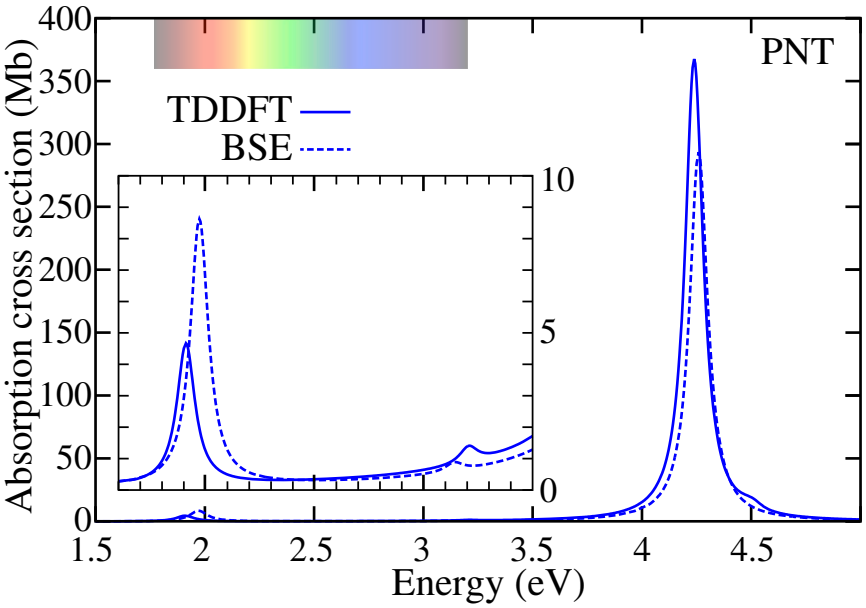

Figure 28: (Color online) Comparison between the computed TDDFT (blue solid line) and BSE (blue dashed line) absorption cross section (in Mb) of molecular PNT as a function of the energy (in eV).

which rises up to 18 Mb. A second small absorption peak (4.7 Mb of amplitude) appears at the upper side of the visible region (more specifically at 2.93 eV). The substituted compound shows his most

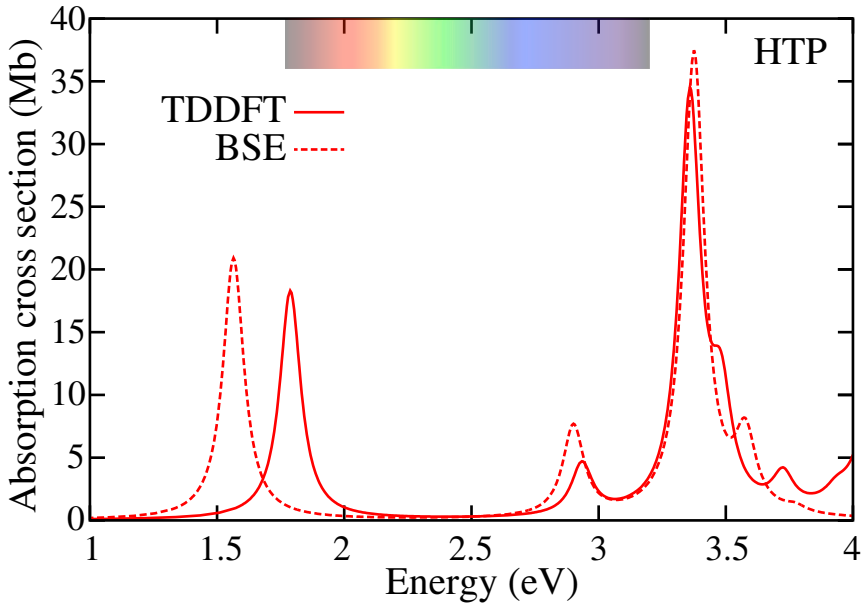

Figure 29: (Color online) Comparison between the computed TDDFT (red solid line) and BSE (red dashed line) absorption cross section (in Mb) of molecular HTP as a function of the energy (in eV).

important absorption structure at the lower edge of the near UV region. This structure presents a main peak (34.5 Mb of amplitude) at 3.35 eV and a shoulder (13.9 Mb) at 3.46 eV.

With respect to the unsubstituted molecule, the HTP globally presents an increasing of absorption in the visible region, due to a combination of increased amplitude of the first absorption peak and a new structure at the upper edge of the visible region. The S-functionalized molecule also presents his most important absorption peak in the very near UV range of energies, in which pentacene does not shows absorption peaks.

Figure 27 shows the comparison between our TDDFT calculated spectrum and the experimental absorption spectrum of hexathiapentacene taken in solution with 1,12-dichlorobenzene at 100 °C[47]. We found good agreement in terms of the position of the main absorption peaks. The differences between the two plots (in particular the redshift of the experimental curve with respect to the calculated one) are mainly due to known effects of the solvent on the measurements of the absorption spectra[169].

In case of Fig. 27 the comparison between the computed and experimental absorption peaks should be performed giving details on the effective oscillator strengths which are proportional to the area beneath the reported structures. Therefore in this case we have, for the experimental peak (A), at 391.8 nm (3.16 eV) a calculated area

530 Mb×nm (which corresponds to an oscillator strength by 0.2) to be compared with theoretical peak at 369.1 nm (3.36 eV) with an area by 455 Mb×nm (oscillator strength 0.17). On the other hand the experimental peak (B) at 730.9 nm (1.7 eV) shows a calculated area of 1613 Mb×nm (with an oscillator strength by 0.59) to be compared with theoretical peak around 693.5 nm (1.79 eV) with 820 Mb×nm area (oscillator strength 0.3).

Aside from the shift in the peak positions (22.7 nm for A and 37.4 nm for B) in the experimental case just discussed before, the high energy structure for HTP shows a better comparison with the computed value when considering the effective oscillator strength (difference of 16 % in the case of A).

In Figs. 28 and 29 we have reported the comparison of the absorption spectra calculated within Time Dependent DFT and the *GW*/BSE method in both cases using the basis set 6-31+G*.

In Fig. 28 the use of the *GW*/BSE produces a principal peak at 4.26 eV nearly coincident with that after TDDFT (aside a 21 % reduction), and a blue shifted small structure at the onset around 2 eV.

In Fig. 29 the two peaks around 2.9 eV and 3.4 eV produced by the two methods are nearly coincident. On the other hand the *GW*/BSE scheme describes an absorption peak at the onset red shifted by 0.23 eV nearly unchanged. For this particular peak it could be demonstrated that the above shift results negligible going from basis set 6-31+G* to AUG-cc-pVTZ.

4.4 BULK PROPERTIES

The electronic band structures for crystalline solid HTP and PNT calculated along high-symmetry lines of the BZ are presented in Figure 30. The coordinates of the high-symmetry points in the reciprocal space are Γ=(0,0,0), Y=($\frac{1}{2}$,0,0), Z=(0,0,$\frac{1}{2}$), A=($\frac{1}{2}$,$\frac{1}{2}$,0), B=(0,$\frac{1}{2}$,0) and D=($\frac{1}{2}$,$\frac{1}{2}$,-$\frac{1}{2}$) (in units of $\frac{2\pi}{a}$, $\frac{2\pi}{b}$, $\frac{2\pi}{c}$).

The direct energy gaps in these high-symmetry points are reported in Table 5. The fundamental gap is located at the A point for PNT and at the Γ point for HTP. As expected, the calculated PBE gap for PNT (0.73 eV) is considerably smaller than the experimental gaps for solid PNT (E_{gap}=2.2-2.4 eV)[105]. Using the B3LYP functional, it reaches 1.6 eV which is a clear improvement but still 0.6-0.8 eV below the experimental value. Note that the calculated *GW*[170] quasiparticle gap (1.9 eV) is also 0.3-0.5 eV too low. For HTP, we are not aware of any measurement of the band gap nor of any *GW* calculations. However, we expect that a similar trend ($E_{\text{gap}}^{\text{B3LYP}} < E_{\text{gap}}^{GW} < E_{\text{gap}}^{\text{Expt.}}$) also holds.

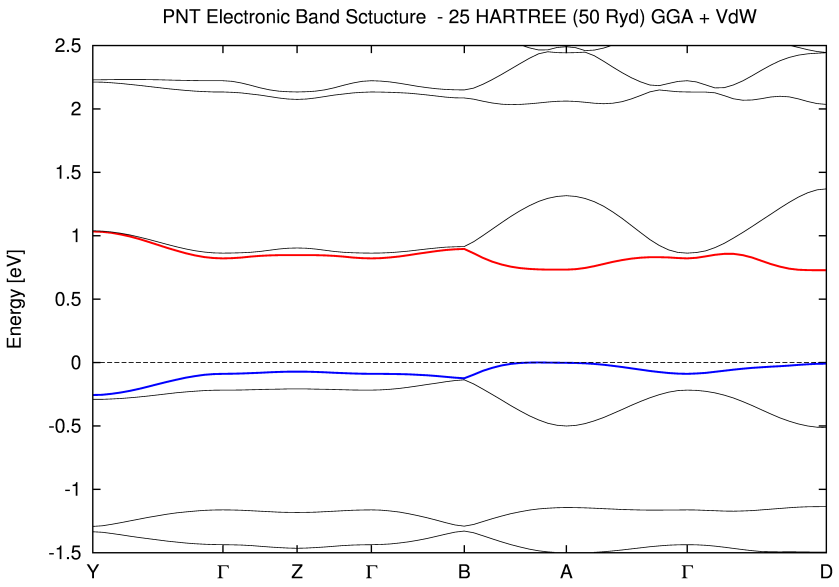

(a)

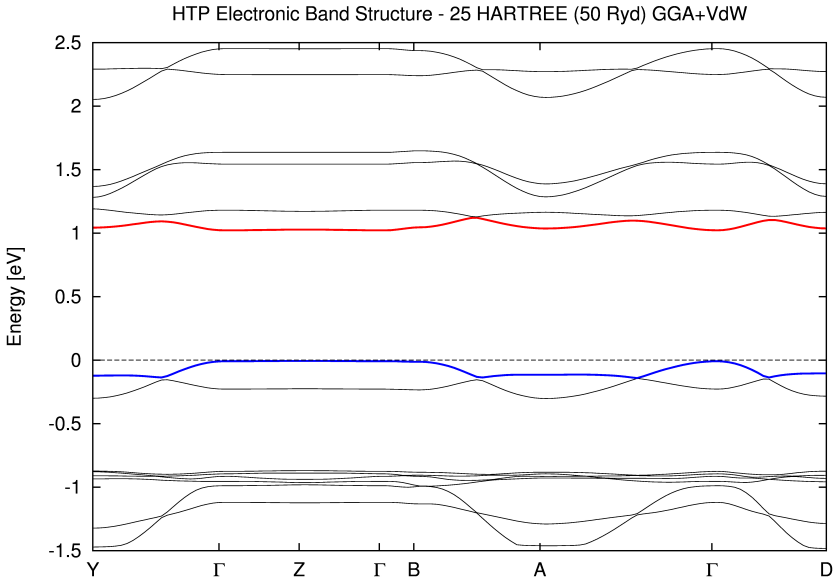

(b)

Figure 30: Electronic band structure of the crystalline solid phases of (a) PNT and (b) HTP at GGA-PBE level (see text) . The lowest conduction and highest valence bands are highlighted in red and blue, respectively.

In the present case, the HTP molecular solid here calculated presents energy bands which show differences with respect to the PNT solid either in the energy gaps and in the dispersion with respect to solid PNT. After present calculations within B3LYP for

Table 5: Values of the direct energy transitions (from valence to conduction) at various high-symmetry points for HTP and PNT calculated using the PBE and B3LYP exchange-correlation functionals. Previous PBE results from Ref. [105] are also reported for PNT. All values are given in eV.

	Γ	Y	Z	B	A	D
HTP (this work)						
PBE	1.03	1.16	1.04	1.06	1.15	1.15
B3LYP	1.95	2.11	1.96	1.99	2.09	2.09
PNT (this work)						
PBE	0.91	1.29	0.92	1.02	0.73	0.74
B3LYP	1.80	2.26	1.81	1.92	1.60	1.61
PNT (from Ref. 105.)						
PBE	0.89	1.29	0.92	1.03	0.71	0.72

the direct gaps solid HTP shows larger values (ranging from 0.1 to 0.5 eV) with respect to the solid PNT aside from point Y of 1STBZ (first Brillouin zone); in fact at this point solid HTP shows a smaller band gap value by 0.15 eV with respect to solid PNT (see Tab. 5). Therefore at the B3LYP level the lower onset energy for optical absorption for solid PNT turns out to be 1,60 eV (direct transition at point A of the 1STBZ) while for solid HTP comes out to be 1,95 eV (direct transition at point Γ of the 1STBZ). Consider that for the molecules (see Tab. 4 for the B3LYP case) the optical onset results at lower energy for HTP molecule than for PNT cluster.

With respect to band dispersion 0.31 eV for PNT and 0.10 eV for HTP for the lowest conduction band (LCB) and 0.26 eV and 0.13 eV respectively for PNT and HTP highest valence band (HVB) result (See Tab. 6). For these bands in the PNT case larger dispersions result.

These effects can be ascribed to a combined action of the different molecular packing and the sulfur substitution in HTP crystal.

Table 6: Band dispersion of the highest valence band (HVB) and lowest conduction band (LCB) of HTP and PNT molecular solids calculated within PBE along various high-symmetry directions (ΓX, ΓZ, ΓB, ΓA, and ΓD) as well as in the full Brillouin zone (BZ). Previous PBE results from Ref. [105] are also reported for PNT. All values are given in eV.

	ΓX	ΓZ	ΓB	ΓA	ΓD	BZ
HTP (this work)						
HVB	0.113	0.003	0.004	0.106	0.096	0.134
LCB	0.021	0.006	0.024	0.015	0.015	0.100
PNT (this work)						
HVB	0.142	0.010	0.022	0.082	–	0.225
LCB	0.188	0.021	0.068	0.107	–	0.305
PNT (from Ref. 105.)						
HVB	0.167	0.017	0.035	0.087	0.080	0.256
LCB	0.121	0.026	0.074	0.088	0.093	0.306

4.5 CONCLUSIONS

We have presented a comparative investigation between the electronic properties of isolated molecules and the corresponding molecular solids in the specific case of hexathiapentacene and pentacene using state of the art computational techniques. We have studied how molecular features are modified within the solid environment.

For the molecular phase using an all-electron code, we have computed ionization energies, electron affinities, quasi-particle gap, optical absorption, and molecular reorganization energies for both holes and electrons. We have found larger electron affinities and ionization energies for HTP, as compared to its parent PNT molecule, which gives rise to a reduction of the quasi-particle gap. The onset energy of the optical absorption spectrum for the molecules is red-shifted following functionalization and the same trend is found for the exciton binding energy. The visible-near UV region of the HTP molecular spectrum shows an enhancing of the absorption due to the red-shift and increased amplitude of the first peak and due to the new large structures in the very near UV.

For the corresponding PNT and HTP crystalline molecular solids, we have observed that different molecular packing stacks and sulfur substitution determine important differences in the electronic prop-

erties of the two systems. We have found that the dispersion of the bands shows differences in the two solids.

In the case of the molecular solids PNT, at the B3LYP level, shows a smaller fundamental gap wit respect to HTP. This finding differs from the gap ordering found for the HTP and PNT mlecules.

5

TRANSPORT PROPERTIES: PNT, DBC, ANT, PYR AFTER PERFLUORINATION

Contents

5.1 INTRODUCTION

A common key parameter for organic-based applications in devices is the charge carrier mobility.[126] In this sense, Graphene Nano-Ribbons (GNRs) are expected to reach the graphene limit of zero band gap (extremely large mobilities) for sufficiently large widths.

The impact of using GNRs in thin-film nanoelectronics or organic field-effect transistors,[171,172] besides improvements in device fabrication processes, is believed to depend not only on the intrinsic charge carrier mobilities of the organic materials but also on the relative positions of the interacting molecules, which is intimately related to the supramolecular ordering of the samples.

In this Chapter we would like thus to address the behavior of angular dibenzochrysene (DBC), compact dibenzochrysene (or anthanthrene, ANT), PYR as a smallest examples of GNRs and compare the intrinsic efficiency of these materials for charge transport in the hopping regime with respect to Pentacene (PNT), which can be considered as a benchmark in the field of organic semiconductors (in particular as hole transporter). We will also perform a comparison of transport performances of this PAHs with ther perfluorinated derivatives: Perfluoro-Pentacene (PFP), Perfluoro-Dibenzochrysene (PF-DBC) Perfluoro-Anthanthrene (PF-ANT) and Perfluoro-Pyrene (PF-PYR).

5.2 COMPUTATIONAL FRAMEWORK

The interplay between electronic and vibronic interactions promotes charge-transfer (CT) at room temperature in organic molecular semi-

conductors. The widely applied idealized mechanism known as Marcus theory[113,173], (as we have seen in Sect. 2.4) describes CT as a self-exchange hole(electron)-transfer chemical reaction between the molecules.

The non-adiabatic transfer rate, k_{CT}, is used to quantitatively analyze these properties. According to the weak-coupling regime, the rate critically depends on two parameters that can be extracted from quantum-mechanical calculations (see Ref. 110,174,175 and Sect. 2.4 for the complete explanation) the intramolecular coupling, or reorganization energy (λ), and the electronic coupling between adjacent molecules, or transfer integral (t). The form of the rate is described as previously seen in the Eq. 58 which we report here for clarity

$$K_{CT} = \frac{4\pi}{h}\frac{t^2}{\sqrt{4\pi\lambda k_B T}}\exp\left(-\frac{\lambda}{4k_B T}\right)$$

The strategy to compute the internal reorganization energy λ uses the so-called *four-point method*[176,177], previously seen in the Sect 2.4, which requires the separate optimization of the geometry of the neutral (E_n) and charged molecules (E_c) and the single-point calculations of the neutral molecule at the charged geometry ($E_n^{(c)}$) and of the charged molecule at the neutral geometry ($E_c^{(n)}$):

$$\lambda = \lambda_1 + \lambda_2 = (E_n^{(c)} - E_n) + (E_c^{(n)} - E_c)$$

The contribution to λ from the reorganization of the surrounding medium after the arrival of the charge (the so-called external contribution to the reorganization energy) has been calculated, and found to be of little significance for closely related molecules[178] and will thus be thereby neglected.

Furthermore, the mobilities not only depend on the intrinsic electronic properties of the materials but also on the dimeric interactions between neighboring molecules.[179] It is possible to use a co-facially stacked dimeric nanostructure to approximate the expected solid packing. For this purpose we have choosen two values of the dimer distance: the equilibrium distance between the two molecules and the distance of 3.5 Å which is is the typical distance of a thin-film packing (greater than the experimental interplanar distance of graphite (3.35 Å)) as suggested by Sancho-Garcia et al. in Ref. [147]. The equilibrium distance for a certain dimer is determined calculating at which distance of two facially stacked molecules, the energy of the dimer is at minimum.

The transfer integral t is thus calculated for the two distances (optimized one and 3.5 Å) by the method known as *energy splitting*

in dimer[180] to obtain a simple yet reliable[125,181] estimate of the electronic coupling for cofacial dimers using the Eq. 59 previously seen in Chapter 2.4:

$$t_{h[e]} = \frac{\varepsilon_{\text{HOMO[LUMO+1]}} - \varepsilon_{\text{HOMO-1[LUMO]}}}{2}$$

5.3 RESULTS

Both the molecular reorganization energy λ and the transfer integral t play an important role in the calculation of the mobilities within the Marcus theory. Since λ coefficient enters in the argument of an exponential, it has a stronger influence in the hopping rate and, as a consequence, on the mobility.

Tab. 7 shows the values of λ and t for all compounds here considered calculated at the dimer equilibrium distance and at the fixed distance of 3.5 Å. For the λ coefficients we can see that the values

	λ_h [eV]	λ_e [eV]	t_h [eV]	t_e [eV]	d_{eq} [Å]	t'_h [eV]	t'_e [eV]
PNT	0.092	0.13	0.213	0.229	3.80	0.342	0.361
PYR	0.15	0.21	0.223	0.219	3.80	0.355	0.346
ANT	0.11	0.15	0.245	0.240	3.73	0.350	0.342
DBC	0.12	0.16	0.233	0230	3.75	0.345	0.339
PFP	0.23	0.24	0.255	0.287	3.45	0.234	0.265
PF-PYR	0.34	0.99	0.261	0.265	3.45	0.240	0.244
PF-ANT	0.26	0.27	0.266	0.268	3.45	0.245	0.247
PF-DBC	0.26	0.25	0.262	0.283	3.45	0.241	0.261

Table 7: Molecular reorganization energies for holes and electrons (λ_h and λ_e), transfer integral at the equilibrium distance for holes and electrons (t_h and t_e), values of equilibrium distances for the dimers (d_{eq}) and transfer integral at fixed distance of 3.5 Å (t'_h and t'_e) .

for the holes are always smaller with respect to the electron cases aside from PF-DBC in which a small inversion results. For the unsubstituted systems we found large differences between electrons and holes λ(with differences in the range $33 \div 41$ %) while for the perfluorinated ones the differences appear small (4%) with the exception of PF-PYR which shows a λ_e nearly tripled with respect to λ_h.

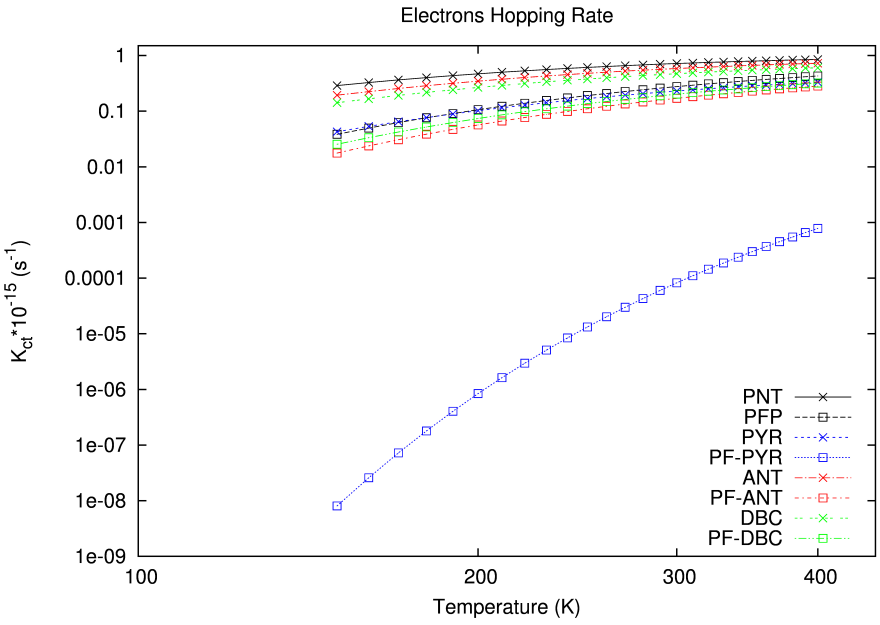

(a)

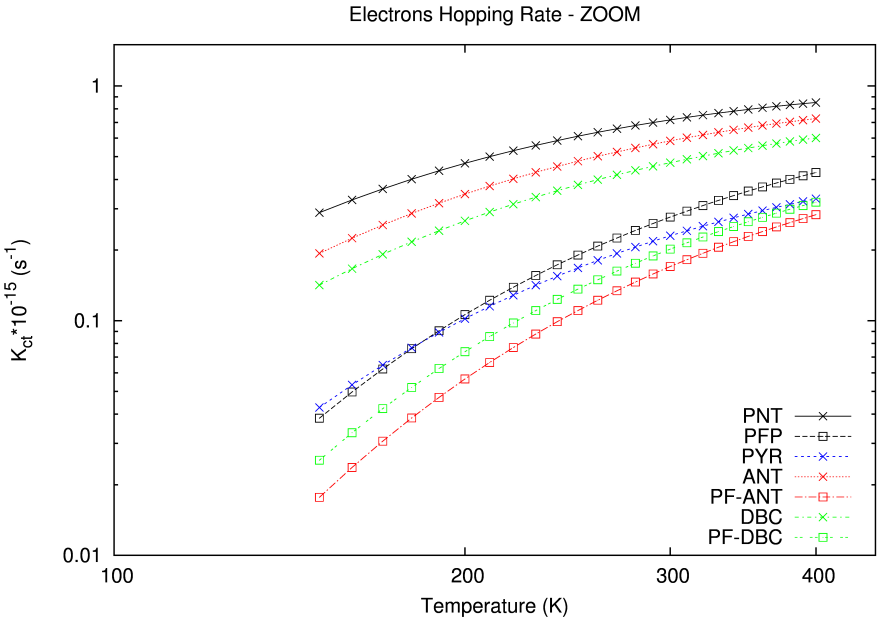

(b)

Figure 31: Electrons hopping rate K_{CT} for all studied compounds, calculated as function of the absolute temperature (T). Colored crosses curves identify pure molecules (black for PNT, red for ANT, green for DBC and blue for PYR); typeface squares curves correspond to the perfluorinated ones.

For the transfer integral t of the perfluoro-compounds, calculated at the equilibrium distance of the dimer, the values for electrons are

always larger than those for the holes (differences always under 13 %). In the case of the pure molecules, for these parameters (aside from PNT), the t values for the holes are larger than those for the electrons ($-1 \div -2$ %; +8 % for PNT). Same behavior we found for the calculations at the distance of 3.5 Å with differences of the same order of magnitude between electrons and holes parameters.

Generally if we make a comparison of the values obtained for the transfer integrals t at the two different distances (equilibrium one and fixed one), the pure PAHs (PNT, PYR, ANT and DBC) show larger values for t'_h and t'_e with respect to t_h and t_e. Perfluorinated molecules show the opposite behavior (t'_h and t'_e smaller with respect to t_h and t_e). This could be considered as a consequence of the reduction (in the case of pure systems) or the increase (for the halogenated ones) of the intermolecular distance in the dimers.

Fig. 31 shows the electron hopping rates (K_{ct}) calculated using the values in Tab. 7 and the Eq. 58 (according to the Marcus semiclassical framework explained in Sect. 2.4). The temperatures range has been chosen here according to what reported in [182].

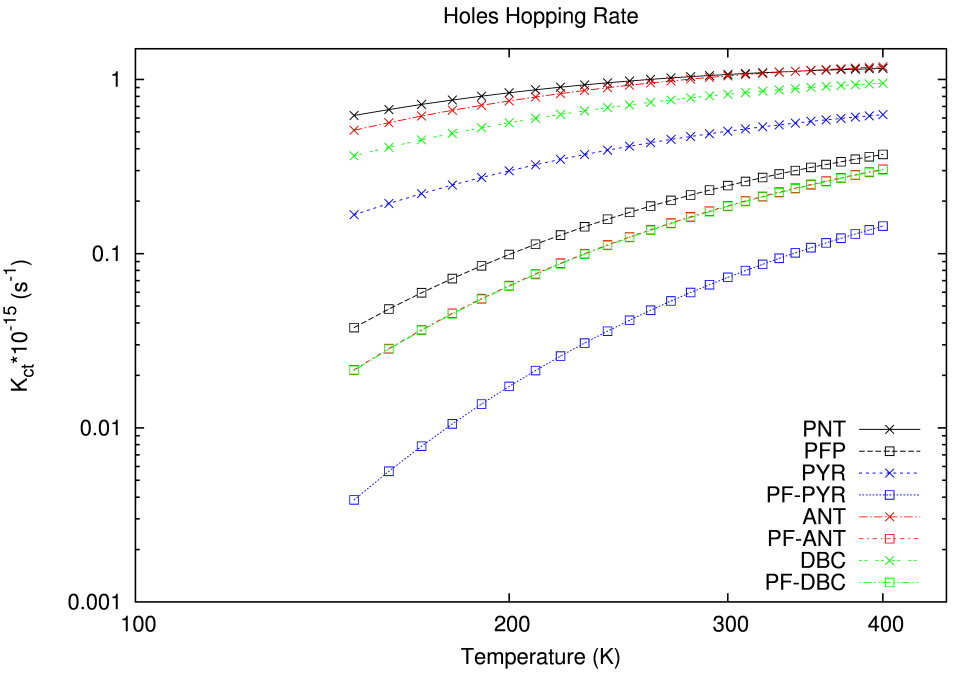

Figure 32: Holes hopping rate K_{CT} for all studied compounds calculated as function of the absolute temperature (T). Colored crosses curves identify pure molecules (black for PNT, red for ANT, green for DBC and blue for PYR); typeface squares curves correspond to the perfluorinated ones.

PF-PYR shows a rather different behavior with respect to the other compounds, with K_{ct} almost $3 \div 6$ order of magnitude lower as compared with other molecules. This particular fact is due to the large λ coefficient for this perfluorinated molecule (see Tab. 7). We consider in Fig. 31-b a limited range for the hopping rates to obtain a more clear vision of the hopping rate values for the other molecules (with this choice the PF-PYR curve results out of range).

DBC and ANT show a behavior similar to PNT in the whole temperature range but with consistent differences in terms of values of K_{ct} which results reduced from 27 % to 49 % in the case of DBC and from 12 % to 30 % in the case of ANT in comparison with PNT. A clear grouping of the pure compounds and the perfluorinated ones results with the only exception of the pure PYR which shows the lowest performance with respect to the other unsubstituted molecules here considered. In all cases the perfluorination determines a lowering of the electron hopping rate within the temperatures range here considered.

The Fig. 32 shows the holes hopping rates (K_{ct}) calculated within the same framework of the electronic ones. In this case the ANT shows a very similar behavior with respect to PNT (with differences under 15 %) and even slightly better in for T>280 K (+6 % at T=400 K).

Comparing Fig. 32 with Fig. 31-a and Fig. 31-b we can see that, in both cases for pure and perfluorinated molecules, each curve for the holes is higher with the corresponding one for the electrons. This is a clear manifestation that, either in the pure state or in the perfluorinated one, for the molecules here considered, the hole mobility plays a dominant role.

Differently from the case of electrons, the hole hopping rate for pure PYR is the lowest in between all the pure systems but remains above the values for all the perfluorinated molecules in the considered temperature range.

In Fig. 33 we report the holes mobilities for different molecules normalized with respect to the mobility of pentacene. The ratio of the charge carriers mobilities (holes or electron) for two different compounds (in this case DBC, ANT, PYR and corresponding perfluorinated, indicated with X, and PNT), can be obtained, according with the Marcus theory, by:

$$\frac{\mu_X}{\mu_{PNT}} = \frac{K_{CT,X}}{K_{CT,PNT}} = \frac{t_X^2}{t_{PNT}^2}\sqrt{\frac{\lambda_{PNT}}{\lambda_X}}e^{\frac{\lambda_{PNT}-\lambda_X}{4k_BT}} \tag{81}$$

This equation provides a simple direct comparison between experimental mobility values and theoretical charge transfer rates ob-

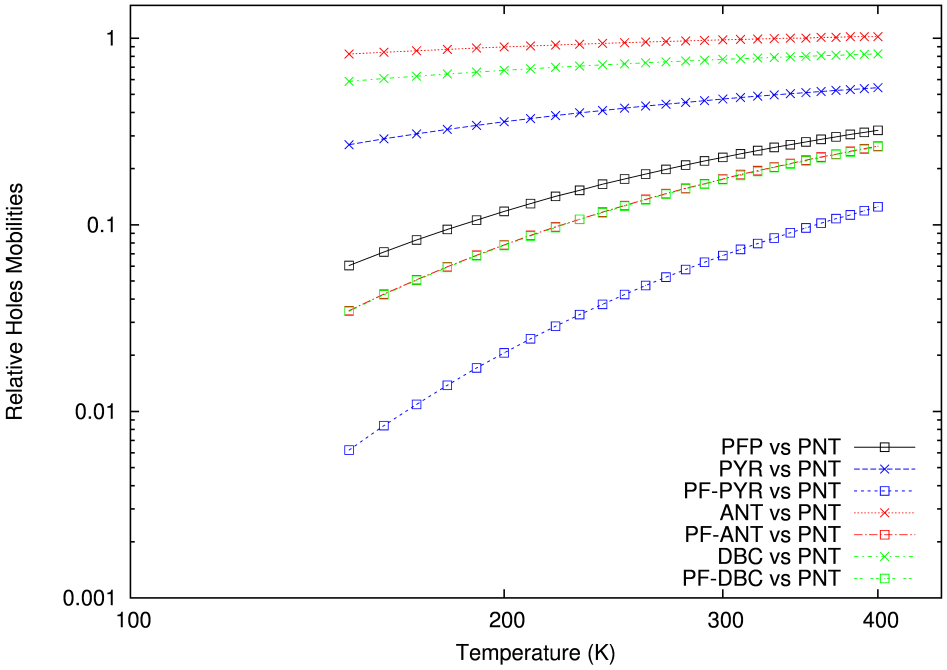

Figure 33: Relative holes mobilities (normalized with respect to PNT) calculated as function of the absolute temperature (T). Colored crosses curves identify pure molecules (red for ANT, green for DBC and blue for PYR); typeface squares curves correspond to the perfluorinated ones.

tained for the various molecules. From the Fig. 33 it is clear that the only compound which presents a comparable hole mobility is the ANT which shows a better performance (+2.3 %) at T=400 K. In general the perfluorinated molecules present always a worsening in the relative mobility if compared with the PNT. PYR and PF-PYR molecules show the worst behavior in terms of relative hole mobility respectively in relation to pure and perfluorinated candidates we considered in this work.

In Fig. 34 shows the electron mobilities normalized with respect to the mobility of PNT. Also in the case of Fig. 34-b PF-PYR curve has been set out of the range, to obtain a better visualization of the curves relative for the other molecules.

For these carriers too, we found the best performance in the case of ANT which is lower by about 15 % in particular at high temperatures.

For the electron relative mobility the PYR presents a very poor performance with respect to the other PAHs with a relative mobility similar (and in one case lower) than those of the fuoro-substituted systems.

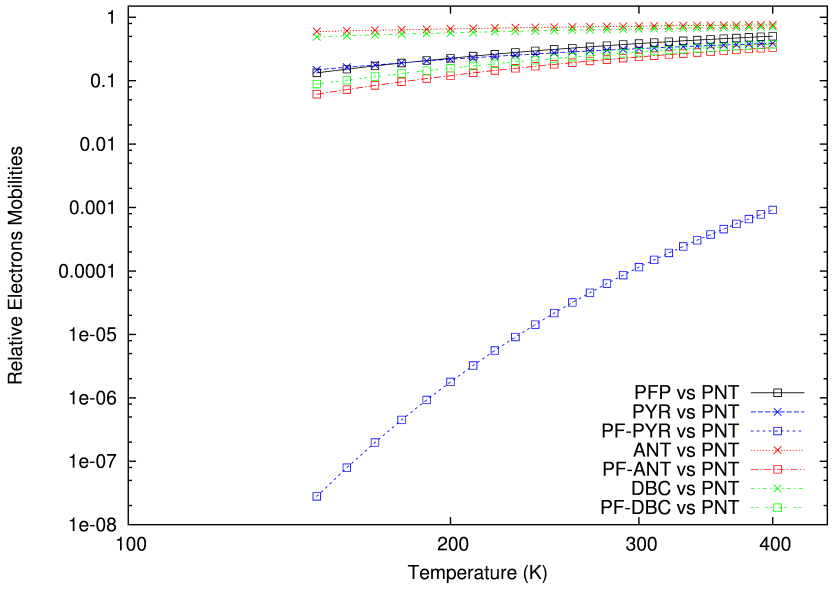

(a)

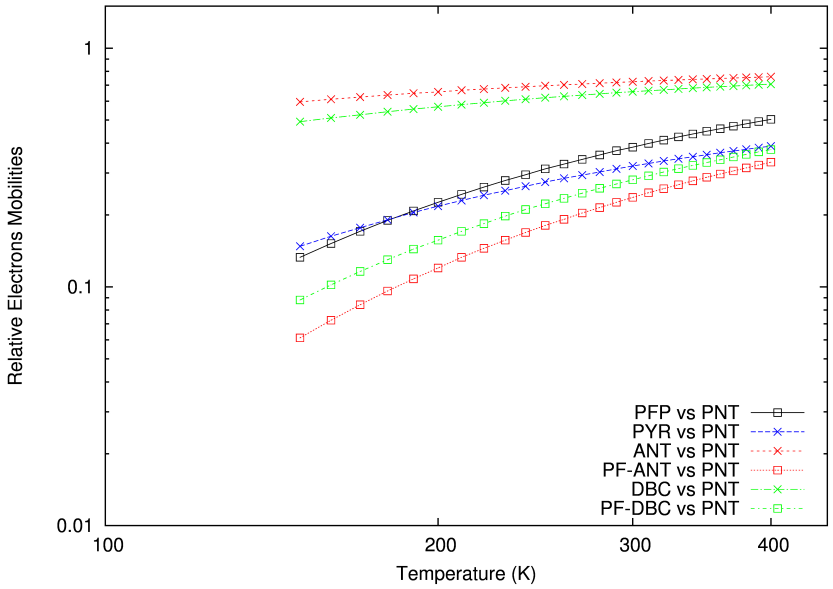

(b)

Figure 34: Relative electrons mobilities (normalized with respect to PNT) calculated as function of the absolute temperature (T). Colored crosses curves identify pure molecules (red for ANT, green for DBC and blue for PYR); typeface squares curves correspond to the perfluorinated ones.

PF-PYR shows the worst performance with a relative mobility from 3 to 7 orders of magnitude lower with respect to that other molecules.

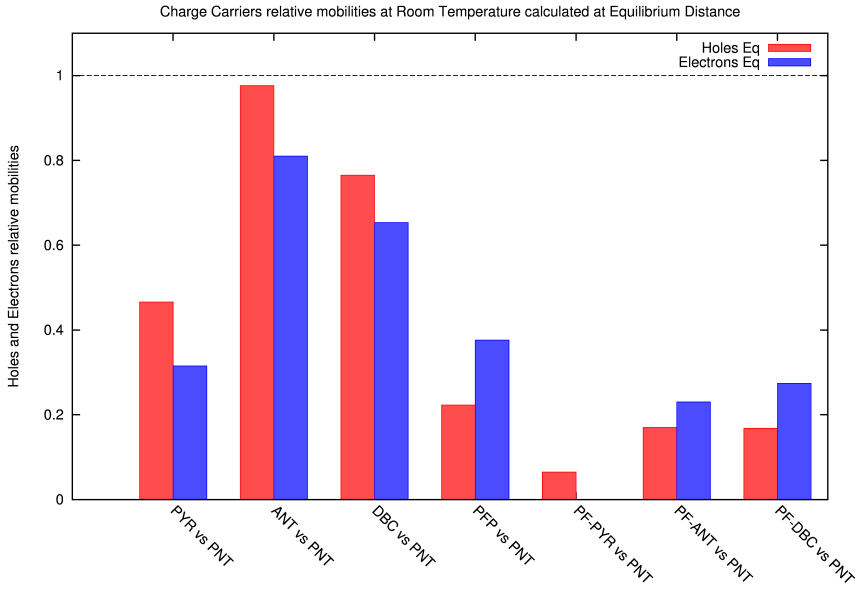

Figure 35: Relative mobilities for holes (red) and electrons (blue) calculated at the equilibrium distance and at T=293,15 K=20 °C

The histograms in Fig. 35 highlight the relative mobilities for the holes and the electrons with respect to PNT at the room temperature (T=20 °C=293,15 K). For all the PAHs is confirmed their hole transporter nature. For these molecules best performance is showed by the ANT but even in this case the value of mobility remains under the value of PNT.

For the perfluorinated systems, aside from PYR, the electrons mobilities perform better than the holes ones. This fact confirms the well known transition from p-type to n-type semiconductor after fluorination[183], with values of electron relative mobilities always below 40%.

In the case of PF-PYR the relative electron mobility result too low to be visible in Fig. 35

We have also performed calculations for the same quantities (hopping rates and relative mobilities for holes and electron) in the case of dimer intermolecular distance d=3.5 Å

Fig. 36 and 37 report the behavior of electrons K_{CT} as a function of temperature, calculated at the distance of 3.5 Å. The second plot is a magnification with the curve of PF-PYR out of the range.

For the electrons K_{CT} the Figures 36 and 37 shows an increase of values for all pure molecules which appear from 2 to 2.5 times larger with respect to the same quantities for the optimized distance, and a moderate lowering in the case of functionalized PAHs by about 15 % . For the pure molecules this behavior is essentially a consequence of

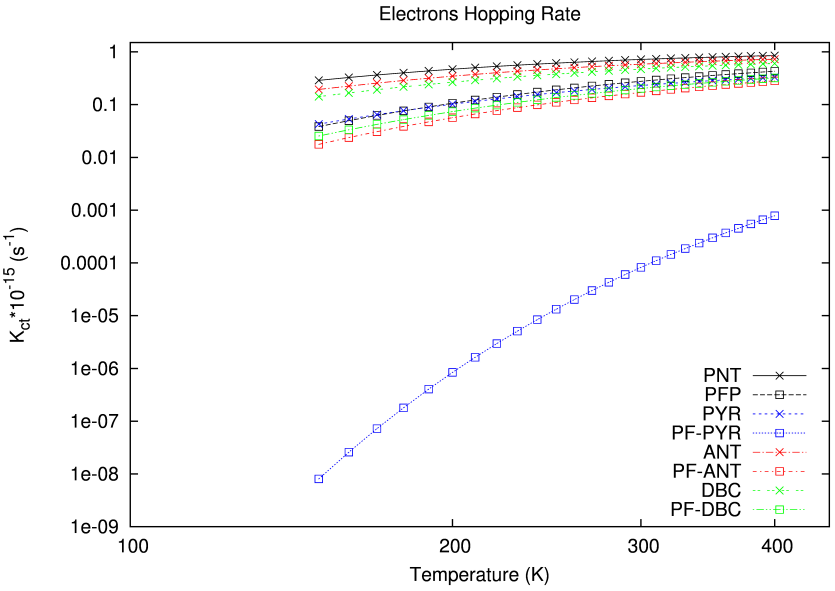

(a)

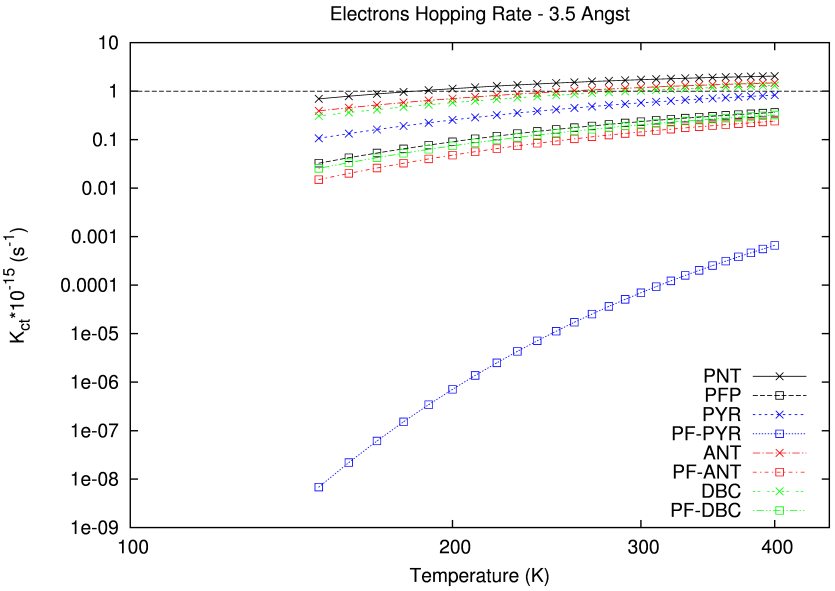

(b)

Figure 36: Electrons hopping rate K_{CT} calculated at dimer distance of 3.5 Å (b) in comparison with the same quantities calculated at d_{eq} (a), as function of the absolute temperature (T). Colored crosses curves identify pure molecules (black for PNT, red for ANT, green for DBC and blue for PYR); typeface squares curves correspond to the perfluorinated ones.

the increase of the transfer integral t due to the reduction of cofacial dimer intermolecular distance (from the equilibrium distance 3.70 ÷

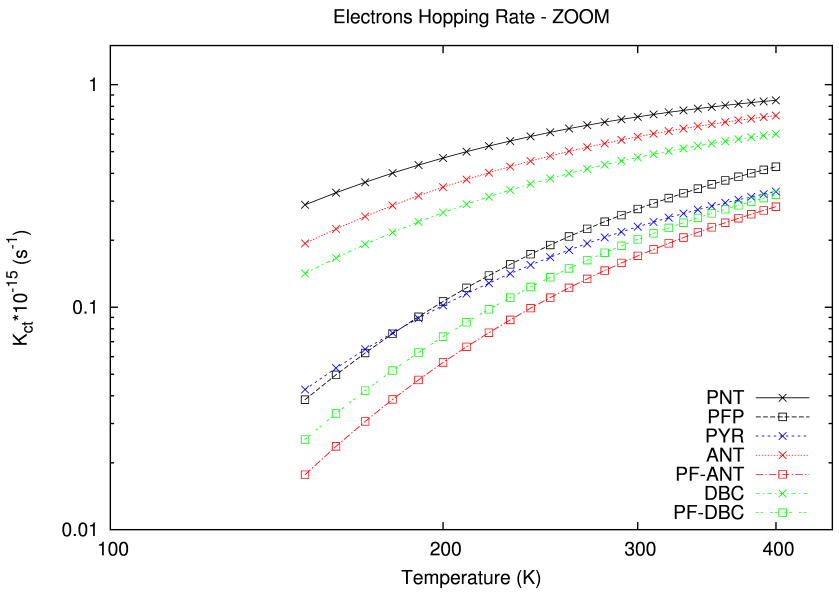

(a)

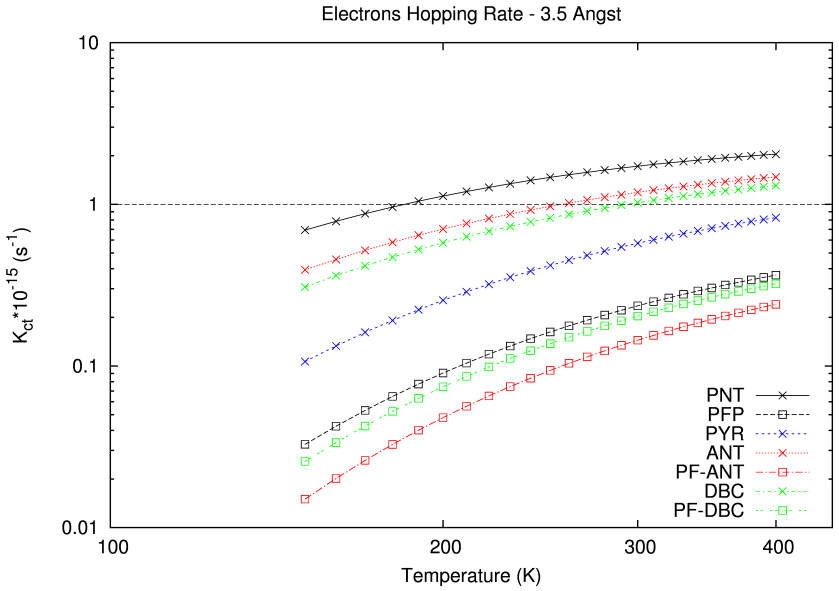

(b)

Figure 37: Magnification of electrons K_{CT} plot calculated at dimer distance of 3.5 Å (b) in comparison with the same quantities calculated at d_{eq} (a), as function of the absolute temperature (T). Here PF-PYR curve is out of the range)
Colored crosses curves identify pure molecules (black for PNT, red for ANT, green for DBC and blue for PYR); typeface squares curves correspond to the perfluorinated ones.

3.80 Å to 3.5 Å). On the other hand the small reduction reported for

the fluoro-compounds of is due to the limited decrease of t caused to the raise of the dimer distance from 3.45 Å to 3.5 Å.

Fig. 38 reports the trend of K_{CT} for the holes at the same distance (3.5 Å) and we can see the same behavior found for the electrons. Even for the holes the hopping rate presents a large raise for the original molecules (same order of the increase of electrons) and a small lowering for the halogenated ones (even in this case of the same order of the reduction previous encountered for the negative carriers). These facts are mainly ascribable to the same reasons seen above for the electrons. Figures 39 and 40illustrate the behavior of the electron relative mobility (respect to PNT) calculated with the parameters at the distance of 3.5 Å using the Eq. 81. Compared with the calculations at the equilibrium distances the mobility shows a reduction for DBC (-9.5 %) and an increasing for PYR ($+4$ %) and ANT ($+5$ %) but even after this increasing, the mobility of ANT (which shows the best performance) remains under the mobility of PNT. We found, instead, large worsening of electron mobility for the pefluorinated compounds with lowering by about 64 % for PFP, PF-ANT, PF-DBC and 58 % for PF-PYR.

In Fig. 41 we can see the trend for the holes relative mobility at the distance of 3.5 Å. Also in this case we found a large reduction for fluoro-substituted compounds (-66 % for all fluorinates) and a smaller reduction for DBC (-12 %) and ANT (-18 %), while the values for PYR remains almost unchanged. Also for the holes mobility, the ANT shows the best response in terms of mobility but even in this case its value remains under the PNT one.

These behaviors are a consequence of the fact that the reduction of the dimer distance from d_{eq} to 3.5 Å enhances even the hopping rate of PNT which remains higher with respect to the new values for holes and electron mobilities and causes a reduction of the ratio defined as 81.

.

5.4 CONCLUSIONS

We have performed a systematic comparison for pure and perfluorinated PAHs relatively to the values of carriers hopping rate (K_{CT}) and relative mobilities (respect to PNT) for holes and electrons. All the observables are calculated at equilibrium distance (d_{eq}) and at the fixed distance $d = 3.5$ Å for the corresponding dimers in a range of temperatures from 150 K to 400 K.

We found that for all molecules and for both holes and electrons, the perfluorination induces a worsening of the performance

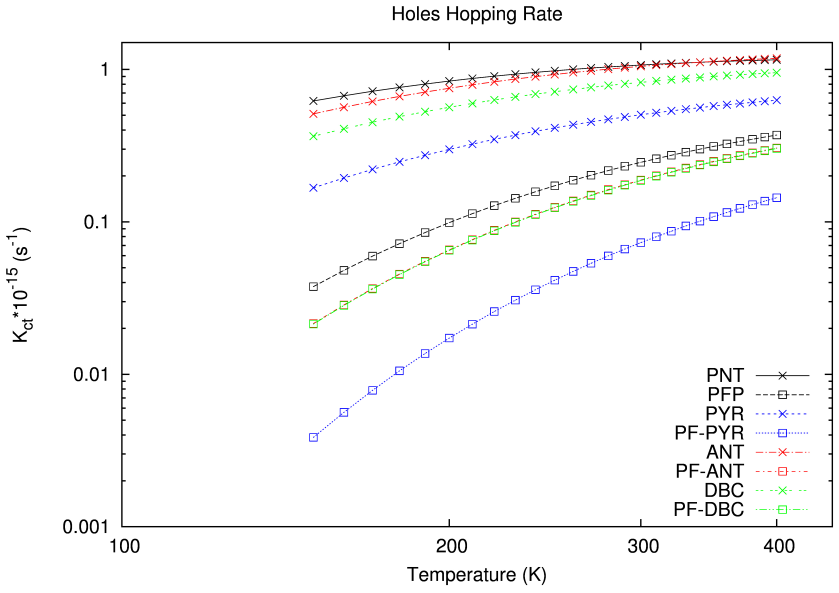

(a)

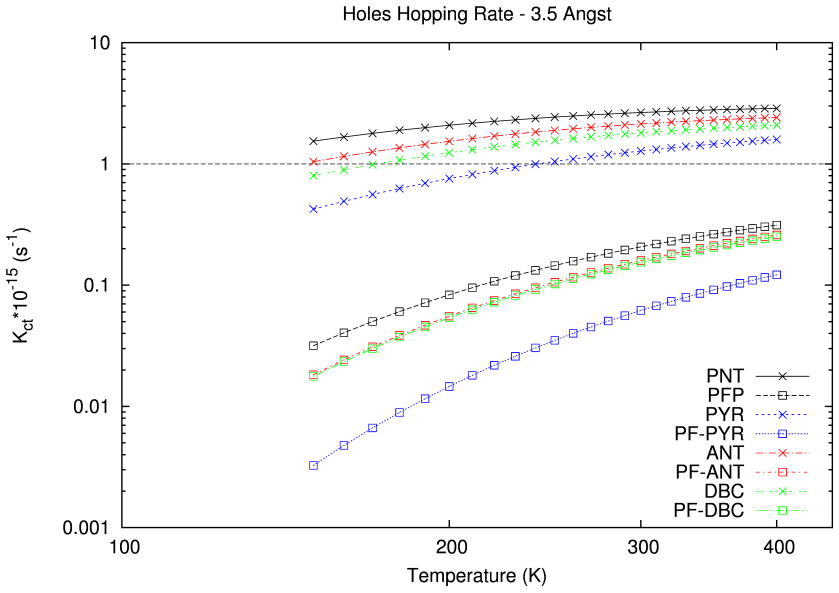

(b)

Figure 38: Holes hopping rate K_{CT} calculated at dimer distance of 3.5 Å (b) in comparison with the same quantities calculated at d_{eq} (a), as function of the absolute temperature (T). Colored crosses curves identify pure molecules (black for PNT, red for ANT, green for DBC and blue for PYR); typeface squares curves correspond to the perfluorinated ones.

in terms of K_{CT} essentially due to the large increasing of molecular reorganization energies (λ_e and λ_h) after the substitution. This

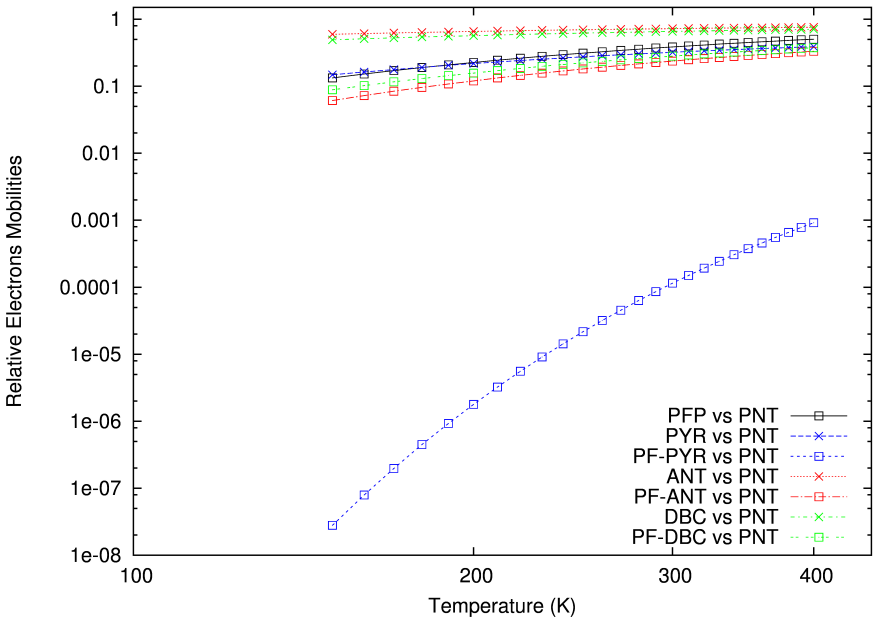

(a)

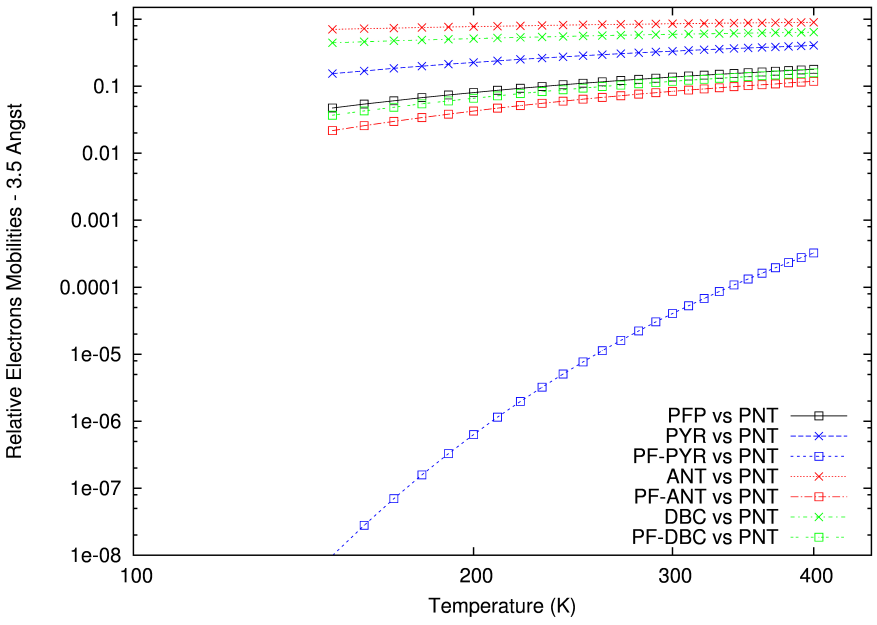

(b)

Figure 39: Relative electrons mobilities (normalized with respect to PNT) calculated at dimer distance of 3.5 Å, as function of the absolute temperature (T). Colored crosses curves identify pure molecules (red for ANT, green for DBC and blue for PYR); typeface squares curves correspond to the perfluorinated ones.

behavior is also confirmed going from d_{eq} to 3.5 Å in the dimer distances. Comparing the hopping rates curves for both carriers at the

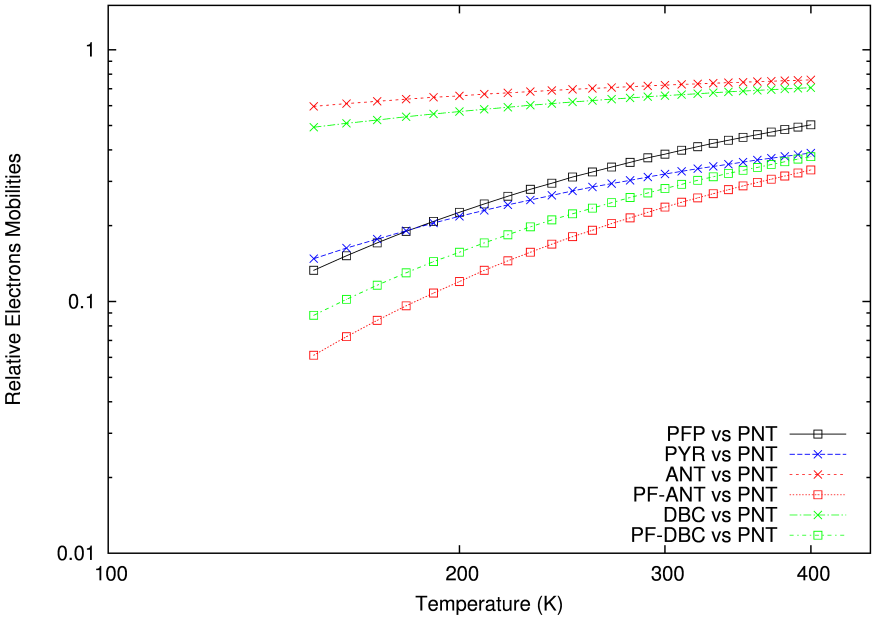

(a)

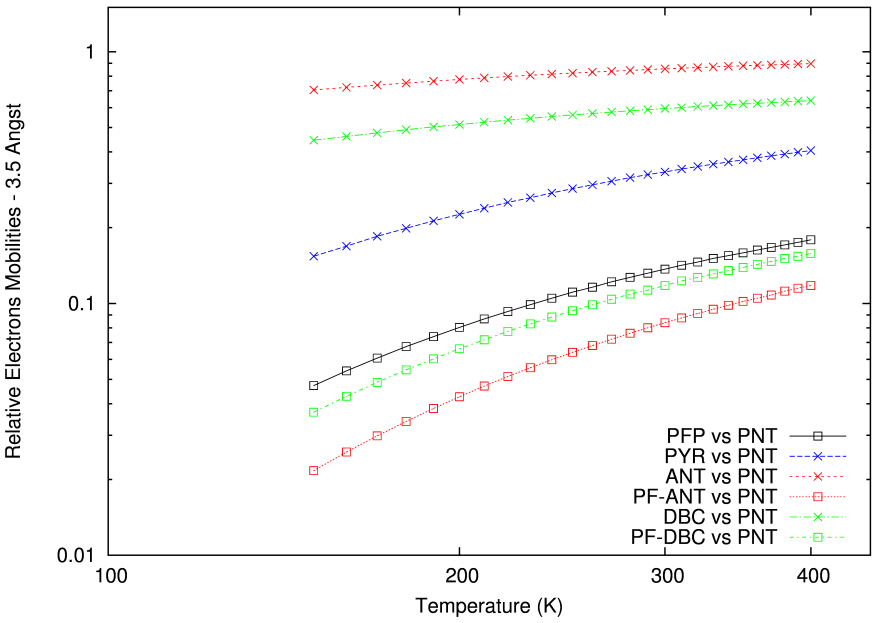

(b)

Figure 40: Magnification of relative electrons mobilities plot (normalized with respect to PNT) calculated at dimer distance of 3.5 Å, as function of the absolute temperature (T). Here PF-PYR curve is out of the range.
Colored crosses curves identify pure molecules (red for ANT, green for DBC and blue for PYR); typeface squares curves correspond to the perfluorinated ones.

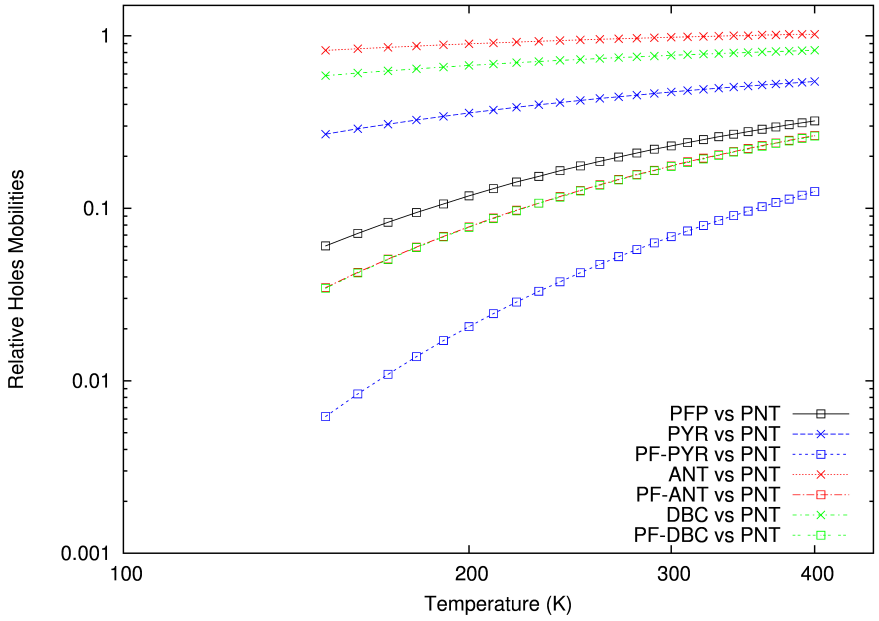

(a)

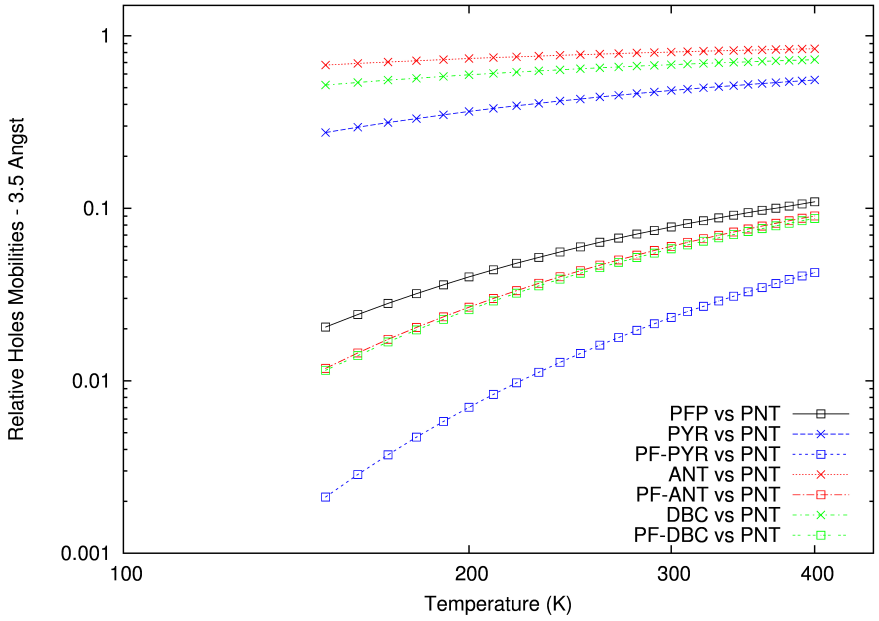

(b)

Figure 41: Relative holes mobilities (normalized with respect to PNT) calculated at dimer distance of 3.5 Å, as function of the absolute temperature (T). Colored crosses curves identify pure molecules (red for ANT, green for DBC and blue for PYR); typeface squares curves correspond to the perfluorinated ones.

two different distances, we found an important increase of K_{CT} at

3.5 Å dimer distance for the pure systems and a slight reduction for the halogenated ones after the transition to the fixed distance.

The relative holes mobilities, evaluated at d_{eq}, results for almost all compounds lower with respect to PNT; the only compound which presents a comparable hole mobility is the ANT which presents a mobility of the order of +2 % larger then that of PNT (but just at temperatures higher with respect to the room temperature). For the electrons relative mobility (in the same conditions) we found always a worsening as compared with that of PNT.

The same quantities, but evaluated at $d = 3.5$ Å present a worsening for all compounds (except for electrons in the case of PYR and ANT, for which the curves remain almost unchanged).

In general at fixed distance, none of the compounds under study presents better mobility as compared to PNT, despite the growth of their respective K_{CT}. The performance of compounds with large aromatic core (ANT and DBC) in comparison with PNT, suggests that systems with even larger conjugated core (e. g.large circumacenes) than ANT and DBC could obtain better performances with respect to PNT even in the presence of fluorination.

6 CONCLUSIONS

In this Thesis we used different computational techniques to perform a systematic comparative study, focused on the effects of chemical substitutions or functionalizations on the electronic, optical and charge-transport properties of several Polycyclic Aromatic Hydrocarbons (PAHs) systems. More specifically, we have extensively studied the effects of partial or total substitutions with electronegative atoms (F, Cl, S) and the addition of Tri-Isopropylsilylethynyl (TIPS) groups.

In the case of molecular systems we used the hybrid exchange-correlation functional B3LYP in conjunction with a gaussian localized basis set as implemented in the all-electrons code NWChem. We computed Electron Affinity (EA), Ionization Energy (IE), Quasi-Particle (QP) gap, exciton binding energies, and molecular reorganization energies for both holes and electrons considering the effects of partial sulfur substitution (Hexathiapentacene, HTP) and complete halogenation and addition of TIPS groups (for Dibenzochrysene (DBC) and Anthanthrene (ANT)).

For HTP we found larger EA and IE as compared to its parent molecule PNT and a reduction of the QP gap. We observed the same behavior in the case of halogen substitutions for both DBC and ANT. Following TIPS functionalization the same molecules show a rise of EA and a lowering of IE. In both compact and angular molecules, the above trends reflect a general reduction of the quasi-particle gap upon chemical modification.

The effect of substitution with electron withdrawing atoms (F, Cl, S) and functionalization with large steric hindrance groups (TIPS) gives rise to a redshift of the onset energy in the optical absorption spectra for all the systems considered. In addition, substituted molecules display more structured spectra in terms of higher intensities (TIPS) and number of transitions occurring in the visible/near-UV range (F, Cl). Analogous behavior is also observed in the case of HTP.

After chemical modifications charge-transport properties of both holes and electrons appear to worsen for all the investigated compounds due to the increase of the molecular reorganization energies. In the case of pure and perfluorinated PAHs this is confirmed by the computed mobilities for both carriers with respect to PNT.

Moreover we studied the crystalline molecular solids of PNT and HTP using the ABINIT code which is based on ionic pseudopotentials and a plane-waves expansion of the electronic wave-functions. The ground-state electronic properties have been determined using the PBE exchange-correlation functional. On the other hand the one particle electronic excitations have been calculated either at the PBE level and within a perturbative B3LYP scheme. By comparing the results for PNT and HTP we could also estimate quantitatively the effect of sulfur substitution on molecular packing.

Overall, the predictions of the ground and excited-state electronic properties for the isolated molecules and the crystalline solids here presented could be used as a term of reference for possible future research plans focused on substituted and functionalized organic compounds.

LIST OF FIGURES

LIST OF TABLES

BIBLIOGRAPHY

[1] S. Ogawa, ed., *Organic Electronics Materials and Devices*. Springer, 1st ed., 2015. (Cited on pages 4, 10, and 105.)

[2] A. Köler and C. E. Bässler, *Electronic Processes in Organic Semiconductors*. Wiley - VCH, April 2015. (Cited on page 3.)

[3] R. M. Pope and C. E. Swenberg, *Electronic Structure: Basic Theory and Practical Methods*. Oxford University Press, 2nd ed., 1999. (Cited on pages 3 and 41.)

[4] A. J. Heeger, "Semiconducting and metallic polymers: The fourth generation of polymeric materials (Nobel Lecture)," *Angewandte Chemie International Edition*, vol. 40, no. 14, pp. 2591–2611, 2001. (Cited on page 4.)

[5] C. K. Chiang, C. R. Fincher, Y. W. Park, A. J. Heeger, H. Shirakawa, E. J. Louis, S. C. Gau, and A. G. MacDiarmid, "Electrical conductivity in doped polyacetylene," *Phys. Rev. Lett.*, vol. 39, pp. 1098–1101, Oct 1977. (Cited on page 4.)

[6] A. Mishra and P. Bäuerle, "Small molecule organic semiconductors on the move: Promises for future solar energy technology," *Angewandte Chemie International Edition*, vol. 51, no. 9, pp. 2020–2067, 2012. (Cited on page 4.)

[7] J. D. Myers and J. Xue, "Organic semiconductors and their applications in photovoltaic devices," *Polymer Reviews*, vol. 52, no. 1, pp. 1–37, 2012. (Cited on pages 7, 8, and 105.)

[8] W. Brütting and C. Adachi, eds., *Physics of Organic Semiconductors*. Wiley-VCH, 2nd ed., 2012. (Cited on pages 6 and 8.)

[9] B. P. Rand, J. Xue, S. Uchida, and S. R. Forrest, "Mixed donor-acceptor molecular heterojunctions for photovoltaic applications. i. material properties," *Journal of Applied Physics*, vol. 98, no. 12, p. 124902, 2005. (Cited on page 7.)

[10] L. Bozano, S. A. Carter, J. C. Scott, G. G. Malliaras, and P. J. Brock, "Temperature- and field-dependent electron and hole mobilities in polymer light-emitting diodes," *Applied Physics Letters*, vol. 74, no. 8, pp. 1132–1134, 1999.

[11] S. A. Choulis, Y. Kim, J. Nelson, D. D. C. Bradley, M. Giles, M. Shkunov, and I. McCulloch, "High ambipolar and balanced carrier mobility in regioregular poly(3-hexylthiophene)," *Applied Physics Letters*, vol. 85, no. 17, pp. 3890–3892, 2004. (Cited on page 7.)

[12] S. Z. Bisri, T. Takenobu, T. Takahashi, and Y. Iwasa, "Electron transport in rubrene single-crystal transistors," *Applied Physics Letters*, vol. 96, no. 18, p. 183304, 2010. (Cited on page 8.)

[13] R. W. I. de Boer, M. E. Gershenson, A. F. Morpurgo, and V. Podzorov, "Organic single-crystal field-effect transistors," *Physica Status Solidi (A)*, vol. 201, no. 6, pp. 1302–1331, 2004.

[14] J. Takeya, M. Yamagishi, Y. Tominari, R. Hirahara, Y. Nakazawa, T. Nishikawa, T. Kawase, T. Shimoda, and S. Ogawa, "Very high-mobility organic single-crystal transistors with in-crystal conduction channels," *Applied Physics Letters*, vol. 90, no. 10, p. 102120, 2007.

[15] M. Yamagishi, J. Takeya, Y. Tominari, Y. Nakazawa, T. Kuroda, S. Ikehata, M. Uno, T. Nishikawa, and T. Kawase, "High-mobility double-gate organic single-crystal transistors with organic crystal gate insulators," *Applied Physics Letters*, vol. 90, no. 18, p. 182117, 2007. (Cited on page 8.)

[16] R. M. Pope and C. E. Swenberg, *Electronic Processes in Organic Crystals and Polymers*. Oxford University Press, 2nd ed., 1999. (Cited on pages 8 and 39.)

[17] W. A. Luhman and R. J. Holmes, "Investigation of energy transfer in organic photovoltaic cells and impact on exciton diffusion length measurements," *Advanced Functional Materials*, vol. 21, no. 4, pp. 764–771, 2011. (Cited on page 9.)

[18] P. E. Shaw, A. Ruseckas, and I. D. W. Samuel, "Exciton diffusion measurements in poly(3-hexylthiophene)," *Advanced Materials*, vol. 20, no. 18, pp. 3516–3520, 2008.

[19] P. Peumans and S. R. Forrest, "Very-high-efficiency double-heterostructure copper phthalocyanine/C_{60} photovoltaic cells," *Applied Physics Letters*, vol. 79, no. 1, pp. 126–128, 2001. (Cited on page 9.)

[20] H. Najafov, B. Lee, Q. Zhou, C. Feldman, and V. Podzorov, "Observation of long-range exciton diffusion in highly or-

dered organic semiconductors," *Nature Materials*, vol. 9, no. 4, pp. 938–943, 2010. (Cited on page 9.)

[21] P. Peumans and S. R. Forrest, "Separation of geminate charge-pairs at donor-acceptor interfaces in disordered solids," *Chemical Physics Letters*, vol. 398, no. 1Ű3, pp. 27 – 31, 2004. (Cited on page 9.)

[22] B. Lucas, T. Trigaud, and C. Videlot-Ackermann, "Organic transistors and phototransistors based on small molecules," *Polymer International*, vol. 61, no. 3, pp. 374–389, 2012. (Cited on pages 11 and 69.)

[23] J. E. Anthony, "Functionalized acenes and heteroacenes for organic electronics," *Chemical Reviews*, vol. 106, no. 12, pp. 5028–5048, 2006. (Cited on pages 11, 12, 69, and 70.)

[24] J. E. Anthony, "The larger acenes: Versatile organic semiconductors," *Angewandte Chemie International Edition*, vol. 47, no. 3, pp. 452–483, 2008. (Cited on page 12.)

[25] A. L. Appleton, S. M. Brombosz, S. Barlow, J. S. Sears, J. Bredas, S. R. Marder, and U. H. F. Bunz, "Effects of electronegative substitution on the optical and electronic properties of acenes and diazaacenes," *Nature Communications*, vol. 1, pp. 1–7, Oct 2010. (Cited on pages 11 and 69.)

[26] K. B. Burke, Y. Shu, P. Kemppinen, B. Singh, M. Bown, I. I. Liaw, R. M. Williamson, L. Thomsen, P. Dastoor, W. Belcher, C. Forsyth, K. N. Winzenberg, and G. E. Collis, "Single crystal X-ray, AFM, NEXAFS, and OFET studies on angular polycyclic aromatic silyl-capped 7,14-bis(ethynyl)dibenzo[b,def]chrysenes," *Crystal Growth & Design*, vol. 12, no. 2, pp. 725–731, 2012. (Cited on pages 11, 12, and 69.)

[27] H.-Y. Chen and I. Chao, "Toward the rational design of functionalized pentacenes: Reduction of the impact of functionalization on the reorganization energy," *ChemPhysChem*, vol. 7, no. 9, pp. 2003–2007, 2006. (Cited on pages 11 and 64.)

[28] O. Lobanova Griffith, N. E. Gruhn, J. E. Anthony, B. Purushothaman, and D. L. Lichtenberger, "Electron transfer parameters of triisopropylsilylethynyl-substituted oligoacenes," *The Journal of Physical Chemistry C*, vol. 112, no. 51, pp. 20518–20524, 2008. (Cited on pages 12, 55, 69, and 70.)

[29] X. Feng, Q. Li, J. Gu, F. A. Cotton, Y. Xie, and H. F. Schaefer, "Perfluorinated polycyclic aromatic hydrocarbons: Anthracene, phenanthrene, pyrene, tetracene, chrysene, and triphenylene," *The Journal of Physical Chemistry A*, vol. 113, no. 5, pp. 887–894, 2009.

[30] O. Lobanova Griffith, J. E. Anthony, A. G. Jones, and D. L. Lichtenberger, "Electronic properties of pentacene versus triisopropylsilylethynyl-substituted pentacene: Environment-dependent effects of the silyl substituent," *Journal of the American Chemical Society*, vol. 132, no. 2, pp. 580–586, 2010. (Cited on pages 12, 55, and 70.)

[31] H. Sun, A. Putta, and M. Billion, "Arene trifluoromethylation: An effective strategy to obtain air-stable n-type organic semiconductors with tunable optoelectronic and electron transfer properties," *The Journal of Physical Chemistry A*, vol. 116, no. 30, pp. 8015–8022, 2012. (Cited on pages 11 and 69.)

[32] M. L. Tang and Z. Bao, "Halogenated materials as organic semiconductors," *Chemistry of Materials*, vol. 23, no. 3, pp. 446–455, 2011. (Cited on pages 11 and 69.)

[33] T. B. Singh, P. Senkarabacak, N. S. Sariciftci, A. Tanda, C. Lackner, R. Hagelauer, and G. Horowitz, "Organic inverter circuits employing ambipolar pentacene field-effect transistors," *Applied Physics Letters*, vol. 89, no. 3, p. 033512, 2006. (Cited on pages 11, 69, and 70.)

[34] M. C. R. Delgado, K. R. Pigg, D. A. da Silva Filho, N. E. Gruhn, Y. Sakamoto, T. Suzuki, R. M. Osuna, J. Casado, V. Hernández, J. T. L. Navarrete, N. G. Martinelli, J. Cornil, R. S. Sánchez-Carrera, V. Coropceanu, and J.-L. Brédas, "Impact of perfluorination on the charge-transport parameters of oligoacene crystals," *Journal of the American Chemical Society*, vol. 131, no. 4, pp. 1502–1512, 2009. (Cited on pages 11, 69, and 70.)

[35] B. A. Jones, M. J. Ahrens, M.-H. Yoon, A. Facchetti, T. J. Marks, and M. R. Wasielewski, "High-mobility air-stable n-type semiconductors with processing versatility: Dicyanoperylene-3,4:9,10-bis(dicarboximides)," *Angewandte Chemie International Edition*, vol. 43, no. 46, pp. 6363–6366, 2004. (Cited on pages 11 and 70.)

[36] M. L. Tang, J. H. Oh, A. D. Reichardt, and Z. Bao, "Chlorination: A general route toward electron transport in or-

ganic semiconductors," *Journal of the American Chemical Society*, vol. 131, no. 10, pp. 3733–3740, 2009. (Cited on pages 11 and 70.)

[37] C. C. Mattheus, A. B. Dros, J. Baas, G. T. Oostergetel, A. Meetsma, J. L. de Boer, and T. T. Palstra, "Identification of polymorphs of pentacene," *Synthetic Metals*, vol. 138, no. 3, pp. 475–481, 2003. (Cited on pages 11 and 70.)

[38] H. Yang, T. J. Shin, M.-M. Ling, K. Cho, C. Y. Ryu, and Z. Bao, "Conducting AFM and 2D GIXD studies on pentacene thin films," *Journal of the American Chemical Society*, vol. 127, no. 33, pp. 11542–11543, 2005.

[39] M. Pedio, B. Doyle, N. Mahne, A. Giglia, F. Borgatti, S. Nannarone, S. Henze, R. Temirov, F. Tautz, L. Casalis, R. Hudej, M. Danisman, and B. Nickel, "Growth of pentacene on Ag(1;1;1) surface: A NEXAFS study," *Applied Surface Science*, vol. 254, no. 1, pp. 103 – 107, 2007.

[40] S. C. B. Mannsfeld, A. Virkar, C. Reese, M. F. Toney, and Z. Bao, "Precise structure of pentacene monolayers on amorphous silicon oxide and relation to charge transport," *Advanced Materials*, vol. 21, no. 22, pp. 2294–2298, 2009. (Cited on page 70.)

[41] J. C. Sancho-Garcia, A. J. Perez-Jimenez, Y. Olivier, and J. Cornil, "Molecular packing and charge transport parameters in crystalline organic semiconductors from first-principles calculations," *Phys. Chem. Chem. Phys.*, vol. 12, pp. 9381–9388, 2010. (Cited on pages 55 and 60.)

[42] J. C. Sancho-Garcia and Perez-Jimenez, "A theoretical study of π-stacking tetracene derivatives as promising organic molecular semiconductors," *Chemical Physics Letters*, vol. 499, pp. 146–151, 2010. (Cited on pages 11 and 55.)

[43] M. D. Curtis, J. Cao, and J. W. Kampf, "Solid-state packing of conjugated oligomers: From π-stacks to the herringbone structure," *Journal of the American Chemical Society*, vol. 126, no. 13, pp. 4318–4328, 2004. (Cited on page 11.)

[44] A. L. Briseno, S. C. Mannsfeld, S. A. Jenekhe, Z. Bao, and Y. Xia, "Introducing organic nanowire transistors," *Materials Today*, vol. 11, no. 4, pp. 38 – 47, 2008. (Cited on pages 11 and 12.)

[45] A. P. H. J. Schenning and E. W. Meijer, "Supramolecular electronics; nanowires from self-assembled π-conjugated systems," *Chem. Commun.*, pp. 3245–3258, 2005. (Cited on page 12.)

[46] F. J. M. Hoeben, P. Jonkheijm, E. W. Meijer, and A. P. H. J. Schenning, "About supramolecular assemblies of π-conjugated systems," *Chemical Reviews*, vol. 105, no. 4, pp. 1491–1546, 2005. (Cited on page 12.)

[47] A. L. Briseno, Q. Miao, M.-M. Ling, C. Reese, H. Meng, Z. Bao, and F. Wudl, "Hexathiapentacene: Structure, molecular packing, and thin-film transistors," *Journal of the American Chemical Society*, vol. 128, no. 49, pp. 15576–15577, 2006. (Cited on pages 12, 70, 73, 74, 76, 78, 79, 107, and 111.)

[48] M. T. Lloyd, A. C. Mayer, S. Subramanian, D. A. Mourey, A. V. Herman, Dave J.ăand Bapat, J. E. Anthony, and G. G. Malliaras, "Efficient solution-processed photovoltaic cells based on an anthradithiophene/fullerene blend," *Journal of the American Chemical Society*, vol. 129, no. 29, pp. 9144–9149, 2007. (Cited on page 12.)

[49] K. N. Winzenberg, P. Kemppinen, G. Fanchini, M. Bown, G. E. Collis, C. M. Forsyth, K. Hegedus, T. B. Singh, and S. E. Watkins, "Dibenzo[b,def]chrysene derivatives: Solution-processable small molecules that deliver high power-conversion efficiencies in bulk heterojunction solar cells," *Chemistry of Materials*, vol. 21, no. 24, pp. 5701–5703, 2009. (Cited on page 12.)

[50] L. Zhang, B. Walker, F. Liu, N. S. Colella, S. C. B. Mannsfeld, J. J. Watkins, T.-Q. Nguyen, and A. L. Briseno, "Triisopropylsilylethynyl-functionalized dibenzo[def,mno]chrysene: a solution-processed small molecule for bulk heterojunction solar cells," *J. Mater. Chem.*, vol. 22, pp. 4266–4268, 2012. (Cited on page 12.)

[51] O. L. Griffith, J. E. Anthony, A. G. Jones, Y. Shu, and D. L. Lichtenberger, "Substituent effects on the electronic characteristics of pentacene derivatives for organic electronic devices: Dioxolane-substituted pentacene derivatives with triisopropylsilylethynyl functional groups," *Journal of the American Chemical Society*, vol. 134, no. 34, pp. 14185–14194, 2012. (Cited on page 12.)

[52] S. C. B. Mannsfeld, M. L. Tang, and Z. Bao, "Thin film structure of triisopropylsilylethynyl-functionalized pentacene and tetraceno[2,3-b]thiophene from grazing incidence X-Ray diffraction," *Advanced Materials*, vol. 23, no. 1, pp. 127–131, 2011. (Cited on page 12.)

[53] W. Kohn, "Electronic structure of matter-wave functions and density functionals (nobel lecture)," *Review of Modern Physics*, vol. 71, p. 1253, 1999. (Cited on pages 15, 21, 55, and 70.)

[54] E. Runge and E. K. U. Gross, "Density-functional theory for time-dependent systems," *Phys. Rev. Lett.*, vol. 52, pp. 997–1000, Mar 1984. (Cited on pages 15 and 29.)

[55] M. Born and J. R. Oppenheimer, "Zur quantentheorie der molekeln," *Annalen der Physik*, vol. 84, pp. 457–484, 1927. (Cited on page 17.)

[56] D. R. Hartree, "The wave mechanics of an atom with a non-coulomb central field. part i. theory and methods," *Mathematical Proceedings of the Cambridge Philosophical Society*, vol. 24, pp. 89–110, 1 1928. (Cited on page 19.)

[57] D. R. Hartree, "The wave mechanics of an atom with a non-coulomb central field. part ii. some results and discussion," *Mathematical Proceedings of the Cambridge Philosophical Society*, vol. 24, pp. 111–132, 1 1928. (Cited on page 19.)

[58] V. Fock, "Näherungsmethode zur lösung des quantenmechanischen mehrkörperproblems," *Zeitschrift für Physik*, vol. 61, no. 1-2, pp. 126–148, 1930. (Cited on page 20.)

[59] J. C. Slater, "Note on Hartree's method," *Phys. Rev.*, vol. 35, pp. 210–211, Jan 1930. (Cited on page 20.)

[60] L. H. Thomas, "The calculation of atomic fields," *Mathematical Proceedings of the Cambridge Philosophical Society*, vol. 23, pp. 542–548, 1927. (Cited on page 21.)

[61] E. Fermi, "Eine statistische methode zur bestimmung einiger eigenschaften des atoms und ihre anwendung auf die theorie des periodischen systems der elemente," *Zeitschrift für Physik*, vol. 48, no. 1-2, pp. 73–79, 1928. (Cited on page 21.)

[62] P. Hohenberg and W. Kohn, "Inhomogeneous electron gas," *Phys. Rev.*, vol. 136, pp. B864–B871, Nov 1964. (Cited on pages 21, 22, and 25.)

[63] W. Kohn and L. J. Sham, "Self-consistent equations including exchange and correlation effects," *Phys. Rev.*, vol. 140, pp. A1133–A1138, Nov 1965. (Cited on pages 22 and 25.)

[64] R. O. Jones, "Density functional theory: Its origins, rise to prominence, and future," *Rev. Mod. Phys.*, vol. 87, pp. 897–923, Aug 2015. (Cited on page 23.)

[65] O. Gunnarsson and B. I. Lundqvist, "Exchange and correlation in atoms, molecules, and solids by the spin-density-functional formalism," *Phys. Rev. B*, vol. 13, pp. 4274–4298, May 1976. (Cited on page 24.)

[66] P. H. Dederichs, S. Blügel, R. Zeller, and H. Akai, "Ground states of constrained systems: Application to cerium impurities," *Phys. Rev. Lett.*, vol. 53, pp. 2512–2515, Dec 1984. (Cited on page 24.)

[67] E. Wigner, "On the interaction of electrons in metals," *Phys. Rev.*, vol. 46, pp. 1002–1011, Dec 1934. (Cited on page 24.)

[68] G. D. Mahan, *Many-Particle Physics*. Kluwer Academic / Plenum Press, 2^{rd} ed., 2000. (Cited on page 24.)

[69] J. P. Perdew, J. A. Chevary, S. H. Vosko, K. A. Jackson, M. R. Pederson, D. J. Singh, and C. Fiolhais, "Atoms, molecules, solids, and surfaces: Applications of the generalized gradient approximation for exchange and correlation," *Phys. Rev. B*, vol. 46, pp. 6671–6687, Sep 1992. (Cited on page 25.)

[70] S. H. Vosko, L. Wilk, and M. Nusair, "Accurate spin-dependent electron liquid correlation energies for local spin density calculations: a critical analysis," *Canadian Journal of Physics*, vol. 58, no. 8, pp. 1200–1211, 1980. (Cited on page 25.)

[71] C. Lee, W. Yang, and R. G. Parr, "Development of the Colle-Salvetti correlation-energy formula into a functional of the electron density," *Phys. Rev. B*, vol. 37, pp. 785–789, Jan 1988. (Cited on page 25.)

[72] J. P. Perdew, K. Burke, and M. Ernzerhof, "Generalized gradient approximation made simple," *Phys. Rev. Lett.*, vol. 77, pp. 3865–3868, Oct 1996. (Cited on pages 25 and 73.)

[73] J. Tao, J. P. Perdew, V. N. Staroverov, and G. E. Scuseria, "Climbing the density functional ladder: Nonempirical meta–generalized gradient approximation designed for

molecules and solids," *Phys. Rev. Lett.*, vol. 91, p. 146401, Sep 2003. (Cited on page 26.)

[74] R. P. Feynman, "Forces in molecules," *Phys. Rev.*, vol. 56, pp. 340–343, Aug 1939. (Cited on page 26.)

[75] A. D. Becke, "Density-functional thermochemistry. III. the role of exact exchange," *Journal of Chemical Physics*, vol. 98, p. 5648, 1993. (Cited on pages 26 and 71.)

[76] R. O. Jones and O. Gunnarsson, "The density functional formalism, its applications and prospects," *Rev. Mod. Phys.*, vol. 61, pp. 689–746, 1989. (Cited on page 27.)

[77] G. Onida, L. Reining, and A. Rubio, "Electronic excitations: density-functional versus many-body Green's-function approaches," *Rev. Mod. Phys.*, vol. 74, p. 601, 2002. (Cited on page 27.)

[78] F. Bechstedt, R. D. Sole, G. Cappellini, and L. Reining, "An efficient method for calculating quasiparticle energies in semiconductors," *Solid State Communications*, vol. 84, no. 7, pp. 765 – 770, 1992. (Cited on page 27.)

[79] G. Malloci, L. Chiodo, A. Rubio, and A. Mattoni, "Structural and optoelectronic properties of unsaturated ZnO and ZnS nanoclusters," *J. Phys. Chem. C*, vol. 116, pp. 8741–8746, 2012. (Cited on page 27.)

[80] G. Malloci, G. Cappellini, G. Mulas, and G. Satta, "Quasiparticle effects and optical absorption in small fullerenelike gap clusters," *Phys. Rev. B*, vol. 70, p. 205429, Nov 2004. (Cited on pages 27 and 71.)

[81] R. O. Jones and O. Gunnarsson, "The density functional formalism, its applications and prospects," *Rev. Mod. Phys.*, vol. 61, pp. 689–746, Jul 1989. (Cited on pages 28 and 71.)

[82] A. U. Carsten, *Time-Dependent Density Functional Theory: concept and applications*. Oxford University Press, 2012. (Cited on pages 29 and 105.)

[83] M. Marques and E. Gross, "Time-dependent density functional theory," *Annual Review of Physical Chemistry*, vol. 55, no. 1, pp. 427–455, 2004. (Cited on pages 30, 55, and 70.)

[84] M. A. L. Marques, A. Castro, and A. Rubio, "Assessment of exchange-correlation functionals for the calculation of dynamical properties of small clusters in time-dependent density functional theory," *The Journal of Chemical Physics*, vol. 115, no. 7, pp. 3006–3014, 2001. (Cited on page 31.)

[85] L. Serra and A. Rubio, "Core polarization in the optical response of metal clusters: Generalized time-dependent density-functional theory," *Phys. Rev. Lett.*, vol. 78, pp. 1428–1431, Feb 1997. (Cited on page 31.)

[86] M. A. L. Marques, X. López, D. Varsano, A. Castro, and A. Rubio, "Time-dependent density-functional approach for biological chromophores: The case of the green fluorescent protein," *Phys. Rev. Lett.*, vol. 90, p. 258101, Jun 2003. (Cited on page 31.)

[87] V. M. Galitskii and A. B. Migdal, "Application of quantum field theory methods to the many body problem," *Sov. Phys. - JETP*, vol. 7, no. 1, pp. 96–104, 1958. (Cited on pages 31 and 33.)

[88] F. Sottile, *Response functions of semiconductors and insulators: from the Bethe-Salpeter equation to time-dependent density functional theory*. PhD thesis, -, Sept. 2003. (Cited on pages 32, 35, and 36.)

[89] G. Mahan, *Many-Particle Physics*. Springer, 3rd ed., 2010. (Cited on page 33.)

[90] P. C. Martin and J. Schwinger, "Theory of many-particle systems. i," *Phys. Rev.*, vol. 115, pp. 1342–1373, Sep 1959. (Cited on page 33.)

[91] L. Hedin, "New method for calculating the one-particle green's function with application to the electron-gas problem," *Phys. Rev.*, vol. 139, pp. A796–A823, Aug 1965. (Cited on page 34.)

[92] G. Onida, L. Reining, and A. Rubio, "Electronic excitations: density-functional versus many-body green's-function approaches," *Rev. Mod. Phys.*, vol. 74, pp. 601–659, Jun 2002. (Cited on pages 34, 37, 38, and 72.)

[93] C. Faber, P. Boulanger, C. Attaccalite, I. Duchemin, and X. Blase, "Excited states properties of organic molecules: from density functional theory to the GW and Bethe-Salpeter

Green's function formalisms," *Philosophical Transactions of the Royal Society of London A: Mathematical, Physical and Engineering Sciences*, vol. 372, no. 2011, 2014. (Cited on page 35.)

[94] E. E. Salpeter and H. A. Bethe, "A relativistic equation for bound-state problems," *Phys. Rev.*, vol. 84, pp. 1232–1242, Dec 1951. (Cited on page 37.)

[95] L. J. Sham and T. M. Rice, "Many-particle derivation of the effective-mass equation for the Wannier exciton," *Phys. Rev.*, vol. 144, pp. 708–714, Apr 1966. (Cited on page 37.)

[96] W. Hanke and L. J. Sham, "Many-particle effects in the optical excitations of a semiconductor," *Phys. Rev. Lett.*, vol. 43, pp. 387–390, Jul 1979.

[97] G. Strinati, "Dynamical shift and broadening of core excitons in semiconductors," *Phys. Rev. Lett.*, vol. 49, pp. 1519–1522, Nov 1982. (Cited on page 37.)

[98] R. J. Elliott, "Intensity of optical absorption by excitons," *Phys. Rev.*, vol. 108, pp. 1384–1389, Dec 1957. (Cited on page 37.)

[99] M. Rohlfing and S. G. Louie, "Excitonic effects and the optical absorption spectrum of hydrogenated Si clusters," *Phys. Rev. Lett.*, vol. 80, pp. 3320–3323, Apr 1998. (Cited on page 37.)

[100] S. Albrecht, L. Reining, R. Del Sole, and G. Onida, "*Ab Initio* calculation of excitonic effects in the optical spectra of semiconductors," *Phys. Rev. Lett.*, vol. 80, pp. 4510–4513, May 1998.

[101] L. X. Benedict, E. L. Shirley, and R. B. Bohn, "Optical absorption of insulators and the electron-hole interaction: An *Ab Initio* calculation," *Phys. Rev. Lett.*, vol. 80, pp. 4514–4517, May 1998. (Cited on page 37.)

[102] M. Rohlfing and S. G. Louie, "Electron-hole excitations and optical spectra from first principles," *Phys. Rev. B*, vol. 62, pp. 4927–4944, Aug 2000. (Cited on page 37.)

[103] P. H. Hahn, W. G. Schmidt, and F. Bechstedt, "Molecular electronic excitations calculated from a solid-state approach: Methodology and numerics," *Phys. Rev. B*, vol. 72, p. 245425, Dec 2005. (Cited on page 37.)

[104] K. Hummer, P. Puschnig, and C. Ambrosch-Draxl, "Lowest optical excitations in molecular crystals: Bound excitons versus

free electron-hole pairs in anthracene," *Phys. Rev. Lett.*, vol. 92, p. 147402, Apr 2004. (Cited on page 37.)

[105] K. Hummer and C. Ambrosch-Draxl, "Electronic properties of oligoacenes from first principles," *Phys. Rev. B*, vol. 72, p. 205205, 2005. (Cited on pages 80, 82, 83, and 111.)

[106] P. Cudazzo, M. Gatti, and A. Rubio, "Excitons in molecular crystals from first-principles many-body perturbation theory: Picene versus pentacene," *Phys. Rev. B*, vol. 86, p. 195307, Nov 2012. (Cited on page 37.)

[107] G. Satta, G. Cappellini, V. Olevano, and L. Reining, "Many-body effects in the electronic spectra of cubic boron nitride," *Phys. Rev. B*, vol. 70, p. 195212, Nov 2004. (Cited on pages 37 and 38.)

[108] C. Rödl, F. Fuchs, J. Furthmüller, and F. Bechstedt, "*Ab initio* theory of excitons and optical properties for spin-polarized systems: Application to antiferromagnetic MnO," *Phys. Rev. B*, vol. 77, p. 184408, May 2008. (Cited on page 37.)

[109] E. L. Shirley, "Many-body effects on bandwidths in ionic, noble gas, and molecular solids," *Phys. Rev. B*, vol. 58, pp. 9579–9583, Oct 1998. (Cited on page 38.)

[110] J.-L. Brédas, D. Beljonne, V. Coropceanu, and J. Cornil, "Charge-transfer and energy-transfer processes in π-conjugated oligomers and polymers: A molecular picture," *Chemical Reviews*, vol. 104, no. 11, pp. 4971–5004, 2004. (Cited on pages 38, 72, and 86.)

[111] K. Hannewald and P. A. Bobbert, "Ab initio theory of charge-carrier conduction in ultrapure organic crystals," *Applied Physics Letters*, vol. 85, no. 9, pp. 1535–1537, 2004.

[112] H. Sirringhaus, P. J. Brown, R. H. Friend, M. M. Nielsen, K. Bechgaard, B. M. W. Langeveld-Voss, A. J. H. Spiering, R. A. J. Janssen, E. W. Meijer, P. Herwig, and D. M. de Leeuw, "Two-dimensional charge transport in self-organized, high-mobility conjugated polymers," *Nature*, vol. 401, no. 6754, pp. 685–688, 1999. (Cited on page 38.)

[113] R. A. Marcus, "Electron transfer reactions in chemistry. theory and experiment," *Rev. Mod. Phys.*, vol. 65, pp. 599–610, Jul 1993. (Cited on pages 38 and 86.)

[114] R. A. Marcus, "Electrostatic free energy and other properties of states having nonequilibrium polarization. I," *The Journal of Chemical Physics*, vol. 24, no. 5, pp. 979–989, 1956. (Cited on page 39.)

[115] R. A. Marcus, "On the theory of electrochemical and chemical electron transfer processes," *Canadian Journal of Chemistry*, vol. 37, no. 1, pp. 155–163, 1959.

[116] R. A. Marcus, "On the theory of oxidation-reduction reactions involving electron transfer. V. Comparison and properties of electrochemical and chemical rate constants," *The Journal of Physical Chemistry*, vol. 67, no. 4, pp. 853–857, 1963. (Cited on page 39.)

[117] P. F. Barbara, T. J. Meyer, and M. A. Ratner, "Contemporary issues in electron transfer research," *The Journal of Physical Chemistry*, vol. 100, no. 31, pp. 13148–13168, 1996. (Cited on page 38.)

[118] I. Leontyev, A. Tovmash, M. Vener, I. Rostov, and M. Basilevsky, "Molecular simulations of outersphere reorganization energies for intramolecular electron and hole transfer in polar solvents," *Chemical Physics*, vol. 319, no. 1-3, pp. 4 – 15, 2005. (Cited on page 39.)

[119] J. R. Reimers, Z.-L. Cai, and N. S. Hush, "A priori evaluation of the solvent contribution to the reorganization energy accompanying intramolecular electron transfer: Predicting the nature of the Creutz-Taube ion," *Chemical Physics*, vol. 319, no. 1-3, pp. 39 – 51, 2005.

[120] A. A. Milischuk, D. V. Matyushov, and M. D. Newton, "Activation entropy of electron transfer reactions," *Chemical Physics*, vol. 324, no. 1, pp. 172 – 194, 2006.

[121] M. V. Vener, A. V. Tovmash, I. V. Rostov, and M. V. Basilevsky, "Molecular simulations of outersphere reorganization energies in polar and quadrupolar solvents. the case of intramolecular electron and hole transfer," *The Journal of Physical Chemistry B*, vol. 110, no. 30, pp. 14950–14955, 2006.

[122] S. R. Manjari, , and H. J. Kim, "Temperature- and pressure-dependence of the outer-sphere reorganization free energy for electron transfer reactions: A continuum approach," *The Journal of Physical Chemistry B*, vol. 110, no. 1, pp. 494–500, 2006. (Cited on page 39.)

[123] K. Senthilkumar, F. C. Grozema, F. M. Bickelhaupt, and L. D. A. Siebbeles, "Charge transport in columnar stacked triphenylenes: Effects of conformational fluctuations on charge transfer integrals and site energies," *The Journal of Chemical Physics*, vol. 119, no. 18, pp. 9809–9817, 2003. (Cited on pages 39 and 42.)

[124] K. Senthilkumar, F. C. Grozema, C. Fonseca Guerra, F. M. Bickelhaupt, F. D. Lewis, Y. A. Berlin, M. A. Ratner, and L. D. A. Siebbeles, "Absolute rates of hole transfer in DNA," *Journal of the American Chemical Society*, vol. 127, no. 42, pp. 14894–14903, 2005. (Cited on page 39.)

[125] E. F. Valeev, V. Coropceanu, D. A. da Silva Filho, S. Salman, and J.-L. Brédas, "Effect of electronic polarization on charge-transport parameters in molecular organic semiconductors," *Journal of the American Chemical Society*, vol. 128, no. 30, pp. 9882–9886, 2006. (Cited on pages 39, 41, 42, and 87.)

[126] V. Coropceanu, J. Cornil, D. A. da Silva Filho, Y. Olivier, R. Silbey, and J.-L. Brédas, "Charge transport in organic semiconductors," *Chemical Reviews*, vol. 107, no. 4, pp. 926–952, 2007. (Cited on pages 39, 41, 42, and 85.)

[127] S. E. Koh, C. Risko, D. A. daSilva Filho, O. Kwon, A. Facchetti, J.-L. Brédas, T. J. Marks, and M. A. Ratner, "Modeling electron and hole transport in fluoroarene-oligothiopene semiconductors: Investigation of geometric and electronic structure properties," *Advanced Functional Materials*, vol. 18, no. 2, pp. 332–340, 2008. (Cited on page 41.)

[128] J. C. Slater, "Atomic shielding constants," *Phys. Rev.*, vol. 36, pp. 57–64, Jul 1930. (Cited on page 42.)

[129] S. F. Boys, "Electronic wave functions. I. A general method of calculation for the stationary states of any molecular system," *Proceedings of the Royal Society of London A: Mathematical, Physical and Engineering Sciences*, vol. 200, no. 1063, pp. 542–554, 1950. (Cited on page 42.)

[130] A. M. Malek, *Chemical Reactivity Indices in Thermodynamic Extension of the Spin Density Functional Theory and its Zero-Temperature Limit*. PhD thesis, -, May 2014. (Cited on pages 45 and 105.)

[131] R. Ditchfield, W. J. Hehre, and J. A. Pople, "Self-consistent molecular-orbital methods IX. an extended gaussian-type basis for molecular-orbital studies of organic molecules," *The Journal of Chemical Physics*, vol. 54, no. 2, pp. 724–728, 1971. (Cited on page 47.)

[132] M. C. Payne, M. P. Teter, D. C. Allan, T. A. Arias, and J. D. Joannopoulos, "Iterative minimization techniques for *ab initio* total-energy calculations: molecular dynamics and conjugate gradients," *Rev. Mod. Phys.*, vol. 64, pp. 1045–1097, Oct 1992. (Cited on pages 48 and 49.)

[133] R. M. Martin, *Electronic Structure: Basic Theory and Practical Methods*. Cambridge University Press (CUP), 2004. (Cited on page 49.)

[134] H. J. Monkhorst and J. D. Pack, "Special points for Brillouin-zone integrations," *Phys. Rev. B*, vol. 13, pp. 5188–5192, Jun 1976. (Cited on page 49.)

[135] F. Jensen, *Introduction to Computational Chemistry*. Wiley, 2^{rd} ed., 2007. (Cited on pages 50, 51, and 52.)

[136] J. Sancho-García, "Assessment of density-functional models for organic molecular semiconductors: The role of hartree–fock exchange in charge-transfer processes," *Chemical Physics*, vol. 331, no. 2–3, pp. 321–331, 2007. (Cited on pages 55, 58, and 72.)

[137] S. Grimme and M. Parac, "Substantial errors from time-dependent density functional theory for the calculation of excited states of large π systems," *ChemPhysChem*, vol. 4, no. 3, pp. 292–295, 2003. (Cited on page 57.)

[138] G. Cappellini, G. Malloci, and G. Mulas, "Electronic excitations of oligoacenes: A time dependent density functional theory study," *Superlattices and Microstructures*, vol. 46, no. 1-2, pp. 14 – 18, 2009. (Cited on pages 57 and 71.)

[139] G. Malloci, G. Cappellini, G. Mulas, and A. Mattoni, "Electronic and optical properties of families of polycyclic aromatic hydrocarbons: A systematic (time-dependent) density functional theory study," *Chemical Physics*, vol. 384, no. 1–3, pp. 19–27, 2011. (Cited on pages 57, 64, 71, 76, and 111.)

[140] B. M. Wong, M. Piacenza, and F. D. Sala, "Absorption and fluorescence properties of oligothiophene biomarkers from

long-range-corrected time-dependent density functional theory," *Phys. Chem. Chem. Phys.*, vol. 11, pp. 4498–4508, 2009. (Cited on page 57.)

[141] (Cited on page 57.)

[142] J.-D. Chai and M. Head-Gordon, "Long-range corrected hybrid density functionals with damped atom-atom dispersion corrections," *Phys. Chem. Chem. Phys.*, vol. 10, pp. 6615–6620, 2008. (Cited on page 57.)

[143] G. Malloci, C. Joblin, and G. Mulas, "On-line database of the spectral properties of polycyclic aromatic hydrocarbons," *Chemical Physics*, vol. 332, pp. 353 – 359, 2007. (Cited on pages 59 and 110.)

[144] G. Malloci, G. Mulas, G. Cappellini, and C. Joblin, "Time-dependent density functional study of the electronic spectra of oligoacenes in the charge states -1, 0, +1, and +2," *Chemical Physics*, vol. 340, no. 1–3, pp. 43–58, 2007. (Cited on pages 59, 71, and 110.)

[145] R. Rieger and K. Müllen, "Forever young: polycyclic aromatic hydrocarbons as model cases for structural and optical studies," *Journal of Physical Organic Chemistry*, vol. 23, no. 4, pp. 315–325, 2010. (Cited on pages 59 and 110.)

[146] S. Grimme, J. Antony, S. Ehrlich, and S. Krieg, "Semiempirical GGA-type density functional constructed with a long-range dispersion correction," *Journal of Computational Chemistry*, vol. 27, no. 15, pp. 1787–1799, 2006. (Cited on page 58.)

[147] J. C. Sancho-Garcia and A. J. Perez-Jimenez, "Charge-transport properties of prototype molecular materials for organic electronics based on graphene nanoribbons," *Phys. Chem. Chem. Phys.*, vol. 11, pp. 2741–2746, 2009. (Cited on pages 58, 64, and 86.)

[148] J. Bromilow, R. T. C. Brownlee, V. O. Lopez, and R. W. Taft, "Para-substituent C-13 chemical shifts in substituted benzenes. I. Updating the σ_r^0 scale and analysis of aprotic solvent effects," *The Journal of Organic Chemistry*, vol. 44, no. 26, pp. 4766–4770, 1979. (Cited on page 64.)

[149] G. Malloci, G. Cappellini, G. Mulas, and A. Mattoni, "A (time dependent) density functional theory study of the optoelectronic properties of bis-triisopropylsilylethynyl functionalized

acenes," *Thin Solid Films*, vol. 543, pp. 32–34, 2013. (Cited on page 67.)

[150] H. Ma, H.-L. Yip, F. Huang, and A. K.-Y. Jen, "Interface engineering for organic electronics," *Advanced Functional Materials*, vol. 20, no. 9, pp. 1371–1388, 2010. (Cited on page 69.)

[151] C. C. Mattheus, A. B. Dros, J. Baas, A. Meetsma, J. L. de Boer, and T. T. M. Palstra, "Polymorphism in pentacene," *Acta Crystallographica Section C*, vol. 57, pp. 939–941, Aug 2001. (Cited on pages 70, 73, 74, and 111.)

[152] F. Anger, R. Scholz, E. Adamski, K. Broch, A. Gerlach, Y. Sakamoto, T. Suzuki, and F. Schreiber, "Optical properties of fully and partially fluorinated rubrene in films and solution," *Applied Physics Letters*, vol. 102, no. 1, p. 013308, 2013. (Cited on page 70.)

[153] M. Mas-Torrent, M. Durkut, P. Hadley, X. Ribas, and C. Rovira, "High mobility of dithiophene-tetrathiafulvalene single-crystal organic field effect transistors," *Journal of the American Chemical Society*, vol. 126, no. 4, pp. 984–985, 2004. (Cited on page 70.)

[154] M. Mas-Torrent and C. Rovira, "Tetrathiafulvalene derivatives for organic field effect transistors," *J. Mater. Chem.*, vol. 16, pp. 433–436, 2006. (Cited on page 70.)

[155] M. Bendikov, F. Wudl, and D. F. Perepichka, "Tetrathiafulvalenes, oligoacenenes, and their buckminsterfullerene derivatives: The brick and mortar of organic electronics," *Chemical Reviews*, vol. 104, no. 11, pp. 4891–4946, 2004. (Cited on page 70.)

[156] M. Valiev, E. Bylaska, N. Govind, K. Kowalski, T. Straatsma, H. V. Dam, D. Wang, J. Nieplocha, E. Apra, T. Windus, and W. de Jong, "Nwchem: A comprehensive and scalable open-source solution for large scale molecular simulations," *Computer Physics Communications*, vol. 181, no. 9, pp. 1477 – 1489, 2010. (Cited on page 71.)

[157] R. Cardia, G. Malloci, A. Mattoni, and G. Cappellini, "Effects of tips-functionalization and perhalogenation on the electronic, optical, and transport properties of angular and compact dibenzochrysene," *The Journal of Physical Chemistry A*, vol. 118, no. 28, pp. 5170–5177, 2014. (Cited on page 71.)

[158] X. Blase, C. Attaccalite, and V. Olevano, "First-principles *GW* calculations for fullerenes, porphyrins, phtalocyanine, and other molecules of interest for organic photovoltaic applications," *Phys. Rev. B*, vol. 83, p. 115103, Mar 2011. (Cited on page 72.)

[159] X. Blase and C. Attaccalite, "Charge-transfer excitations in molecular donor-acceptor complexes within the many-body Bethe-Salpeter approach," *Applied Physics Letters*, vol. 99, no. 17, p. 171909, 2011.

[160] D. Jacquemin, I. Duchemin, and X. Blase, "Benchmarking the Bethe-Salpeter formalism on a standard organic molecular set," *Journal of Chemical Theory and Computation*, vol. 11, no. 7, pp. 3290–3304, 2015. (Cited on page 72.)

[161] X. Gonze, B. Amadon, P.-M. Anglade, J.-M. Beuken, F. Bottin, P. Boulanger, F. Bruneval, D. Caliste, R. Caracas, M. Côté, T. Deutsch, L. Genovese, P. Ghosez, M. Giantomassi, S. Goedecker, D. Hamann, P. Hermet, F. Jollet, G. Jomard, S. Leroux, M. Mancini, S. Mazevet, M. Oliveira, G. Onida, Y. Pouillon, T. Rangel, G.-M. Rignanese, D. Sangalli, R. Shaltaf, M. Torrent, M. Verstraete, G. Zerah, and J. Zwanziger, "ABINIT: First-principles approach to material and nanosystem properties," *Computer Physics Communications*, vol. 180, no. 12, pp. 2582 – 2615, 2009. (Cited on page 73.)

[162] X. Gonze, G.-M. Rignanese, M. Verstraete, J.-M. Beuken, Y. Pouillon, R. Caracas, F. Jollet, M. Torrent, G. Zerah, M. Mikami, P. Ghosez, M. Veithen, J.-Y. Raty, V. Olevano, F. Bruneval, L. Reining, R. Godby, G. Onida, D. Hamann, and D. Allan., "A brief introduction to the ABINIT software package.," *Zeitschrift fur Kristallographie - Crystalline Materials*, vol. 220, pp. 558 – 562, 2005.

[163] X. Gonze, J.-M. Beuken, R. Caracas, F. Detraux, M. Fuchs, G.-M. Rignanese, L. Sindic, M. Verstraete, G. Zerah, F. Jollet, M. Torrent, A. Roy, M. Mikami, P. Ghosez, J.-Y. Raty, and D. Allan, "First-principles computation of material properties: the {ABINIT} software project," *Computational Materials Science*, vol. 25, no. 3, pp. 478 – 492, 2002. (Cited on page 73.)

[164] N. Troullier and J. L. Martins, "Efficient pseudopotentials for plane-wave calculations," *Phys. Rev. B*, vol. 43, pp. 1993–2006, Jan 1991. (Cited on page 73.)

[165] S. Grimme, J. Antony, S. Ehrlich, and S. Krieg, "A consistent and accurate ab initio parametrization of density functional dispersion correction (DFT-D) for the 94 elements H-Pu," *Journal of Chemical Physics*, vol. 132, p. 154104, 2010. (Cited on page 73.)

[166] S. Grimme, S. Ehrlich, and L. Goerigk, "Effect of the damping function in dispersion corrected density functional theory," *Journal of Computational Chemistry*, vol. 32, no. 7, pp. 1456–1465, 2011. (Cited on page 73.)

[167] M. Marques, J. Vidal, M. Oliveira, L. Reining, and S. Botti, "Density-based mixing parameter for hybrid functionals," *Phys. Rev. B*, vol. 83, p. 035119, 2011. (Cited on page 74.)

[168] J. Skone, M. Govoni, and G. Galli, "Self-consistent hybrid functional for condensed systems," *Phys. Rev. B*, vol. 89, p. 195112, 2014. (Cited on page 74.)

[169] D. Varsano, R. Di Felice, M. A. L. Marques, and A. Rubio, "A TDDFT study of the excited states of DNA bases and their assemblies," *The Journal of Physical Chemistry B*, vol. 110, no. 14, pp. 7129–7138, 2006. (Cited on page 79.)

[170] M. L. Tiago, J. E. Northrup, and S. G. Louie, "*Ab initio* calculation of the electronic and optical properties of solid pentacene," *Phys. Rev. B*, vol. 67, p. 115212, 2003. (Cited on page 80.)

[171] H. Klauk, ed., *Organic Electronics: Materials, Manufacturing, and Applications*. Wiley - VCH, 1^{st} ed., 2006. (Cited on page 85.)

[172] T. Mori, "Molecular materials for organic field-effect transistors," *Journal of Physics: Condensed Matter*, vol. 20, no. 18, p. 184010, 2008. (Cited on page 85.)

[173] R. Marcus and N. Sutin, "Electron transfers in chemistry and biology," *Biochimica et Biophysica Acta (BBA) - Reviews on Bioenergetics*, vol. 811, no. 3, pp. 265 – 322, 1985. (Cited on page 86.)

[174] J. Cornil, D. Beljonne, J.-P. Calbert, and J.-L. Brédas, "Interchain interactions in organic π-conjugated materials: Impact on electronic structure, optical response, and charge transport," *Advanced Materials*, vol. 13, no. 14, pp. 1053–1067, 2001. (Cited on page 86.)

[175] F. C. Grozema and L. D. Siebbeles, "Mechanism of charge transport in self-organizing organic materials," *International Reviews in Physical Chemistry*, vol. 27, no. 1, pp. 87–138, 2008. (Cited on page 86.)

[176] Y. A. Berlin, G. R. Hutchison, P. Rempala, M. A. Ratner, and J. Michl, "Charge hopping in molecular wires as a sequence of electron-transfer reactions," *The Journal of Physical Chemistry A*, vol. 107, no. 19, pp. 3970–3980, 2003. (Cited on page 86.)

[177] K. M. Rosso and M. Dupuis, "Electron transfer in environmental systems: a frontier for theoretical chemistry," *Theoretical Chemistry Accounts*, vol. 116, no. 1-3, pp. 124–136, 2006. (Cited on page 86.)

[178] J. E. Norton and J.-L. Brédas, "Polarization energies in oligoacene semiconductor crystals," *Journal of the American Chemical Society*, vol. 130, no. 37, pp. 12377–12384, 2008. (Cited on page 86.)

[179] W.-Q. Deng, , and W. A. G. III, "Predictions of hole mobilities in oligoacene organic semiconductors from quantum mechanical calculations," *The Journal of Physical Chemistry B*, vol. 108, no. 25, pp. 8614–8621, 2004. (Cited on page 86.)

[180] M. D. Newton, "Quantum chemical probes of electron-transfer kinetics: the nature of donor-acceptor interactions," *Chemical Reviews*, vol. 91, no. 5, pp. 767–792, 1991. (Cited on page 87.)

[181] F. Castet, P. Aurel, A. Fritsch, L. Ducasse, D. Liotard, M. Linares, J. Cornil, and D. Beljonne, "Electronic polarization effects on charge carriers in anthracene: A valence bond study," *Phys. Rev. B*, vol. 77, p. 115210, Mar 2008. (Cited on page 87.)

[182] F. Ortmann, F. Bechstedt, and K. Hannewald, "Charge transport in organic crystals: interplay of band transport, hopping and electron-phonon scattering," *New Journal of Physics*, vol. 12, no. 2, p. 023011, 2010. (Cited on page 89.)

[183] F. Babudri, G. M. Farinola, F. Naso, and R. Ragni, "Fluorinated organic materials for electronic and optoelectronic applications: the role of the fluorine atom," *Chem. Commun.*, pp. 1003–1022, 2007. (Cited on page 93.)

COLOPHON

This document was typeset using the typographical look-and-feel `classicthesis` developed by André Miede. The style was inspired by Robert Bringhurst's seminal book on typography "*The Elements of Typographic Style*". `classicthesis` is available for both LaTeX and LyX:

http://code.google.com/p/classicthesis/

Final Version as of February 23, 2016 (`classicthesis`).